An Investigation on the Nonlinear Vibration Behavior of Mistuned Bladed Disk Assemblies

Hooman Zoka

A Thesis

In the Department of

Mechanical, Industrial and Aerospace Engineering

Presented in Partial Fulfillment of the Requirements

For the Degree of

Master of Applied Science (Mechanical, Industrial and Aerospace Engineering)

at Concordia University

Montreal, Quebec, Canada

December 2022

CONCORDIA UNIVERSITY

SCHOOL OF GRADUATE STUDIES

This is to certify that the thesis prepared

By: Hooman Zoka

Entitled: An Investigation on the Nonlinear Vibration Behavior of Mistuned Bladed Disk Assemblies

and submitted in partial fulfillment of the requirements for the degree of

Master of Applied Science (Mechanical, Industrial and Aerospace Engineering)

complies with the regulations of the University and meets the accepted standards with respect to originality and quality.

Signed by the final examining committee:

_____Chair
Dr. Mojtaba Kheiri

_____Examiner
Dr. Mojtaba Kheiri

_____Examiner
Dr. Ghazanfarah Hafeez

_____Thesis Supervisor
Dr. Behrooz Yousefzadeh

Approved by _____
           Dr. Muthukumaran Packirisamy, Graduate Program Director

December 14, 2022

_____
Dr. Mourad Debbabi, Dean
Faculty of Engineering and Computer Science

ABSTRACT

An Investigation on the Nonlinear Vibration Behavior of Mistuned Bladed Disk Assemblies

Hooman Zoka

One of the critical components of turbomachinery is the bladed disk assembly (BDA). BDAs operate in a harsh environment and under dynamic pressure during operation. In aero engines, the pressure inhomogeneities in airflow and friction forces due to contact at different locations can cause vibrations of the blades and disk. These vibrations result in a range of damages to the machine, from damage to the blade and casing, such as wear, to catastrophic engine failure. The following two factors may have a critical influence on the vibrations of BDAs: (i) the contact between the blade root and disk, (ii) the unavoidable imperfections in manufacturing or mounting of the blades, referred to as mistuning. The former leads to friction forces between the blade root and disk, while the latter adds a significant amount of uncertainty to the system and may lead to the localization of vibration energy to a few blades. The friction forces at the joints and other contact areas introduce nonlinear terms into the governing equations. The analysis of nonlinear vibrations of BDAs is a time-consuming process. Many studies have focused on the separate effects of nonlinearity and mistuning on the vibration characteristics of BDA in turbomachinery. The combined effects of these two phenomena, however, are not well understood. This area has attracted great interest in recent years, and engineers are working to uncover the correlation between mistuning and nonlinearity and their effects on the vibration characteristics of BDAs.

This study is concerned with the mathematical modeling, numerical analysis, and statistical analysis of vibration characteristics of BDAs, including both nonlinear forces and mistuning. The governing equations are written for a lumped parameter model replicating the behavior of BDA with six blades. The nonlinear forces are due to the dry friction between the roots of the blades and the disk. The nonlinear governing equations are then solved for the tuned BDA. The steady-state forced response of the mistuned nonlinear system is then computed, with mistuning introduced as a small blade-to-blade deviation in the elasticity of the blades with respect to the tuned BDA. The effects of changing the mistuning and excitation levels are investigated. Two different mistuning

realizations are considered to study the effect of mistuning on the vibrations of a BDA. A preliminary statistical analysis is then performed on an ensemble of 150 realizations of mistuned BDAs.

Dedication

This dissertation is dedicated to my beloved parents and sisters

for their endless love, support, and encouragement

Acknowledgment

I would like to express my sincere thanks to my supervisor Behrooz Yousefzadeh for his assistance and invaluable guidance at every stage of the research process. He gave me a chance to be in his research group and showed me how to do in-depth research, write better research articles, and how I could improve my work.

I would like to acknowledge all the administrative staff in MIAE, especially the graduate program coordinator, Leslie Hosein, for all her assistance with administrative matters.

Special thanks go to all my close friends and office mates: Graeme Macdermid, Céleste Grimard, Armin Rasooli, Hossein Vatandoost, Nader Mohseni, Ali Kogani, Jiuda Wu, Mohsen Delavari, Mostafa Abdalaziz, Sina Tavassoli, and Mohamed Ghanem.

I would like to thank my girlfriend, Asiyeh, for her endless love and support. Dealing with all obstacles was difficult and challenging for me without her presence.

Last but certainly not least, I would like to extend my thanks to my parents, my sisters and their husbands, Golnaz and Ahmad, and Negar and Ali, my dear niece, Mahpari, and my nephew, Bijan, for their continued love, support, and encouragement throughout this journey.

Table of Contents

Table of Contents

LIST OF FIGURES

List of Tables

Nomenclature

$\boldsymbol{A_T}$	Matrix of coefficients of the state vector's derivatives
$\boldsymbol{A(\omega)}$	Matrix defining linear dynamics of the system
$\boldsymbol{B_T}$	Matrix of coefficients of the state vector
b	Vector of force coefficient
c	Damping coefficient of each DOF
$\boldsymbol{C}$	Damping matrix
c_k	Cosine coefficient of the Fourier series
$\boldsymbol{C_T}$	Matrix of internal and external force
d_m	Mistuning level
F	Amplitude of excitation (excitation level)
$\boldsymbol{F_{ex}}$	External force matrix
f_{ex}	External force
$\boldsymbol{F_{nl}}$	Nonlinear force matrix
f_{nl}	Nonlinear force
f_x	Jacobian of f
$\mathbb{I}_{\boldsymbol{n}}$	Identity matrix with the order of n
$\boldsymbol{K}$	Stiffness matrix
k_m	Mistuned stiffness
k_t	Tuned stiffness
$\boldsymbol{M}$	Mass matrix
m	Mass of each DOF

N	Normal load at the contact surface
N_b	Total number of sectors
N_H	Harmonic number
$Q(t)$	vector including sine and cosine series
s	Curve variable
s_k	Sine coefficient of the Fourier series
t_n	Tangent vector
T	Period of the force or response
y_i	State variables
$\dot{y}_i$	Derivative of state variables
Y	State vector
$\dot{Y}$	Derivative of state vector
$\|X\|$	Norm of amplitude
X_i	Steady-state forced response of ith mass
z	Vector of displacement coefficient
α	Bifurcation parameter
β	Nonlinear stiffness coefficient
γ	Linear stiffness coefficient
$\Delta\alpha$	Iteration step
ε	Degree of regularization
λ	Vector of control or bifurcation parameter
μ	Mean

μ_0	Friction coefficient
ξ	Random deviation
σ	Standard deviation
Ω	Excitation frequency
$\otimes$	Kronecker tensor product

1.   Chapter 1: Introduction

1.1   Bladed Disk Assemblies

Jet aircraft engines, hydroelectric or thermal turbines in power plants, pumps, and turbochargers are examples of turbomachinery. The rotors of these machines are made of disks installed on a shaft connected to a stationary housing. The rotating disk of these machines contains blades. The rotating components are primarily manufactured in two ways: (i) as an integrated and single component, named a blisk, or (ii) as a multi-component structure with several identical blades mounted on a disk referred to as a Bladed Disk Assembly (BDA). Blisks are lighter than BDAs because they do not require bolts, screws, and dovetail joints. However, a blisk's lower structural damping than a BDA results in a higher amplitude of vibration in blisks [1], [2].

BDAs receive energy and momentum from the gas flow in a turbomachine and transfer it to the shafts in a turbine. In an airplane's engine, a BDA operates under extreme conditions with high temperature levels between 850˚C and 1700˚C. These thermal loads, static fluid pressure, and rotation-induced centrifugal loads lead to static stress. In addition, BDAs are subjected to various dynamic loads in this harsh operating environment. Some of the loads are described below:

- **Engine Order Excitation:** The interaction between the blade and the airflow is called Engine Order Excitation [3]. There are pressure inhomogeneities because of the aerodynamic interactions of blade row and non-uniform airflow inside the system. The non-uniform airflow can be formed by the non-symmetric conditions in the flow path, for instance, because of the casing ovality or struts. The operation of the rotating blade inside this pressure inhomogeneities causes dynamic forces [4]. Because adjacent blades experience the same pressure inhomogeneity with a constant time delay, these forces are experienced as a traveling wave by an observer on BDA. This dynamic load contains frequencies at integer multiples of the rotational frequency of the engine.
- **Rubbing:** In turbines, it is necessary to minimize the clearance between the blade tips and casing to increase the aerodynamic efficiency of the turbines. However, reducing the clearance increases the risk of destructive contact between blade tips and their casing,

called rub. The rub can result in various damage types, ranging from small damage such as blade wear to significant damage like blade detachment. On June 23, 2014, the engine of an F-35A aircraft fired because of excessive rubbing between the blades and cowling. This accident resulted in the grounding of this aircraft throughout the fleet [5]. The rub phenomena will be discussed in detail in section 1.3.

Two factors significantly influence the vibrations of BDAs: (i) mistuning, and (ii) nonlinear behavior. Mistuning, a common problem in BDAs, refers to slight structural differences between the blades. Mistuning is inevitable because of imperfection in manufacturing, material inhomogeneity, and imperfect assembly of rotating systems. In BDAs, mistuning increases the levels of blade vibrations compared to their tuned counterparts [3], [5], [6]. Mistuning in BDAs can result in the localization of vibration energy to only a few blades in the assembly. Furthermore, mistuning leads to premature fatigue failure. The study of the influence of mistuning on the vibrations of BDAs dates back to the 1960s.

There are diverse approaches to mitigate the excessive vibration of BDAs. The excitation of the resonant frequencies could be avoided by modifying the natural frequency of the system, for instance, by adjusting the number of blades in each row. When avoiding the resonance frequencies is not feasible, damping can be used to mitigate vibrations. Material damping is negligible compared to the energy loss that occurs at the joints [4]. The most effective damping mechanism at the joints is the friction caused by sliding in the contact interfaces. However, frictional damping results in wear at the location of contact.

There are two primary sources for friction in BDAs: (i) intrinsic to BDA, such as the interaction between the disk and the dovetail joint of the blade, and (ii) additional external damping, for instance, underplatform dampers. Figure 1-1 represents the common friction joints in BDAs: The root joints (a), the shrouds installed at the tip of the blades (b), the underplatform dampers (c), wire dampers (d), and pins dampers (e).
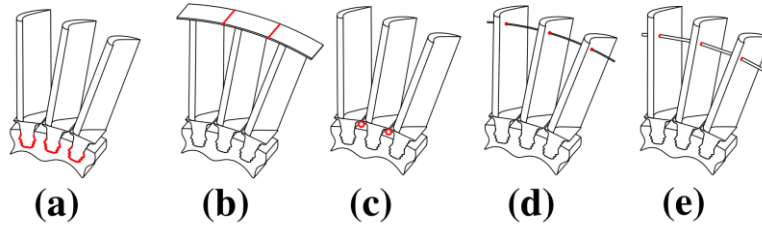
Figure 1-1: Types of friction joints [4]

The next sections review and synthesize the literature on nonlinear vibrations of mistuned BDAs. This thesis is focused entirely on structural vibrations in BDAs. It is assumed that the fluid-loading effects (fluid-structure interactions) are adequately captured by the engine-order excitation. Aeroelastic effects such as flutter are not considered in this work [4]. While there are wide ranges of studies on the effects of nonlinear forces and mistuning on the vibration of BDAs, the combined effects of these two phenomena are not well understood. Only a few investigations are dedicated to studying this topic in recent years.

1.2 Mistuning in BDAs

Although a bladed disk is typically designed to have identical blades, there are always deviations among the blades caused by manufacturing tolerances, slight material discrepancies, wear, and other causes. Such deviations are referred to as mistuning. Even though mistuning is typically small (e.g., the natural frequencies of blades differ on the order of a few percent of the nominal values), mistuned BDAs can have drastically higher forced response levels than their tuned counterparts [7]–[9]. The higher forced response leads to an increase in stresses, which results in high cycle fatigue (HCF) of the blades. The ensuing blade failure is a safety issue and will affect the reliability of turbo engines and lead to high repair costs. The National Airlines flight 27 on November 1973 is an example of aviation incidents related to HCF and blade loss. When the DC-10 aircraft was flying from Miami to San Francisco at 39000 feet, engine number 3 fell apart completely [10]. An annual report from Defense Technical Information Center estimated that in 1994, HCF-related maintenances cost over $400 million per year [11].

It is essential to identify the existence of mistuning in a manufactured BDA. For a BDA, mistuning can be identified by measuring the blade-alone natural frequencies. Measuring each blade's natural frequencies is not feasible for a blisk because the natural frequency of each blade cannot be measured separately. Hence, mistuning identification techniques are introduced based

on experimental measurements of the system response. The identification of mistuning can also be used for structural health monitoring of a turbine, for example, to identify cracks on the blades. A crack may have a negligible effect on the blade-alone frequencies; however, it could be the reason for significant changes in the system mode shapes [3]. Whitehead [12] developed a formula to estimate the boundary for the maximum forced response magnification in a mistuned BDA as a function of the number of blades. Martel and Corral [13] considered tuned traveling modes near the resonance as the active modes. They improved Whitehead's model by considering the number of active modes in a blade mode family instead of the number of blades in Whitehead's formula.

The spatial confinement of vibrations caused by mistuning is strongly dependent on the strength of structural coupling between adjacent blades. It can be explained by considering each blade as a single oscillator (a spring-mass system) connected to its adjacent blades by a spring. It can be shown that the degree of localization is related to the ratio of the overall mistuning in the blade elasticity to the coupling elasticity [3]. The adverse effects of mistuning can therefore be mediated by controlling the elastic coupling between the blades. The inter-blade coupling can be either structural (through the disk or shrouds) or, to a smaller extent, aerodynamic [3]. Indeed, mistuning effects can become negligible when the structural coupling between adjacent blades is strong [4]. The localization of mode shapes in a mistuned system is sometimes called Anderson localization due to a similar phenomenon observed in condensed matter physics [14].

A tuned BDA is a structure with cyclic symmetry built from identical sectors. A sector includes one blade and the corresponding segment of the disk. The cyclic symmetry enables a significant model reduction when analyzing the structural dynamics of tuned BDAs. However, mistuning breaks the cyclic symmetry of BDA. Hence, instead of a single sector model, the whole structure needs to be considered to predict the dynamic response. The mistuning amplification (also known as mistuning magnification or amplification factor) is defined as the ratio of the maximum vibration amplitude of a mistuned system to the maximum vibration amplitude of the corresponding tuned BDA.

A standard method to account for the uncertainty caused by mistuning is the Monte Carlo simulations. In this method, different values for uncertain parameters are chosen randomly, and multiple runs are required. Monte Carlo simulation has two drawbacks: (i) there is no guideline to determine how many samples are needed to describe the mistuning amplification using Monte

Carlo simulation [1], (ii) nonlinear simulations are time-consuming; for instance, finding the nonlinear frequency response curve for each sample on a PC equipped with an i7 processor can take one hour of calculation [1]. Thus, reaching the desirable sampling number considered in a linear context is a computational burden for systems involving nonlinearity [1].

There are several studies on the best blade arrangement with respect to mistuning [15], [16]. Furthermore, there are investigations to find the optimum mistuning pattern in terms of aeroelastic stability and forced response amplification. Indeed, the worst-case scenario study is of interest to researchers and engine manufacturers [17], [18]. Finding the worst-case scenario is crucial for assessing the maximum blade forced response. This offers a metric of the mistuning sensitivity and the study of reliability during the design process of BDA [3]. In addition, studying the worst-case scenario of the mistuning pattern and looking for the best-case mistuning pattern can help minimize the blade's forced response [3]. For linear systems, it is shown that the performance of the optimal mistuning pattern is susceptible to small changes in the value of mistuning [19], [20]. The variation of the mistuning pattern is inevitable during the operation of the engine. The challenge is to find a mistuning pattern that is less sensitive to random mistuning and can be used in the nominal design, known as intentional mistuning [3]. Intentional mistuning increases the stability of BDA's design when BDA is facing flutter [4], [21]. Also, it can be used to decrease the forced response of BDA [2], [22]. However, applying intentional mistuning on BDA to mitigate the forced response of the blade is not a standard mitigation strategy.

1.3   Nonlinear Vibrations in BDAs

Turbines blades with frictional contact (rub between the blade tip and the casing) and growing fatigue crack (variable stiffness because of closing and opening of the crack) are subjected to nonlinear forces at the joints and interfaces.

Analysis based on linearized models is equipped with powerful theoretical and experimental tools to predict the dynamic behavior of BDAs. However, in some cases, the influence of nonlinear forces is significant enough that a linear model cannot predict the correct dynamic behavior of a BDA. For example, to improve aero engine efficiency, it is needed to decrease the weight of the design by manufacturing lightweight-thin blades, resulting in more flexible structures prone to higher-amplitude motion. Moreover, it could be possible to decrease the clearance between the

blades and the casing (thereby increasing the overall efficiency) if the designer has a proper understanding of the nonlinear effects due to contact and friction [23].

In the following section, the dominant sources of nonlinearity in BDAs are discussed. Two categories of simulations used for nonlinear models are mentioned in section 1.3.2.

1.3.1 Dominant Source of Nonlinearities in BDAs

Contact Nonlinearity

Contact nonlinearity refers to friction forces at joints and contact forces due to rubbing between blade tips and casing. At the dovetail joints, the contact between the blade root and the disk holds the inserted blade in its place. The blade can be pulled due to centripetal acceleration and rubbed against the disk at their contact surfaces, as it is shown in Figure 1-2. As a result of rubbing, fretting occurs, which initiates fatigue cracks and blade failure. At the tip of the blade, the clearance between the blade and casing leads to tip flow leakage and reduced efficiency [5], [18]. Decreasing this clearance reduces fuel consumption and, subsequently, both the operating costs and carbon emissions [24]. Figure 1-3 shows the blade-casing clearance in a section view of a turbomachine.
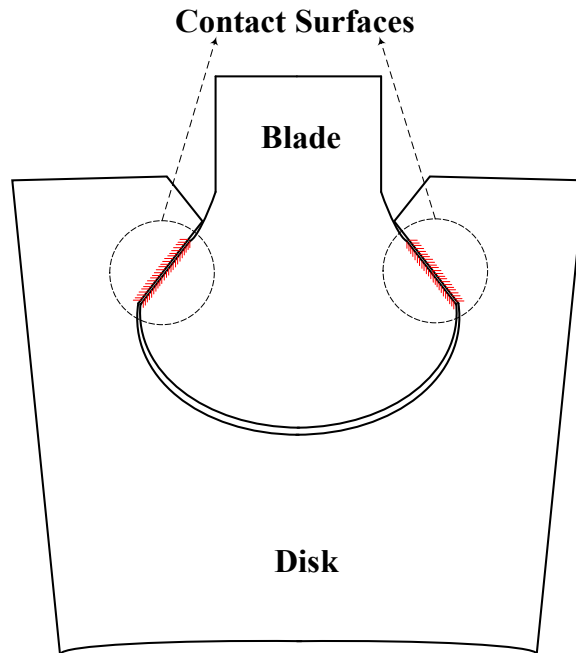
Figure 1-2: Demonstration of dovetail joint in one sector of BDA

6
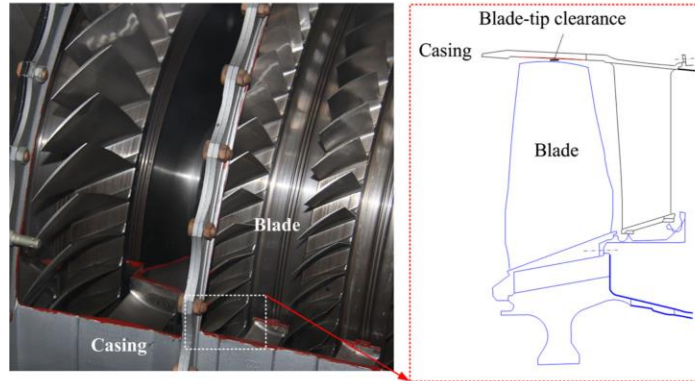
Figure 1-3: Radial distance between blade tip and casing or blade tip clearance [5]

Rubbing between blade tips and the engine casing in aero engines is a common source of friction in BDAs. Figure 1-4 demonstrates the typical places where contact between the rotor-stator or blade-casing occurs [10]. Rubbing usually takes place at the seals and barely between the casing and the blades. Because the linear velocity at the blade tip is high (and so is the impact energy), contact between the blade and casing is the most hazardous. The high level of energy involved in this contact can affect the dynamic behavior of the rotor [5].
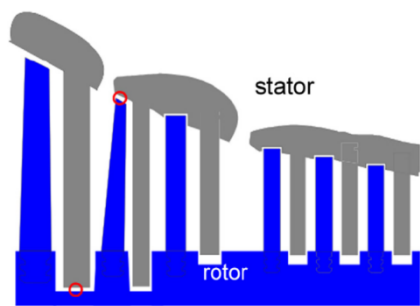
Figure 1-4: Probable places of rotor-stator or blade-casing contact [10]

Using abradable coating material on the inner side of the casing is a way to make the operating clearance near zero and prevent the disastrous penetration of the blade into the bare metal casing. The abradable coating wears due to contact with the blade and leaves a trail, such as the one shown in Figure 1-5 [5], [18]. This contact may lead to high-amplitude vibrations, possibly leading to blade failure [26]. Accurate modeling of friction, wear, and impact during the contact event is challenging [5]. While the effect of adopting different rubbing models to calculate blade response and contact forces is negligible at low rotational speeds, it is significant for high rotational speeds [5].

The vibrations of systems with dry friction can be complicated because of the nonlinear nature of the friction forces, including the local sticking, sliding, and liftoff [4]. In two separate computational studies on the compressor impeller of a helicopter engine, Batailly et al. [25], [26] showed that higher harmonics might be generated because of the nonlinear nature of the unilateral contact force. The generation of harmonics is an inherently nonlinear phenomenon that cannot be captured by a linear model.

Figure 1-5: Effect of rubbing on abradable coating mounted on casing [27]

Geometric Nonlinearity

Geometric nonlinearity refers to nonlinear forces that become significant due to the high amplitude of motion. Thin and elastic structures, such as blades in BDA, are more likely to be affected by geometric nonlinearity. Because large deflection during the operation of BDA is not confined to a specific region, the geometric nonlinearity is not localized as opposed to the contact nonlinearity.

1.3.2 Simulation Methods for Systems with Nonlinearities

The numerical analysis of nonlinear equations can be classified into two categories: (i) frequency-domain methods and (ii) time-domain methods.

The Harmonic Balance Method (HBM) is a common frequency-domain method for the computation of the steady-state response of nonlinear systems. It requires knowledge of the dominant frequency of the response, which can be obtained from experiments or direct integration in the time domain [10]. A truncated Fourier series approximates the response. In computing the forced response, the frequency of the input is the fundamental frequency of the Fourier series, e.g., the frequency of the engine order excitation. The accuracy of the response computed using HBM generally increases with the number of terms included in the truncated Fourier series. HBM has

become a standard method in turbomachinery [28]. HBM could suffer from issues of convergence and accuracy for non-smooth nonlinearities, such as blade-casing contact [17]. HBM is typically combined with numerical continuation techniques to obtain the response of nonlinear systems [29], [30].

The time-domain methods are based on numerical integration methods, such as Runge-Kutta, Newmark, and time forward integration methods. While the time-domain methods are more time-consuming than frequency-domain methods, they do not assume any types of solutions. The study of transient phenomena, which is critical in the study of contact-initiated interactions, typically requires the use of direct integration of the governing equations [1]. The precision of the time integration methods is highly affected by contact and separation, as well as the minimum time step [10]. The prediction of the exact time interval to reach the periodic steady-state response is another disadvantage of the time integration method [30].

1.4 Combined Effects of Mistuning and Nonlinearity

Analyzing the forced response of nonlinear systems is challenging. Unlike the linear system in which the response is independent of the amplitude of motion, in systems with nonlinearity, the amplitude of motion affects the response. Hence, linear models are unable to predict the response of systems involving nonlinearities correctly. The models developed for the tuned system are not applicable to the mistuned system. The symmetrical feature of the tuned systems helps to consider one sector of BDA instead of the entire system. Mistuning breaks the symmetry of the system and can result in keeping all DOFs in the model. There are many studies on the separate effects of mistuning and nonlinearity in turbomachinery; however, the combined effects of structural mistuning and nonlinearity require more investigations.

One of the inexpensive models to study different phenomena in BDA, such as uncertainty, is the lumped parameter model. Lumped parameter models offer a simple phenomenological examination of the vibration behavior of turbomachinery. To investigate the effect of uncertainty due to mistuning in nonlinear models and study the worst-case scenario, using statistical analysis with many random mistuned patterns is helpful. The lumped parameter models reduce the computational burdens of nonlinear systems under variable mistuning patterns and provide well-estimated results of real-world systems. The lumped parameter model is used in various studies,

considering the mistuning effect, using one single degree of freedom model [31]–[33], and multiple degrees of freedom model [29], [34]–[39]. While some papers considered the nonlinear effect due to the geometric nonlinearity [33], [38], [39], others consider contact between the blade root and the disk [36], [37], blade tip and the casing, or between blades at the shrouds [34] as the source of nonlinear forces.

Joannin et al. [35] used a lumped parameter model, Figure 1-6, to study the vibrations of mistuned BDAs with dry friction nonlinearities. The friction force is applied to the blade-disk joint to model dry friction between the blade's root and the disk. For a tuned system, the pairs of equal natural frequencies related to double modes are observed. In the presence of mistuning, each pair of double modes is split into two distinct natural frequencies with two different mode shapes, which increases the chance of occurrence of resonance in the forced response of the system.

In Ref. [35], the mode shapes of the system are studied for two reasons. First, to study the effective modal damping as a function of the vibration amplitude. Second, to provide a better understanding of the shape of the forced vibration response under traveling wave excitations. Considering the mode shape and free response time series, the time series for the tuned system is in the form of the traveling wave, while for the mistuned system, it is in the form of stationary waves. Consequently, the study of forced response in the tuned system, considering all sectors of BDA, unveiled that either in the vicinity or far from resonance, the response is in the form of traveling waves. In contrast, for the mistuned system, while the forced response far from resonances appears as a combination of traveling and stationary waves, it is in the form of stationary waves close to the resonances. Moreover, the effect of using an optimum mistuning pattern is studied by providing two random mistuning patterns. For a given mistuning pattern, the degree of mistuning (its amplitude) changes the effective modal damping.
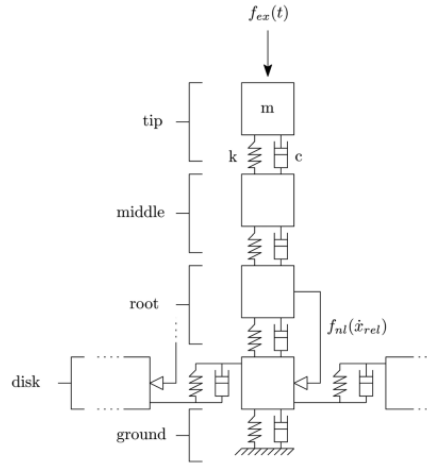
Figure 1-6: Lumped parameter model of BDA including dry friction nonlinearity between the blade root and the disk [35]

To study the combined effects of mistuning and nonlinearity due to the blade-casing contact, Joachim et al. [1] used a 2D model of a BDA (Figure 1-7). They observed that mistuning has a more significant effect on the response of nonlinear systems than linear ones. Moreover, they found no connection between linear and nonlinear amplification. These findings suggest that vibration mitigation methods designed based on linear models, such as new blade designs or intentional mistuning patterns, might not necessarily be helpful when nonlinear contact forces are taken into account.

(a) linear configuration ($n_d = 5$): circular load (→) and boundary dof (→)   (b) nonlinear configuration ($n_d = 5$): deformed casing (▢)
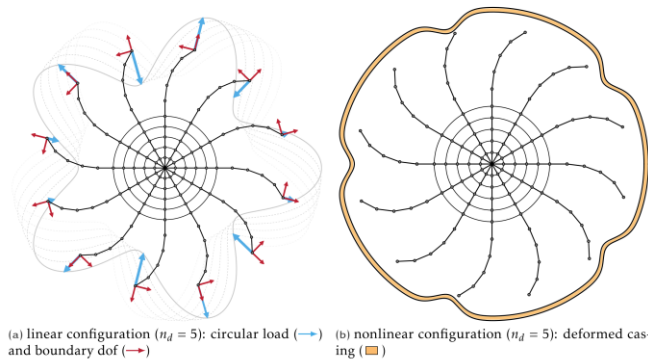
Figure 1. 2D bladed disk model.

Figure 1-7: 2D model of BDA for linear and nonlinear configurations [1]

Using a finite element (FE) model provides a more accurate simulation of a BDA. However, the large number of degrees of freedom (DOF) involved in a full FE model makes such computations expensive. Reduced Order Models (ROMs) are therefore developed to condense the number of DOFs while retaining the main characteristics of the structure. When both mistuning and nonlinear effects are combined in BDA, creating a ROM to both reduce the size of the model

and provide reasonably accurate estimation becomes very challenging. In this case, the nonlinear DOFs can be large in number, and the cyclic symmetry of the system cannot be retained due to mistuning. The geometric nonlinearity adds complications, in which the model reduction techniques are unable to condense the model's DOFs and result in keeping all DOFs [29]. Joannin et al. [29] extended the Craig-Bampton Component Mode Synthesis (CMS) method to provide a ROM that reduces computational time. To do so, they used the normal modes of the nonlinear system [40], [41].

Both mistuning and nonlinearity introduce uncertainties to the system. For a system including mistuning, the level, pattern, and source of mistuning are identified as uncertainties that strongly influence the dynamic behavior of the system [42]. Systems with nonlinearity often have uncertainties due to the nonlinear interaction law, such as friction contact law and sliding interfaces [17], [43]. Statistical analysis approaches are computationally expensive to study uncertainties in the presence of nonlinearities. Researchers use two approaches to avoid the computational burden of such systems: (i) developing efficient models, such that the analytical analyses become applicable, and (ii) working on methods to face uncertainty with fewer numbers of nonlinear simulations.

Most papers working on uncertainties focus on the average of acquired results from different samples (the ensemble average). Butlin et al. [44], [45], however, focused on predicting upper and lower response bounds, representing worst-case and best-case scenarios of the response, respectively. They presented a new approach faster than using the Monte Carlo method alongside the HBM. The root of the uncertainty in their paper is the nonlinear frictional couplings, and experimental tests validate this approach. Figure 1-8 shows the test setup and friction dampers assembly used in Ref. [44], [45]. Because of the highly uncertain nature of nonlinearity, they defined nonlinearity as a general constraint instead of a specific law. This approach is practical when computing the functional form of nonlinearity is challenging, such as the blade-casing contact or at the blade-disk joints. For example, the constraints that can be introduced for blade-casing contact are (i) the dissipative nature of the frictional contact, (ii) the friction coefficient between the blade tip and casing, and (iii) the radial displacement of the blade [18]. Using optimization and applying these constraints, the worst-case metric can be sought without considering a specific constitutive law for nonlinearity.

(a)   **(b)**
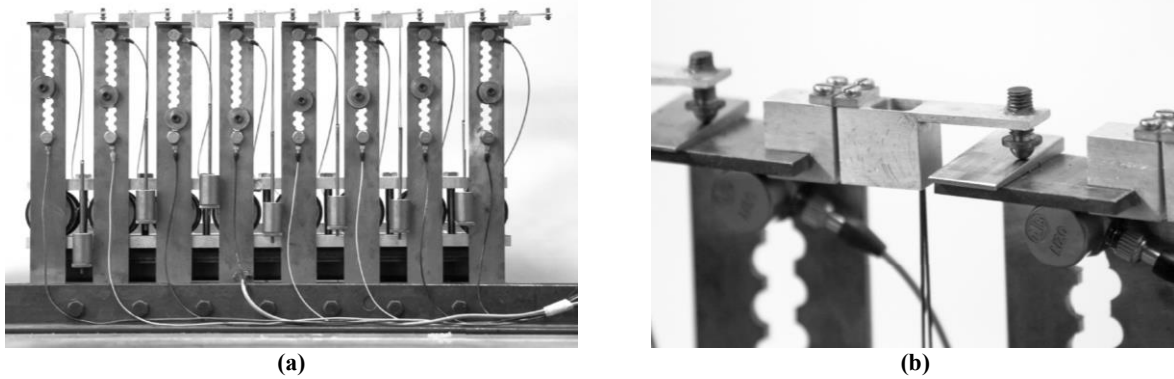
Figure 1-8: Experimental test setup used in [44], [45]**: (a) Beam elements including friction dampers, (b) Detailed view of friction dampers**

1.5   Current Study and Contributions

Significant progress has been made in understanding how mistuning and nonlinear forces in the joints and blade tips influence the vibration behavior of BDA separately. However, the combined effects of mistuning and nonlinearity are not well understood yet, and more studies are required to provide a better vision for researchers and engine manufacturers.

In the present work, a lumped parameter model of a BDA structure is considered to study the combined effects of mistuning and nonlinearity. The source of nonlinearity is the dry friction at the contact interfaces of the blade root and the disk. The external force is applied as a traveling force excitation (engine-order excitation) on the tips of the blades. Mistuning is modeled as a small deviation (with respect to the tuned system) in the stiffness coefficients of the tip and middle sectors of blades The effect of mistuning on vibration characteristics of a single mistuned BDA is discussed first, followed by a statistical investigation on 150 realizations of mistuned BDAs.

1.6   Thesis Organizations

The rest of this thesis is organized in four chapters. Chapter 2 is dedicated to the detailed mathematical modeling and various simulation methods to solve the nonlinear governing equations of the tuned BDA. Furthermore, the method that is chosen to calculate the forced response of the tuned system is verified with the results of the direct integration method and the results reported by Joannin *et al.* [35].

After introducing mistuning to the blades in chapter 3, the mathematical method developed in the previous chapter is established to calculate the steady-state forced response of the mistuned

system. To do so, two different mistuning patterns are considered. In two different studies, the effects of excitation level and mistuning level on the forced response of the mistuned BDA are investigated.

A statistical analysis with many mistuned patterns is performed in chapter 4 to study the effect of uncertainty in the nonlinear model. 150 mistuning realizations are generated, and for each pattern, the steady-state forced response is calculated within a specific range of frequencies. In the next step, different statistical parameters are studied during the investigation on the effect of variable excitation level and mistuning level.

The major findings and contributions along with some future remarks, are summarized in chapter 5.

2. Chapter 2: Vibrations of a Tuned BDA

In this chapter, the vibration behavior of a tuned BDA is studied. First, a simplified lumped parameter model of a tuned BDA with a nonlinear force between the blade root and the disk is presented. The mathematical model and the so-called frictionless and bonded frequencies are calculated to be used in the expression of the nonlinearity effect. Second, some of the available methods to calculate the forced response of the system, including the time domain method, the Harmonic Balance (HB) method, and numerical continuation, are introduced in this chapter. Then, the forced response of blade tips is calculated and verified with the available results provided by another scholar under a traveling wave excitation. Finally, the effect of changing the excitation level in a specific range is investigated to show the activation of the nonlinearity and its effect on the forced response curves. Moreover, the effect of changing the excitation level on different results, including forced response, backbone curve, compliance, and the time series of the blade tips, are studied in this chapter.

2.1 Mathematical Modeling

A tuned BDA can be considered a structure with cyclic symmetry built from identical sectors. Each sector can be simplified as a lumped parameter model. Several identical sectors are connected and make the whole BDA. Figure 2-1 shows a 2D demonstration of a sector of a BDA, including one blade and the corresponding segment of the disk. Each sector contains four different DOFs: three DOFs to make blade sections, including the tip, middle, and root of the blade. The fourth DOF represents the portion of the disk corresponding to the sector. The whole BDA contains six sectors, so the entire BDA has 24 DOFs. Various researcher groups have used this lumped parameter model to study the vibration characteristics of a BDA [29], [34], [35], [46], [47]. In Figure 2-1, m, c, and k refer to the mass, damping, and stiffness coefficients of each DOF, respectively. The external force, f_{ex}, applies to the tip mass of each sector. f_{nl} is the nonlinear force due to the friction force between the root of the blade and the disk. The disk mass is connected to the adjacent disk mass on both sides to complete the cyclic pattern of a tuned BDA. Note that the DOFs in Figure 2-1 correspond to a modal representation of the bending motion of the blades and the tangential motion of the disk.

15

The values of the structural parameters presented in Figure 2-1 are listed in Table 2-1 [35]. The values of the mass are chosen to represent the mass distribution in a real BDA [35]. The values of the stiffness coefficients are then determined such that the natural frequencies of the system represent those of a real BDA. This model is tuned to reproduce the results of the first family of bending modes of a real BDA [35].

In Figure 2-1, considering only one sector, the governing equations are written as follows:

$$m_1 \ddot{x}_1 + c_1 \dot{x}_1 - c_1 \dot{x}_2 + k_1 x_1 - k_1 x_2 = -f_{ex}^1(t) \tag{2-1}$$

$$m_2 \ddot{x}_2 - c_1 \dot{x}_1 + (c_1 + c_2) \dot{x}_2 - c_2 \dot{x}_3 - k_1 x_1 + (k_1 + k_2)x_2 - k_2 x_3 = 0 \tag{2-2}$$

$$m_3 \ddot{x}_3 - c_2 \dot{x}_2 + (c_2 + c_3) \dot{x}_3 - c_3 \dot{x}_4^1 - k_2 x_2 + (k_2 + k_3)x_3 - k_3 x_4^1 + f_{nl}(\dot{x}_{rel}) = 0 \tag{2-3}$$

$$m_4 \ddot{x}_4^1 - c_3 \dot{x}_3 + (c_3 + c_4 + 2c_c) \dot{x}_4^1 - c_c \dot{x}_4^2 - c_c \dot{x}_4^6 - k_3 x_3 + (k_3 + k_4 + 2k_c)x_4^1$$
$$- k_c x_4^2 - k_c x_4^6 + f_{nl}(\dot{x}_{rel}) = 0 \tag{2-4}$$
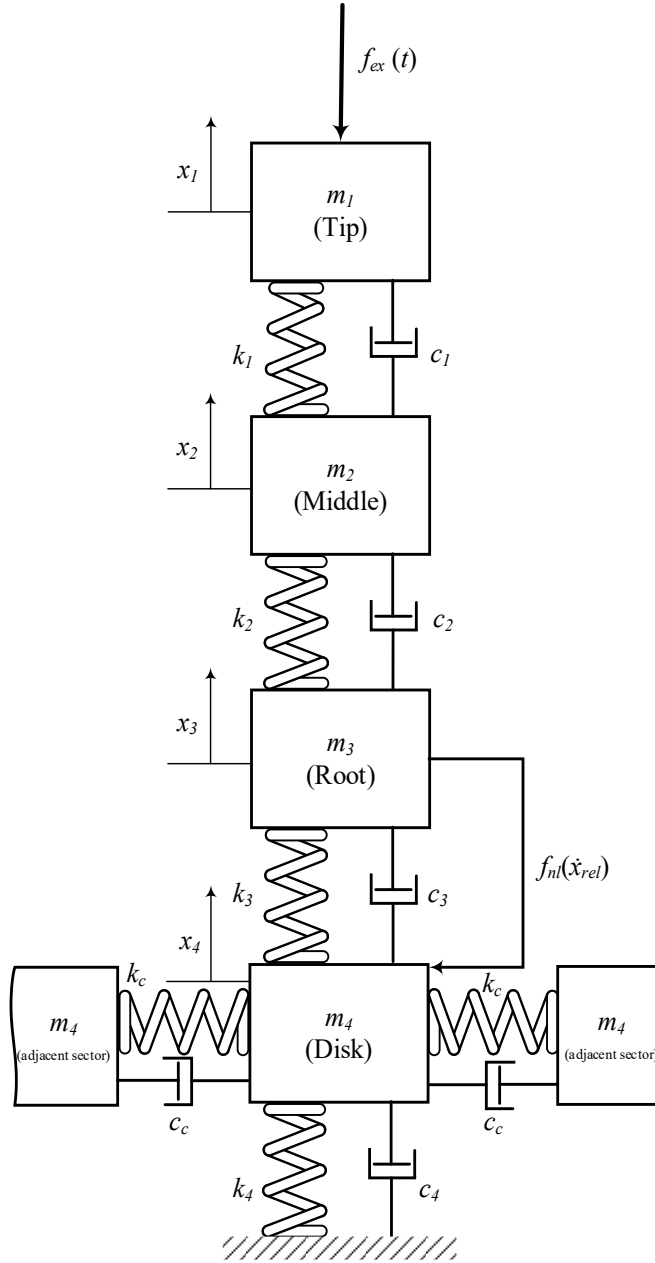
Figure 2-1: Lumped parameter model of each sector of BDA

Table 2-1: Value of parameters used in the sector of BDA [35]

Parameters (unit)	Tip	Middle	Root	Disk	Ground
m (10^{-3} kg)	5	5	15	120	--
c (N.s/m)	0.1	0.1	0.1	0.1	0.1
k (10^5 N/m)	6	10	300	100	25

In the Eqs. (2-1) - (2-4), subscripts 1, 2, 3, c, and 4 refer respectively to the sector's tip, middle, root, disk, and ground sections. Superscripts 1, 2, and 6 correspond to sectors 1, 2, and 6,

17

respectively. The dots refer to the derivatives with respect to the time, t. The parameter $\dot{x}_{rel}$ is the relative velocity between the blade root and the disk.

The governing equations for the whole model in a matrix format can be written in the following form:

$$M\ddot{X}(t) + C\dot{X}(t) + K X(t) + F_{nl}(\dot{X}) = F_{ex}(t) \tag{2-5}$$

where M, C, and K are mass, damping, and stiffness matrices, respectively. F_{nl} and F_{ex} are nonlinear force and external force matrices.

The engine order excitation of the system can be represented as an external force applied to the tip mass of the kth sector can be expressed as:

$$f_{ex}^k(t) = F\cos\left(\Omega t + \frac{2\pi k}{N_b}\right) \tag{2-6}$$

where Ω, F, and N_b are the excitation frequency, the amplitude of excitation, and the total number of sectors, respectively. Considering $T = 2\pi/\Omega$, the excitation can be computed over one forcing period, T. The normalized time series of excitation is demonstrated in Figure 2-2. The amplitude of excitation at $t/T=0$ for each blade is shown in Figure 2-3.
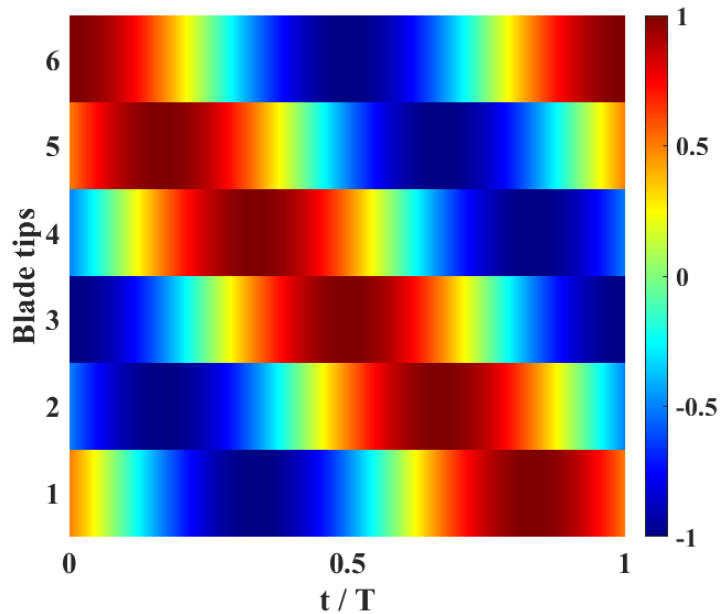
Figure 2-2: Normalized time series of excitation as a time-traveling wave through all sectors
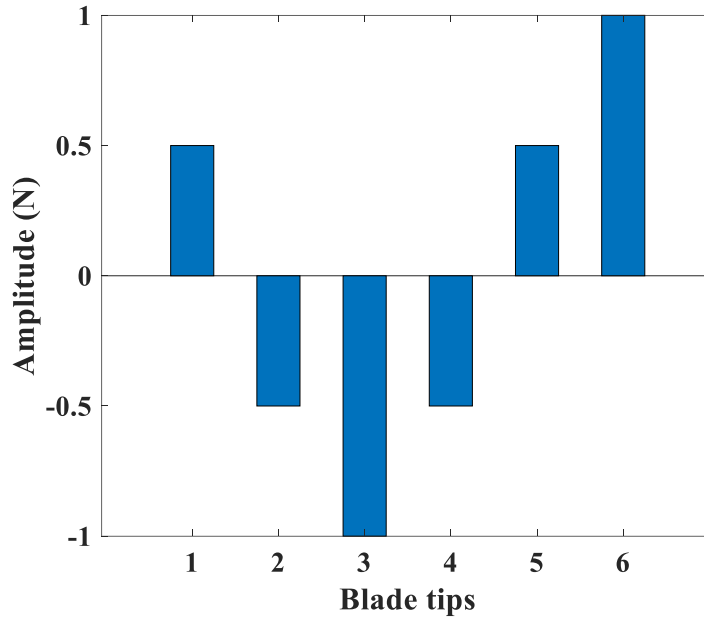
Figure 2-3: Amplitude of excitation at *t/T=0* applied at each blade tip

Ignoring the terms corresponding to the nonlinear and external forces in Eq. (2-5), the first family of natural frequencies for the tuned linear system is reported in Table 2-2. In this table, two different sets of natural frequencies are provided, named frictionless and bonded. The frictionless interface assumption means that the nonlinear force (friction force) between the blade root and the disk has been ignored. Bonded interface expresses the assumption in which there is no relative motion between the blade root and disk, and their masses are summed up together, and c_{root} and k_{root} are ignored. For all results, the bonded frequencies have a higher value than the frictionless frequencies. The reason is the stiffer stiffness between the blade root and the disk in the bonded model versus the softer stiffness in the contact interface in the frictionless assumption.

Table 2-2: Natural frequencies of the tuned linear system for the first family of bending mode, considering frictionless and bonded assumptions

Frequency (Hz)	f_1	f_2	f_3	f_4	f_5	f_6
Frictionless	652.6	1189.1	1189.1	1243.8	1243.8	1248.2
Bonded	653.6	1201.5	1201.5	1256.5	1256.5	1260.8

Table 2-2 shows that two pairs of natural frequencies (f_2, f_3, and f_4, f_5) are equal. The first pair corresponds to the double mode with one nodal diameter, and the second pair is the natural frequencies of the double mode with two nodal diameters [35]. f_1 and f_6 are the natural frequencies associated with a single mode with zero and three nodal diameters, respectively. In a circular

membrane, the nodal diameter or nodal line is defined as the line with zero deflection while the rest of the membrane oscillates.

This study uses Coulomb's dry friction law to model the friction force between the blade root and the disk. Coulomb's law can be modeled using the sign function and relative velocity between the root and the disk. A way to approximate the sign function is by using a hyperbolic tangent. The non-smooth sign function is replaced with a smooth hyperbolic tangent function, which is differentiable at all points. Moreover, we avoid the force discontinuity at $\dot{x}_{rel} = 0$, which results in computational burden [48]. Therefore, the nonlinear force can be formulated as follow:

$$f_{nl}(\dot{x}) = \mu_0 N \tanh \frac{\dot{x}_{rel}}{\varepsilon}, \tag{2-7}$$

where N and μ_0 are the normal load at the contact interface and friction coefficient, respectively. Throughout this study, the value for N is equal to the centrifugal force of the blade, which is constant and equal to 1000 N [35]. Also, the value for μ_0 is constant, equal to 0.3 [35]. In Eq. (2-7), ε represents the degree of regularization, which can be varied based on the amplitude of vibrations. A comparison between two different values of ε ($\varepsilon=10^{-3}$ and $\varepsilon=10^{-5}$) is provided in Figure 2-4. The small value of ε results in a closer approximation to the sign function; however, it takes a longer computation time [35]. In this study, the value for ε is constant and equal to 10^{-3}, which provides an acceptable agreement between the accuracy of results and the computational burden of simulation.
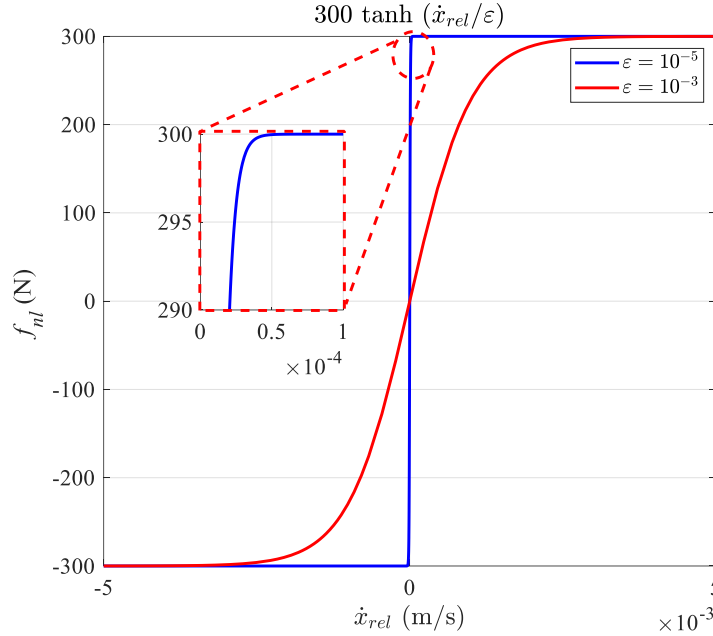
Figure 2-4: Comparison between two different values of ε ($\varepsilon=10^{-3}$ and $\varepsilon=10^{-5}$) for the hyperbolic tangent representation of Coulomb's dry friction law

2.2 Steady-state forced response of the nonlinear system

Three numerical methods are used for computing the steady-state forced response of the BDA in this study. These methods are described in this section.

2.2.1 Time-Domain Method

This method uses the direct integration of governing equations of the system. In this study, MATLAB is used to carry out the time-domain analysis. The *ode* command in MATLAB provides various solvers to solve differential equations with different orders. The order is defined as the highest-order derivative of the time-dependent variable in the equation. In order to use the *ode* command in MATLAB, the order of differential equations should be one. The governing equations of the system for the introduced model in this study, Eqs. (2-1)-(2-4) are second order. So, the first step is to reduce the order of the differential equations to one. In order to rewrite the Eqs. (2-1)-(2-4) for one sector of BDA, the state variables (y_i and $\dot{y}_i$) are assumed as follows:

$$
\begin{array}{llll}
x_1 = y_1 & x_2 = y_3 & x_3 = y_5 & x_4^1 = y_7 \\
\dot{x}_1 = \dot{y}_1 = y_2 \;\; ; & \dot{x}_2 = \dot{y}_3 = y_4 \;\; ; & \dot{x}_3 = \dot{y}_5 = y_6 \;\; ; & \dot{x}_4^1 = \dot{y}_7 = y_8 \\
\ddot{x}_1 = \dot{y}_2 & \ddot{x}_2 = \dot{y}_4 & \ddot{x}_3 = \dot{y}_6 & \ddot{x}_4^1 = \dot{y}_8
\end{array}
\tag{2-8}
$$

21

This assumption can be made for all six sectors of BDA. By substituting state variables from Eq. (2-8) in governing equations (Eqs. (2-1)-(2-4)), we have:

$$\dot{y}_1 = y_2 \tag{2-9}$$

$$m_1 \dot{y}_2 = -c_1 y_2 + c_1 y_4 - k_1 y_1 + k_1 y_3 - f_{ex}^1(t) \tag{2-10}$$

$$\dot{y}_3 = y_4 \tag{2-11}$$

$$m_2 \dot{y}_4 = c_1 y_2 - (c_1 + c_2) y_4 + c_2 y_6 + k_1 y_1 - (k_1 + k_2) y_3 + k_2 y_5 \tag{2-12}$$

$$\dot{y}_5 = y_6 \tag{2-13}$$

$$m_3 \dot{y}_6 = c_2 y_4 - (c_2 + c_3) y_6 + c_3 y_8 + k_2 y_3 - (k_2 + k_3) y_5 + k_3 y_7 - f_{nl}(\dot{x}_{rel}) \tag{2-14}$$

$$\dot{y}_7 = y_8 \tag{2-15}$$

$$m_4 \dot{y}_8 = c_3 y_6 - (c_3 + c_4 + 2c_c) y_8 + c_c y_{16} + c_c y_{48} + k_3 y_5 - (k_3 + k_4 + 2k_c) y_7$$
$$+ k_c y_{15} + k_c y_{47} - f_{nl}(\dot{x}_{rel}) \tag{2-16}$$

Eqs. (2-9)-(2-16) describe the motion of a single sector as a system of first-order equations. There are similar equations for the other sectors. Combining the equations for all sectors, the governing equations for the assembly in the matrix format can be summarized as:

$$\boldsymbol{A_T}\dot{Y} = \boldsymbol{B_T}Y + \boldsymbol{C_T} \tag{2-17}$$

where $\dot{Y}$ is the derivative of state vector Y, and it is defined as:

$$\dot{Y} = \begin{Bmatrix} \dot{y}_1 \\ \dot{y}_2 \\ \dot{y}_3 \\ \vdots \\ \dot{y}_{2n} \end{Bmatrix} \quad ; \qquad\qquad Y = \begin{Bmatrix} y_1 \\ y_2 \\ y_3 \\ \vdots \\ y_{2n} \end{Bmatrix} \tag{2-18}$$

where n is the number of degrees of freedom of the system. The matrices $\boldsymbol{A_T}$, $\boldsymbol{B_T}$, and $\boldsymbol{C_T}$ contain the coefficients of the derivatives of the state vector, coefficients of the state vector, and the matrix of the internal and external force, respectively. The dimension of $\boldsymbol{A_T}$ and $\boldsymbol{B_T}$ matrices are $2n \times 2n$, and for matrix $\boldsymbol{C_T}$, it is $2n \times 1$. Considering the model used in this study, the dimension of $\boldsymbol{A_T}$ and $\boldsymbol{B_T}$ matrices will be 48×48, and matrix $\boldsymbol{C_T}$ has a dimension of 48×1.

Now that the governing equations are converted to first-order equations, the *ode45* command in MATLAB can be used to solve this system of equations. In general, this command is the first recommended solver to solve differential equations that provide acceptable accuracy [49]. The

ode45 command is based on the 4th-order Runge-Kutta method. The details of this method can be found in the numerical methods textbooks [50], [51].

2.2.2 HBM Solution

Considering a general form of the governing Eq. (2-5) for n DOFs system under harmonic periodic excitation, we have:

$$M\ddot{X} + C\dot{X} + KX + F_{nl}(X, \dot{X}) = F_{ex}(\omega, t)$$
(2-19)

Here, the nonlinear force is a function of displacement and velocity.

The periodic response and forces, including external forces and nonlinear forces in the form of $f(x, \dot{x}, \omega, t) = F_{ex}(\omega, t) - F_{nl}(X, \dot{X})$ can be approximated by a truncated Fourier series as follow:

$$x(t) = \frac{c_0^x}{\sqrt{2}} + \sum_{k=1}^{N_H} \left(s_k^x \sin\left(\frac{k\omega t}{v}\right) + c_k^x \cos\left(\frac{k\omega t}{v}\right) \right)$$
(2-20)

$$f(t) = \frac{c_0^f}{\sqrt{2}} + \sum_{k=1}^{N_H} \left(s_k^f \sin\left(\frac{k\omega t}{v}\right) + c_k^f \cos\left(\frac{k\omega t}{v}\right) \right)$$
(2-21)

where N_H is the harmonic number. The unknown cosine and sine coefficients of the Fourier series are c_k and s_k, respectively. The superscripts x and f represent the Fourier coefficients of displacement $x(t)$ and force $f(t)$, respectively. Eq. (2-20) can be simplified to the format below:

$$x(t) = (Q(t) \otimes \mathbb{I}_n)z$$
(2-22)
$$f(t) = (Q(t) \otimes \mathbb{I}_n)b$$
(2-23)

where $\otimes$, $\mathbb{I}_n$ and $Q(t)$ are Kronecker tensor product, the identity matrix with the order of n, and the vector including sine and cosine series, respectively. The vector Q is:

$$Q(t) = \left[\frac{1}{\sqrt{2}} \quad \sin\left(\frac{\omega t}{v}\right) \quad \cos\left(\frac{\omega t}{v}\right) \quad \cdots \quad \sin\left(\frac{N_H \omega t}{v}\right) \quad \cos\left(\frac{N_H \omega t}{v}\right) \right]$$
(2-24)

z and b are the coefficients of displacements and force collected in two vectors with the dimension of $(2N_H+1)n$ as follow:

$$z = \left[(c_0^x)^T \quad (s_1^x)^T \quad (c_1^x)^T \quad \cdots \quad \left(s_{N_H}^x\right)^T \quad \left(c_{N_H}^x\right)^T \right]^T \tag{2-25}$$

$$b = \left[(c_0^f)^T \quad (s_1^f)^T \quad (c_1^f)^T \quad \cdots \quad \left(s_{N_H}^f\right)^T \quad \left(c_{N_H}^f\right)^T \right]^T \tag{2-26}$$

Considering Eq. (2-22), the velocity and acceleration are defined as follow:

$$\dot{x}(t) = \left(\dot{Q}(t) \otimes \mathbb{I}_n\right)z = \left((Q(t)\nabla) \otimes \mathbb{I}_n\right)z \tag{2-27}$$

$$\ddot{x}(t) = \left(\ddot{Q}(t) \otimes \mathbb{I}_n\right)z = \left((Q(t)\nabla^2) \otimes \mathbb{I}_n\right)z \tag{2-28}$$

where

$$\nabla_k = \begin{bmatrix} 0 & & & & \\ & \ddots & & & \\ & & \nabla_k & & \\ & & & \ddots & \\ & & & & \nabla_{N_H} \end{bmatrix}, \qquad \nabla\nabla = \nabla^2 = \begin{bmatrix} 0 & & & & \\ & \ddots & & & \\ & & \nabla_k^2 & & \\ & & & \ddots & \\ & & & & \nabla_{N_H}^2 \end{bmatrix} \tag{2-29}$$

∇ and ∇^2 are described as:

$$\nabla_k = \begin{bmatrix} 0 & -\dfrac{k\omega}{\nu} \\ \dfrac{k\omega}{\nu} & 0 \end{bmatrix}, \qquad \nabla_k^2 = \begin{bmatrix} -\left(\dfrac{k\omega}{\nu}\right)^2 & 0 \\ 0 & -\left(\dfrac{k\omega}{\nu}\right)^2 \end{bmatrix} \tag{2-30}$$

After substituting Eqs. (2-22), (2-23), (2-27), and (2-28) in Eq. (2-19) and considering the mixed-product property of Kronecker tensor product[1], it yields:

$$\left((Q(t)\nabla^2) \otimes M\right)z + \left((Q(t)\nabla) \otimes C\right)z + (Q(t) \otimes K)z = (Q(t) \otimes \mathbb{I}_n)b \tag{2-31}$$

Applying the Galerkin procedure on the orthogonal trigonometric basis $Q(t)$ results in finding the different Fourier coefficients and removing the time dependency:

---

[1] $(A \otimes B)(C \otimes D) = (AC) \otimes (BD)$

$$\left(\left(\frac{2}{T}\int_0^T Q^T(t)Q(t)dt\,\nabla^2\right)\otimes M\right)z + \left(\left(\frac{2}{T}\int_0^T Q^T(t)Q(t)dt\,\nabla\right)\otimes C\right)z$$

$$+\left(\left(\frac{2}{T}\int_0^T Q^T(t)Q(t)dt\right)\otimes K\right)z = \left(\left(\frac{2}{T}\int_0^T Q^T(t)Q(t)dt\right)\otimes \mathbb{I}_n\right)b \tag{2-32}$$

Knowing that

$$\frac{2}{T}\int_0^T Q^T(t)Q(t)dt = \mathbb{I}_{2N_H+1} \tag{2-33}$$

T is the period of the external force. The equations of motion in the frequency domain are as follows:

$$(\nabla^2\otimes M)z + (\nabla\otimes C)z + \left(\mathbb{I}_{2N_H+1}\otimes K\right)z = \left(\mathbb{I}_{2N_H+1}\otimes \mathbb{I}_n\right)b \tag{2-34}$$

or

$$\underbrace{(\nabla^2\otimes M) + (\nabla\otimes C) + \left(\mathbb{I}_{2N_H+1}\otimes K\right)}_{A(\omega)} z = \left(\mathbb{I}_{2N_H+1}\otimes \mathbb{I}_n\right)b \tag{2-35}$$

Eq. (2-35) can be written in the compact form

$$\boldsymbol{A}(\boldsymbol{\omega})z - b(z) = 0 \tag{2-36}$$

where $\boldsymbol{A}(\boldsymbol{\omega})$ is a $(2N_H+1)n \times (2N_H+1)n$ matrix defining the linear dynamics of the system as follows:

$$\begin{bmatrix} -K & & & & & \\ & K-\left(\frac{\omega}{v}\right)^2 M & -\frac{\omega}{v}C & & & \\ & \frac{\omega}{v}C & K-\left(\frac{\omega}{v}\right)^2 M & & & \\ & & & \ddots & & \\ & & & & K-\left(N_H\frac{\omega}{v}\right)^2 M & -N_H\frac{\omega}{v}C \\ & & & & N_H\frac{\omega}{v}C & K-\left(N_H\frac{\omega}{v}\right)^2 M \end{bmatrix} \tag{2-37}$$

Substituting the root of Eq. (2-36) in Eq. (2-22) results in the solution of (2-19).

Eq. (2-36) contains nonlinear algebraic equations which can be solved using different methods. One way is to use iterative methods, such as the Newton-Raphson method, using the FSOLVE command in MATLAB software.

In the HB method, increasing the number of harmonics in the truncated Fourier series is necessary to achieve an answer with sufficient accuracy. Increasing the number of harmonics increases the size of Eq. (2-37), and results in large systems with multiple degrees of freedom, this results in a heavy computational workload [30], [52].

The HBM method, described above, is often unable to handle complicated nonlinear forces such as the Coulomb friction model, because of the hyperbolic tangent function [30], [52]. In the current work, the nonlinear forces contain velocity terms inside the hyperbolic tangent function. Consequently, it is difficult to extract sine and cosine coefficients in Eqs. (2-20) and (2-21) using the HBM formulation. An alternative to the HBM is the Alternating Frequency-Time (AFT) formulation. This method uses inverse Fourier transform, for example, inverse fast Fourier transform (iFFT), and discrete Fourier transform, such as fast Fourier transform (FFT), to switch between the time domain and frequency domain representations of the response. The algorithm of AFT is illustrated in Figure 2-5 [30]. An initial estimation of the response in the frequency domain can be transferred to the time domain using iFFT. Then, the nonlinear forces can be evaluated by the response in the time domain. The nonlinear forces in the time domain are then converted to harmonic coefficients (sines and cosines coefficients) using FFT and used to evaluate the response for the next iteration. The details of HBM and AFT-HB can be found in nonlinear vibrations textbooks [30].
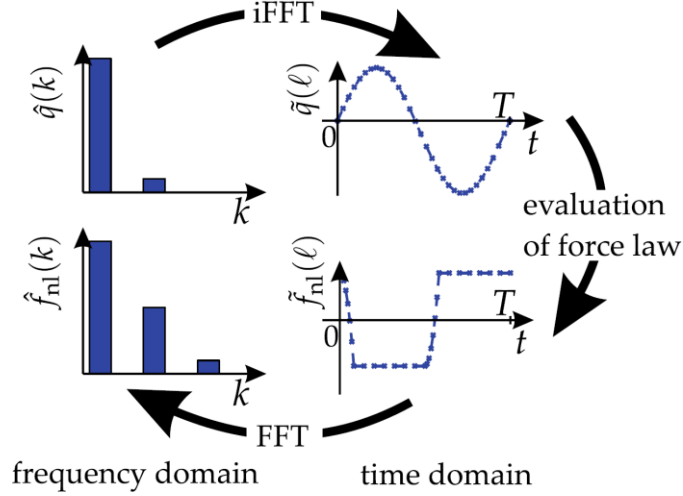
Figure 2-5: Illustration shows the algorithm behind the AFT method [30]

2.2.3   Numerical Continuation

The numerical continuation method makes it possible to find successive points of a response curve (solution curve). A common technique in numerical continuation is the application of predictor and corrector steps. The predictor-corrector method predicts a new point of the response curve. Then the predicted point will be corrected to provide the new sequential point for the next prediction.

The main difficulty in using continuation techniques is to find a good approximation of the initial point close to the solution curve, especially near turning points and branches [53]. Different techniques for numerical continuation can be found in the literature, such as sequential or natural parameter continuation, pseudo-arclength continuation, simplicial or piecewise linear continuation, and Davidenko-Gauss-Newton continuation [53]. The primary difference between these algorithms is in the details of the predictor and corrector steps.

To showcase the effectiveness of continuation methods, we use the Duffing system as an example. The governing equation for this system are:

$$\ddot{x} + C\dot{x} + \gamma x + \beta x^3 = F\cos(\omega t) \tag{2-38}$$

where γ and β are the linear and nonlinear stiffness coefficients, respectively. Assuming only one term in the Fourier series approximation of the response, $N_H=1$, and $\nu=1$ in Eq. (2-20) and applying standard HBM to the above equation, we have:

27

$$x(t) = s_1^x \sin(\omega t) + c_1^x \cos(\omega t) \tag{2-39}$$

$$\dot{x}(t) = \omega s_1^x \cos(\omega t) - \omega c_1^x \sin(\omega t) \tag{2-40}$$

$$\ddot{x}(t) = -\omega^2 s_1^x \sin(\omega t) - \omega^2 c_1^x \cos(\omega t) = -\omega^2 x(t) \tag{2-41}$$

Note that the cubic stiffness only creates odd harmonics; as a result, the even terms in Eq. (2-39) have been dropped [30], [35]. After substituting Eqs. (2-39) - (2-41) in Eq. (2-38) and applying a Galerkin projection procedure, we derive the following two nonlinear algebraic equations:

$$\frac{3}{4}\beta c_1^{x3} + (\alpha - \omega^2)c_1^x + \frac{3}{4}\beta c_1^x s_1^{x2} + C\omega s_1^x = F \tag{2-42}$$

$$\frac{3}{4}\beta s_1^{x3} + (\alpha - \omega^2)s_1^x + \frac{3}{4}\beta s_1^x c_1^{x2} + C\omega c_1^x = 0 \tag{2-43}$$

in which the coefficients of the sine and cosine functions (the amplitudes) are unknown. Assuming $C = 0.05$ Ns/m, $\alpha = 1$, $\beta = 0.04$, and $F = 0.5$ N, the system of equations in Eqs. (2-42) and (2-43) can be solved for different frequencies to find the unknowns. Using the FSOLVE command in MATLAB, these algebraic equations can be solved. The response at the frequency far from the resonance can be provided and used as the initial values to solve the system of equations and find the nonlinear response curve. However, the FSOLVE algorithm has trouble following the turning point, and numerical continuation can be used instead for this purpose.

Here, the sequential continuation and pseudo-arclength continuation methods are explained briefly. A detailed explanation in the context of mechanical vibrations can be found in Refs. [30], [54].

Sequential Continuation

The first method is sequential or natural parameter continuation, in which the prediction starts from an initial solution point (α_0, x_0). Then it continues by increasing α, as $\alpha_1 = \alpha_0 + \Delta\alpha$, to the next point by taking small steps, $\Delta\alpha$, and assuming that in the following prediction point x is the same as the first one, i.e. $(\alpha_1, x_1) = (\alpha_1, x_0)$. In the next step, using an iteration method, such as Newton-Raphson, the prediction corrects by solving $f(x_2, \alpha_1)=0$ for x_2 to find the next accurate solution point $(\alpha_2, x_2) = (\alpha_1, x_2)$. New solution points can be found by considering the new solution point,

(α_2, x_2), as the new starting point, (α_0, x_0), for the next prediction and repeating the same steps. A demonstration of sequential continuation is shown in Figure 2-6 (a).

This method requires taking small steps, $\Delta\alpha$, where the solution curve has steep gradients, which results in a computational burden. Also, as it is shown in Figure 2-6 (a), this method cannot follow the solution curve in the area with a turning point (the last point of Figure 2-6 (a)). Thus, other methods, such as the pseudo-arclength continuation, should be used to follow the solution curve at turning points.

Figure 2-6: Demonstrations of two numerical continuation methods to find the solution curve. (a) Sequential continuation; (b) Pseudo-arclength continuation [53]

Pseudo-Arclength Continuation

Pseudo-arclength continuation makes a linear prediction step in the direction of the solution curve tangent. This prediction is corrected perpendicular to the curve tangent in the next step. A new constraint called Euclidian arclength normalization, also known as the pseudo-arclength constraint, is considered in this method to find all unknowns. By moving in the tangent direction of a known solution point on the solution curve, it is possible to find the next prediction. After considering point 0 in Figure 2-6 (b) as a known solution point, a step of Δs can be taken to find the prediction point, point 1. By adopting a small value of Δs, the new prediction point can be close to the solution point. As the next step, this prediction corrects perpendicular to the tangent vector (utilizing Newton-Raphson iteration) to find the new solution point (point 2). Assuming this new solution point, point 2, as a starting point for the next iteration, point 0, the whole procedure can

be repeated to find the next solution point. The pseudo-arclength continuation algorithm is presented in detail in [53].

Using numerical continuation to solve the governing equations of the SDOF Duffing oscillator, the same equations as Eqs. (2-42) and (2-43) are considered with a difference that ω is also considered an unknown. The pseudo-arclength constraint can provide another equation to determine all unknowns.

Solving all the system of equations containing Eqs. (2-42), (2-43) and pseudo-arclength constraint will capture the turning curve in the response curve of the SDOF Duffing equation. The norm of amplitude, $\|X\|$, and the phase angle are shown in Figure 2-7 and Figure 2-8, respectively. Furthermore, in these figures, the response curve without continuation, the red dashed line, is included. In Figure 2-7, the response curve cannot demonstrate the turning point and drops to stable results before reaching the turning point.
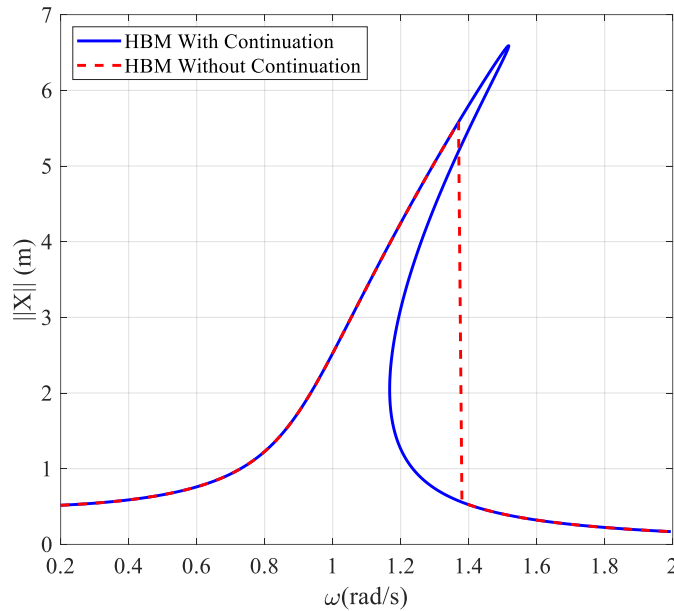
Figure 2-7: Comparison of the norm of amplitude, using HBM by considering N_H=1, with and without continuation
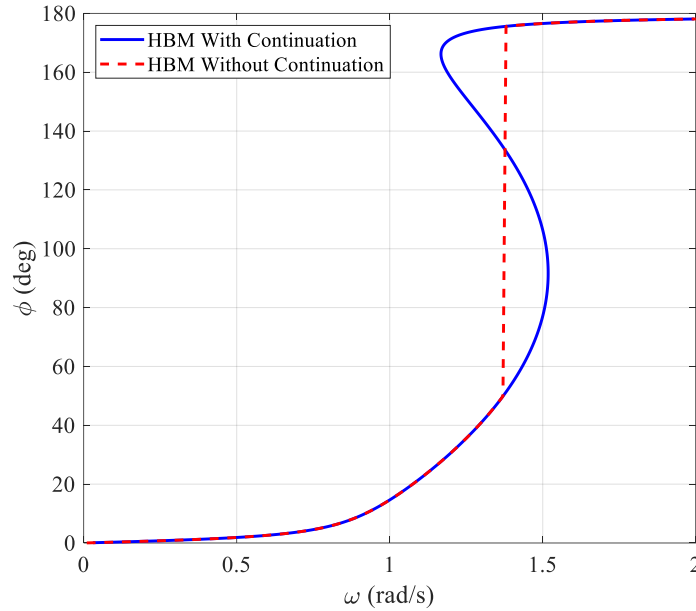
Figure 2-8: Comparison of phase delay, using HBM by considering N$_H$=1; with and without continuation

MatCont is an open-source package developed in MATLAB to carry out numerical continuation and bifurcation analysis of dynamical systems [55]. The first version of the MatCont package was developed in the 1970s. The current version is available in two different types. The first type is the graphical user interface version, which usually is called MatCont and has a user-friendly environment to enter the required equations and set the desired settings. The second type is a command-line version, CL_MatCont, in which the parameters and equations should be entered in the MATLAB M-file environment.

In the current study, the CL_MatCont has been used to compute the amplitude response curve of the nonlinear BDA system. The forced response calculated using CL_MatCont for the tuned system is verified, comparing with two different results: (i) the results provided in Joannin's study [35] and (ii) the results found using the direct integration method. All the results are presented and discussed in the next section.

2.3   Results and Discussion

Figure 2-9 shows the steady-state forced response of the tip mass of the first sector (X_1), assuming an amplitude of 2 N for the external force. To verify the results, the calculated frequency response curves are compared to those reported by Joannin et al.[35]. Figure 2-9 shows a good

31

agreement between the two sets of results. Moreover, in this figure, the time-series of the response at a particular frequency (1199.2 Hz) is shown.

While the time integration method is reliable for calculating the system's forced response, using this method is time-consuming. For example, calculating the response curve presented in Figure 2-10 took around 17 hours on a computer with an Intel(R) Xeon(R) CPU and 32 GB of RAM.
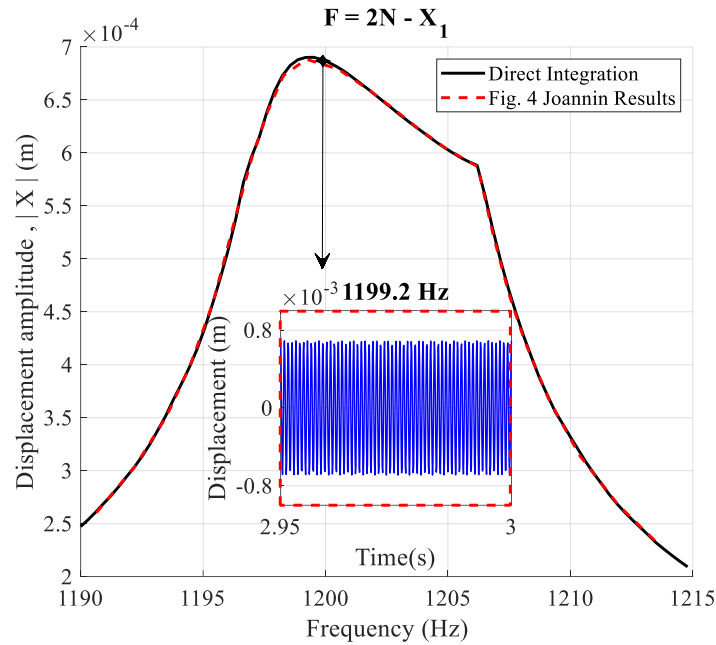
Figure 2-9: Comparison of the steady-state forced response of the tip mass of the first sector, Considering the direct integration method and Joannin's results [35]**, F = 2N**

For the current study, multiple runs with varying external forces from small to high values are required. Using direct numerical integration for this purpose is a heavy burden and can last several weeks. Instead, we use numerical continuation, as implemented in MatCont, for these computations. The advantage of this approach is that the transient response is not computed at each step. Figure 2-10 compares the forced response for the tip mass of the first blade computed using direct numerical integration, numerical continuation, and published results [35]. The simulation time for numerical continuation was 16 minutes, which is about 60 times faster than direct numerical integration (17 hours).
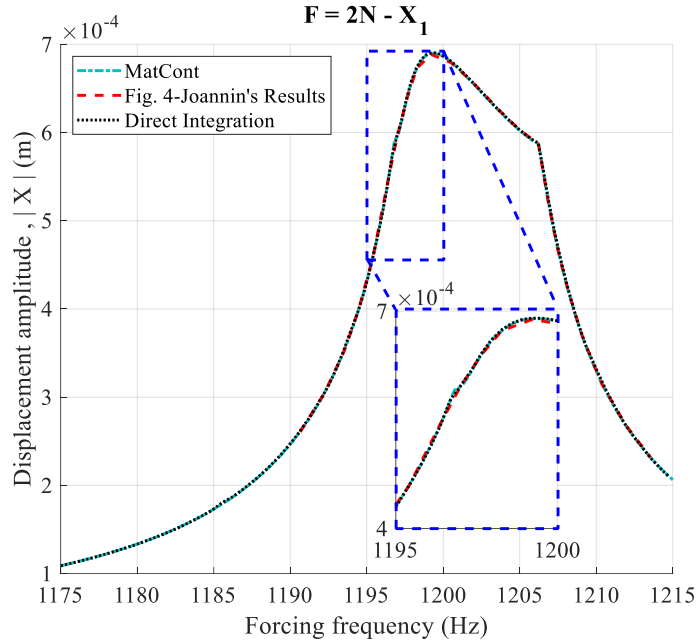
Figure 2-10: Comparison between the results Using the MatCont package, direct integration, and Joannin's results [35]

The steady-state forced response of the tip mass of each sector versus the exciting frequency is plotted in Figure 2-11. As expected, the steady-state displacement amplitude of the six blades is uniform across the BDA.

The steady-state forced response of the tip of the first blade (X_1) with respect to forcing frequency for different values of the external force is plotted in Figure 2-12. The tuned system shows one peak around the first pair of modes of the linear system when the excitation level is low. The exact peak with the same amplitude is observed for the tip mass of other sectors. Moreover, the backbone curve can be plotted by tracing the peak of the forced response curve for different external forces. The natural frequency of the free response occurs in the vicinity of the backbone curve. After increasing the excitation level, the resonance frequency for each curve, and consequently the backbone curve, shifts to lower frequencies.
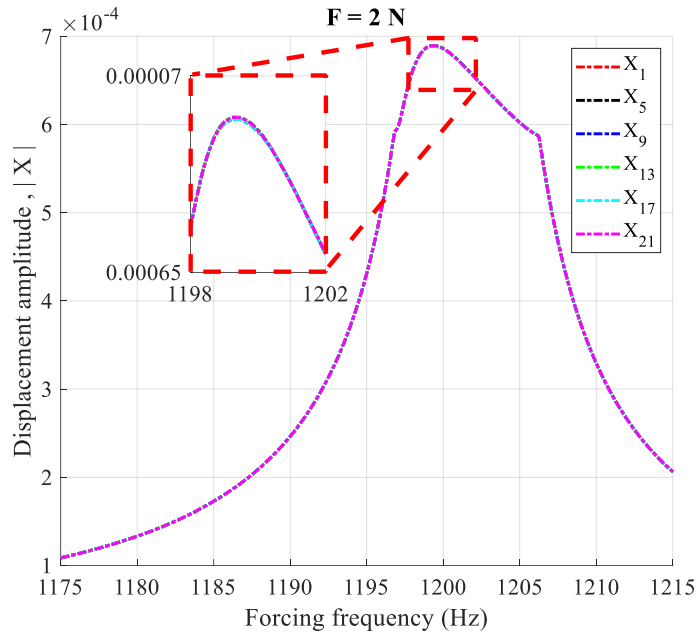
Figure 2-11: Comparison between the displacement amplitudes of the blade tips in the tuned system

In Figure 2-13, the time series for the tip masses of all sectors are plotted before, at, and after the peak of the response curve for F = 2 N. The time series confirms a traveling-wave response in compliance with the external force in Eq. (2-6). After the peak of the response, i.e., after natural frequency, a phase delay of π can be observed between the time series of the response and excitation, similar to the linear behavior of the system (at low amplitudes).
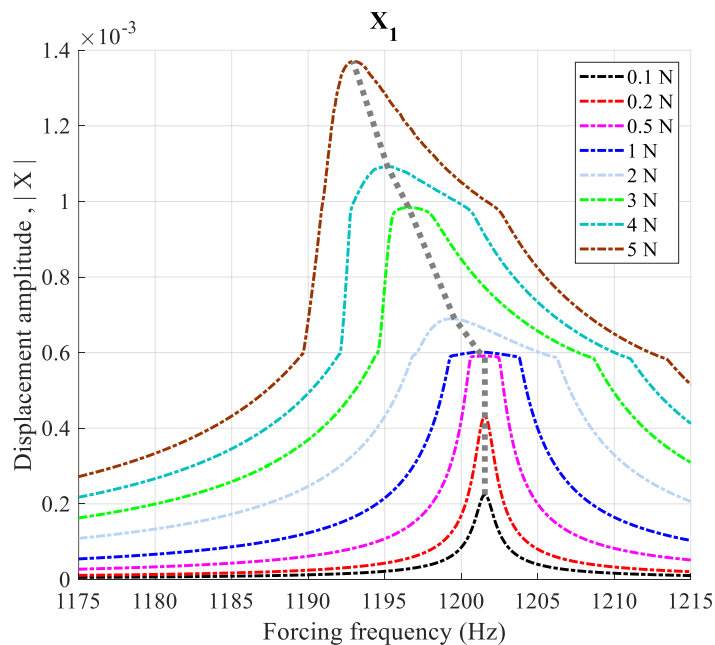
Figure 2-12: Steady-state forced response of the tip of the first blade for different external force levels

34
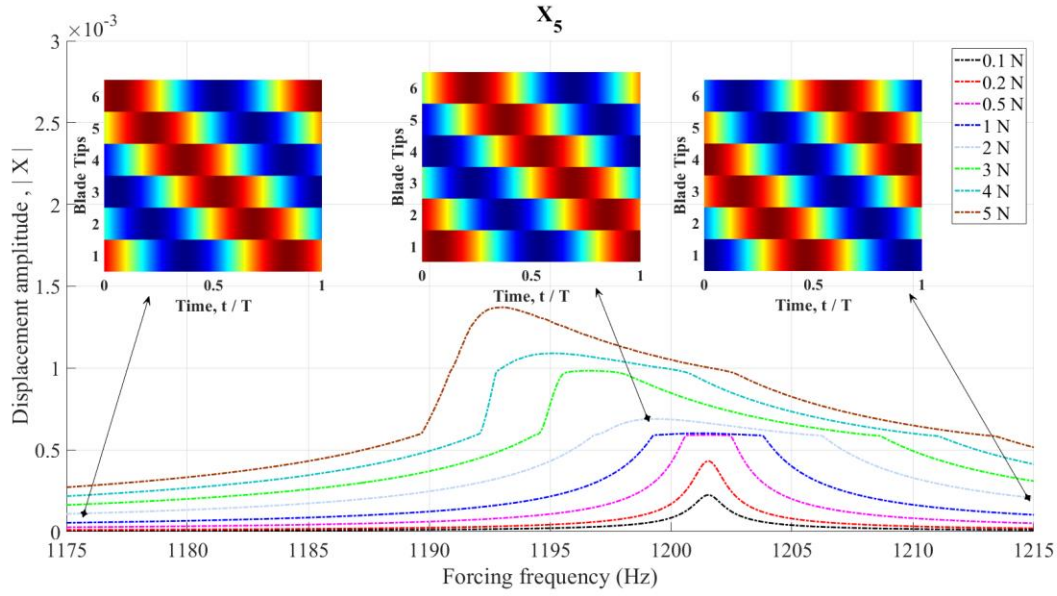
Figure 2-13: Time series of the tip of the second blade for various frequencies at F = 2N

In Figure 2-13, the peak of the response curve gradually shifts to the left (lower frequencies) after increasing the amplitude of the external force. This shift can be observed more clearly when the excitation is increased beyond 5 N, up to 15 N, in Figure 2-14. The backbone curve is plotted in Figure 2-15 for forcing amplitudes in the range between 0.1 N and 15 N. Unlike the linear system in which the natural frequency is independent of the excitation force, the natural frequency in a nonlinear system can depend on the amplitude of motion. Considering lower excitation, the natural frequency for each excitation is constant and equal to the natural frequency presented in Table 2-2 for the linear system with bonded DOF assumption. Observing the natural frequency close to the natural frequency of the linear system with bonded assumption can be interpreted as the stationary sticking state at the contact interface. The bonded frequency is represented with a vertical asymptote in the detailed view of Figure 2-15. At a higher amplitude of excitation, the natural frequency shifts to the left (lower frequency) toward the natural frequency of the linear system with the frictionless assumption. The same behavior was observed in systems including friction nonlinearities [56], [57]. The reason is that the nonlinearity introduced by friction has a softening effect on the dynamic behavior of the system. It reduces the natural frequency of the system. The start of the slipping between DOFs in the contact interface is the reason for the activation of the nonlinearity. The shift continues up to a particular value of excitation and does not change when it reaches the vertical asymptote shown in Figure 2-15.

35
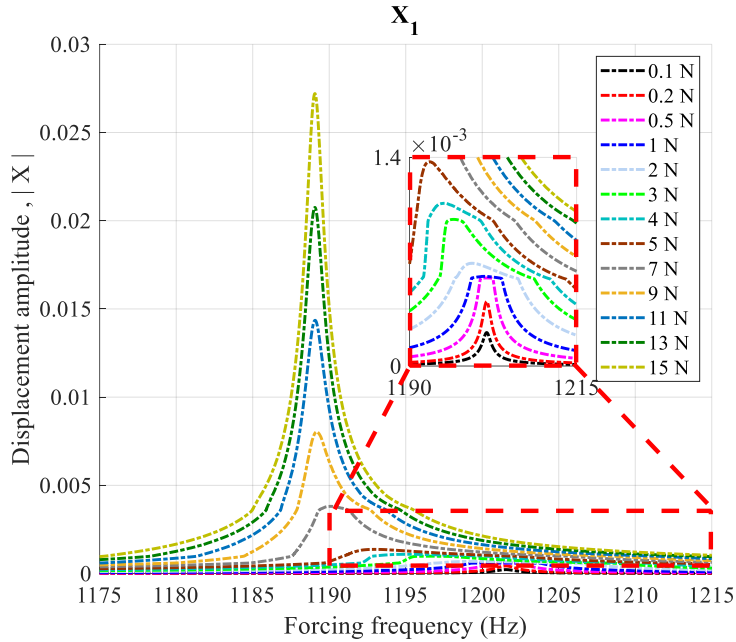
Figure 2-14: Forced response of the tip of the first blade for different levels of excitation
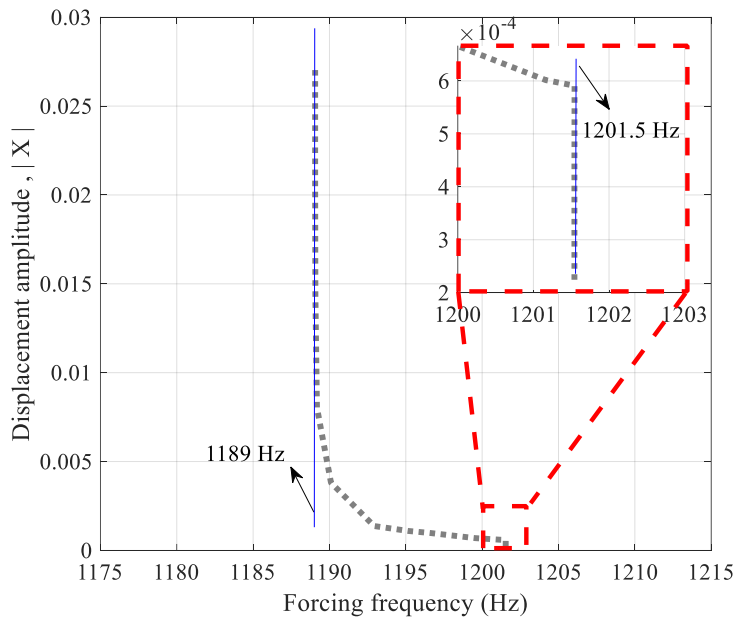

Figure 2-15: Backbone curve based on the forced response of vibration between 0.1-15 N

In Figure 2-16, the resonance shift can be observed after plotting the compliance of the response for a range of excitation forces between 0.1 N and 15 N. Additionally, the effect of increasing damping due to friction can be seen in Figure 2-16. After increasing the excitation level from 0.1 N to 5 N, along with resonance shifting to lower frequencies, the compliance peak decreases due to an increase in damping. The maximum damping can be obtained by exciting the

36

system with a force of 5 N, where the peak of compliance is minimum. The maximum damping is a result of being in the partial-slip condition [35], [57]. After 5 N, the compliance peak increases again for the rest of the excitation range.
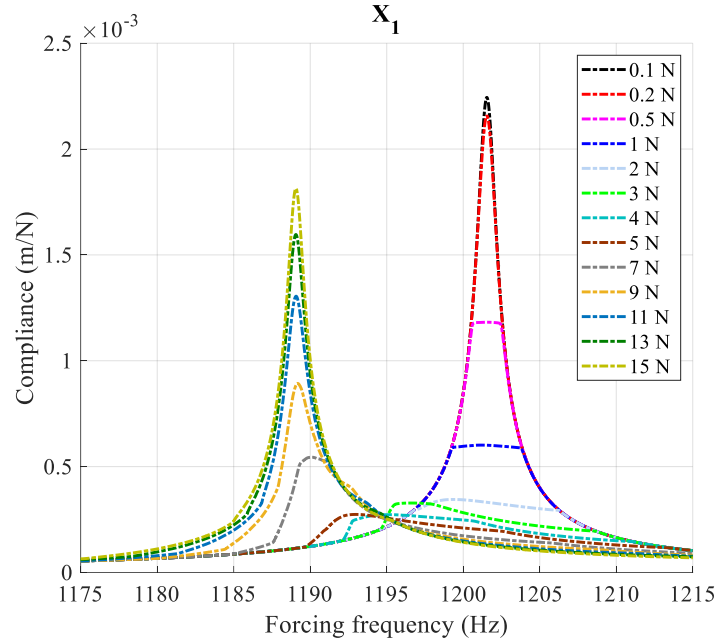
Figure 2-16: Compliance for various excitation forces at the tip of the first blade

2.4   Conclusion

This chapter introduced the lumped parameter model of a tuned BDA. The forced response of blade tips to engine-order excitation is calculated using direct numerical integration and numerical continuation. The calculated results were verified, and the effect of changing the excitation level was investigated. The results showed the effect of nonlinear forces due to the friction between the blade root and the disk on each sector of BDA. The forced response showed only one peak within the desired range of exciting frequencies. The response amplitude for all blade tips under the same excitation amplitude is the same. Due to the nonlinear effect between the blade root and the disk, the resonance frequency shifts from the bonded frequency to the frictionless frequency as a function of the forcing amplitude. Also, the time series of the response, considering one excitation level, kept its traveling wave feature within the investigated range of exciting frequencies. Moreover, the compliance showed that the maximum damping happened when the excitation level was about 5 N.

3. Chapter 3: Effect of Mistuning

In this chapter, the effect of adding a structural mistuning to the BDA model is investigated. Mistuning is introduced to the model by adding a random perturbation with continuous uniform distribution to the tip and middle stiffnesses of the blades. Two distinct realizations are provided to study the effect of mistuning on the frequency response of BDA. A wide range of excitation levels is selected to investigate the effect of the nonlinear force between the blade root and the disk. Moreover, the effect of changing the magnitude of the mistuning realizations is analyzed by considering a constant excitation level and various quantities as the mistuning levels.

3.1 Parameters

Mistuning is modeled as a random parameter in the valued of the middle and tip stiffness of each blade. Thus, the stiffness of the middle (k_2) and tip (k_1) for each blade is represented using the following equation:

$$k_m = k_t(1 + \xi \, d_m)$$
(3-1)

where the parameter ξ represents the random deviation from exact cyclic symmetry, which is multiplied by the level of mistuning, d_m. The value of ξ is taken from a uniform distribution in the range of $[-10^{-3}, 10^{-3}]$ [35]. The value of the mistuning level is assumed to be 100, resulting in about a 2% difference between the first pair of natural frequencies of the tuned linear system in Table 2-2 [35]. Other values for the model remain the same as in Chapter 2.

In this chapter, two different realizations of mistuning are considered to present the effect of mistuning on the forced response of the system. Table 3-1 shows the values of the calculated stiffnesses for the middle and tip stiffnesses with a random pattern for each blade.

	Tip stiffness (k_1) [N/m]		Middle Stiffness (k_2) [N/m]	
	First Realization	**Second Realization**	**First Realization**	**Second Realization**
Blade 1	652287.70	634767.58	1048737.69	1028463.05
Blade 2	594946.36	568244.01	921184.08	944253.15
Blade 3	568857.41	593762.37	1036312.09	1067411.29
Blade 4	631667.75	608322.98	992652.12	1094215.05
Blade 5	631119.29	547368.17	942432.64	1069274.58
Blade 6	628877.77	599554.67	919703.75	1001199.89

The natural frequencies of the linear mistuned system, with two assumptions named frictionless and bonded, are listed in Table 3-2 and Table 3-3 for the first and second realizations, respectively.

Table 3-2: Natural frequencies of the first linear mistuned system for the first family of bending mode, considering frictionless and bonded assumptions

Frequency (Hz)	f_1	f_2	f_3	f_4	f_5	f_6
Frictionless	652.5	1175.6	1191.5	1229.9	1248.1	1252.4
Bonded	653.5	1187.6	1203.9	1242.2	1260.8	1265.0

Table 3-3: Natural frequencies of the second linear mistuned system for the first family of bending mode, considering frictionless and bonded assumptions

Frequency (Hz)	f_1	f_2	f_3	f_4	f_5	f_6
Frictionless	652.8	1179.1	1202.3	1235.7	1253.8	1268.2
Bonded	653.8	1191.0	1215.1	1247.9	1266.7	1281.4

Considering two mistuned realizations in the model and comparing the natural frequencies of the mistuned system with the tuned system, there are no pairs of equal natural frequencies in the former. Mistuning results in the splitting of the pairs of repeated natural frequencies into two separate natural frequencies. Consequently, two different mode shapes will be observed that will be discussed in more detail in section 3.2.

The next step is the calculation of the forced response of the system using (i) direct numerical integration method and (ii) numerical continuation. In the next section, the forced response of the system under different excitation levels and mistuning levels will be presented for the two realizations of mistuning.

3.2 Results and Discussion

3.2.1 Effect of Changing the Excitation Level

The forced response of the first blade tip (X_1) under an external force of 2 N for the first and second realizations is shown in Figure 3-1 and Figure 3-2. The results acquired by numerical continuation (MatCont) and direct numerical integration are mostly similar. However, there is a significant difference between the computational time for these two methods. Calculating the nonlinear forced response of the BDA model using the time integration method for one external force (2 N) took about 120 hours (5 days) for the first realization and 100 hours for the second one. Performing the same calculation using MatCont took 3 hours for the first realization and 2.5 hours for the second one. All the calculations are performed on a computer with an Intel(R) Xeon(R) CPU (@3.4GHz) and 32 GB of RAM.
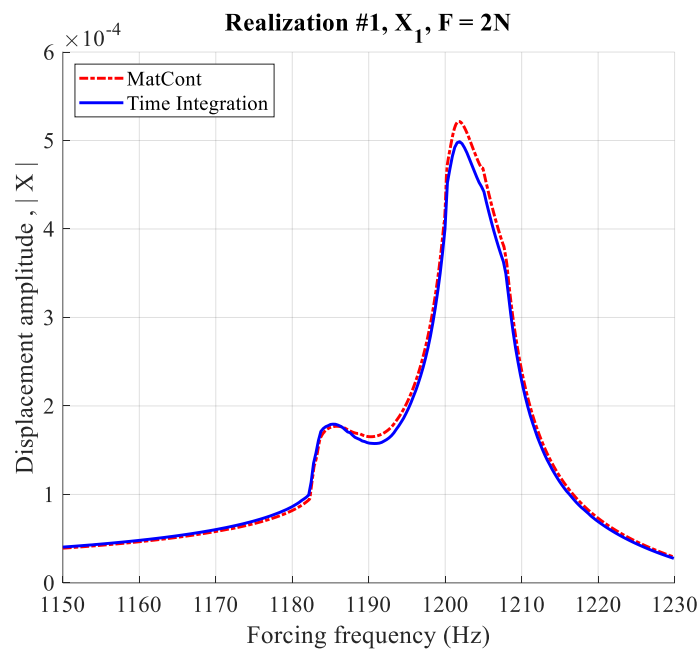
Figure 3-1: Comparison of the steady-state forced response of the tip mass of the first sector, using direct integration method and MatCont package, first mistuning realization, F = 2 N
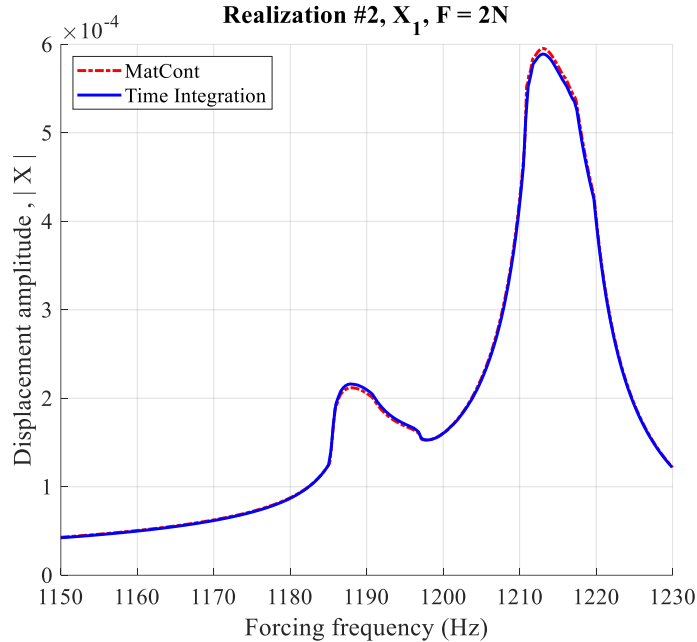
Figure 3-2: Comparison of the steady-state forced response of the tip mass of the first sector, using direct integration method and MatCont package, second mistuning realization, F = 2 N

The steady-state forced response of the tip of the first blade (X_1) versus forcing frequency for a range of external forces between 0.1 N to 5 N and the first mistuned realization are plotted in Figure 3-3. In contrast with the response curve for the tuned system (Figure 2-12), two peaks can be observed for the mistuned system in the same range of exciting frequencies. The splitting of pairs of natural frequencies into two different frequencies, as described in Table 3-2, is the reason for having two peaks.

Figure 3-3, Figure 3-4, and Figure A 1 of Appendix A together show the forced response curves for the blade tip of all six blades for the first mistuning realization. Unlike the tuned system, the frequency response curves of the six blades are no longer identical in the mistuned system. For example, the response curves of blades number one (X_1) and four (X_{13}), two (X_5) and five (X_{17}), and three (X_9) and six (X_{21}) are similar to each other, but their amplitudes are different. Moreover, for all blade tips, except blade number two and five, the amplitude of the second peak is higher than the first peak. The same behavior can be observed for the first and second blade tips by considering the second mistuning realization in Figure 3-5 and Figure 3-6. The rest of the forced response for the second mistuning realization is presented in Figure A 2 in Appendix A. The gray dashed line represents the backbone curve of the response. The backbone curves in all figures are plotted by tracing the maximum values of the response curves for each peak.

41

As in the previous chapter, the effect of nonlinearity on the response curve can be observed, i.e., the natural frequency of the nonlinear system is dependent on the amplitude of excitation. In Figure 3-3 - Figure 3-6, for the low level of excitations, the resonance frequencies remain unchanged and equal to the values of bonded frequencies for the linear system in Table 3-2 and Table 3-3. At this excitation level, there is a stationary sticking state at the contact interface of the blade and disk [58]. After increasing the level of exciting forces and the occurrence of slipping between the blade and disk contact interfaces, the peaks of response curves shift to lower frequencies. Consequently, the backbone curve for each peak is shifting to lower frequencies. The natural frequency for the free response occurs in the vicinity of the backbone curve, so the natural frequency changes by changing the external forces. After increasing the amplitude of excitation to 13 N, the effect of shifting the peaks is clear for the first and second realizations in Figure 3-7 and Figure 3-8, respectively. For the sake of brevity, the results for other blades are presented in Figure A 3 and Figure A 4 of Appendix A.
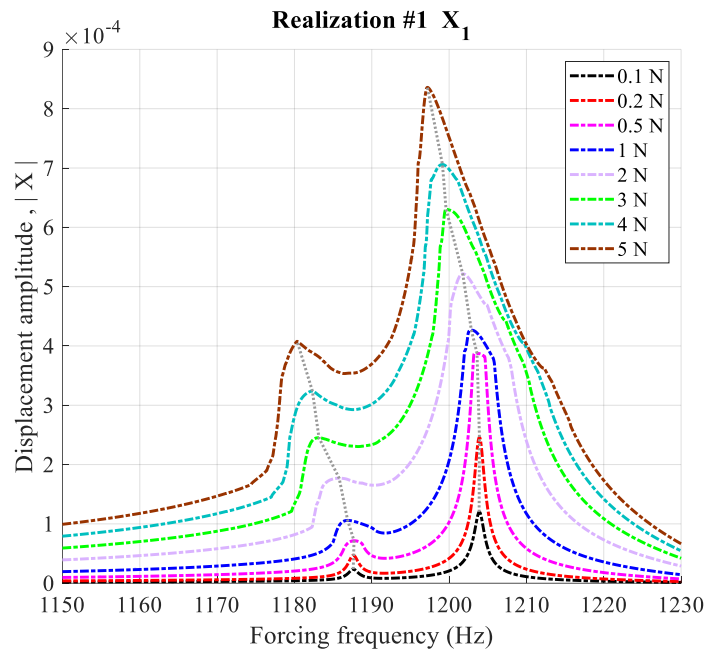
Figure 3-3: Steady-state forced response of the tip of the first blade for a range of external forces between 0.1N and 5N, first mistuning realization
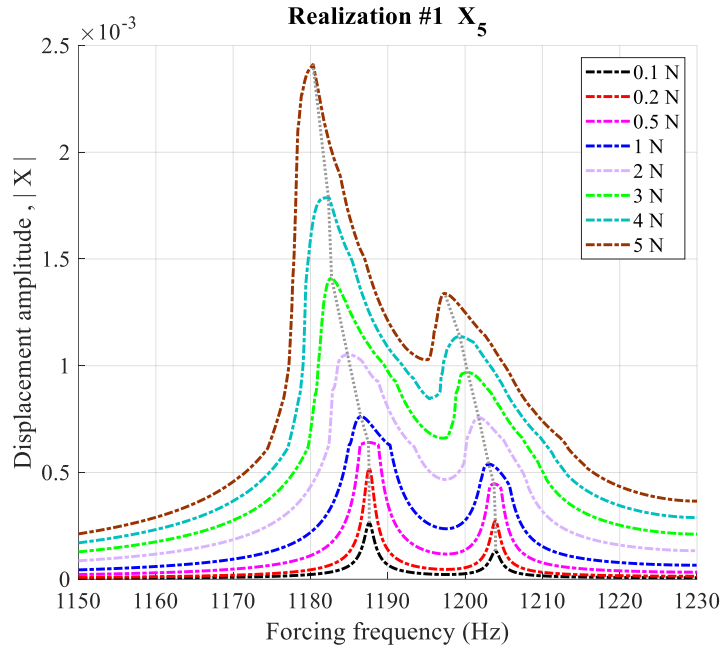
Figure 3-4: Steady-state forced response of the tip of the second blade for a range of external forces between 0.1N and 5N, first mistuning realization
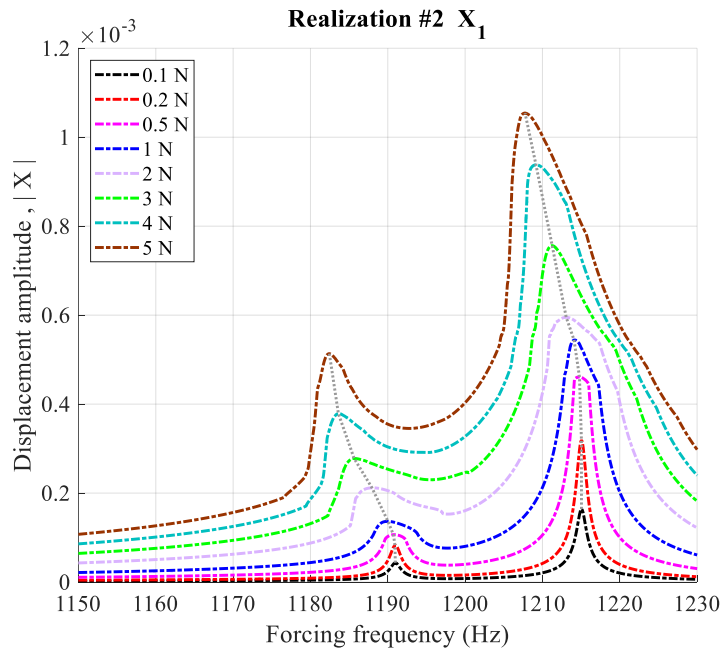
Figure 3-5: Steady-state forced response of the tip of the first blade for a range of external forces between 0.1N and 5N, second mistuning realization
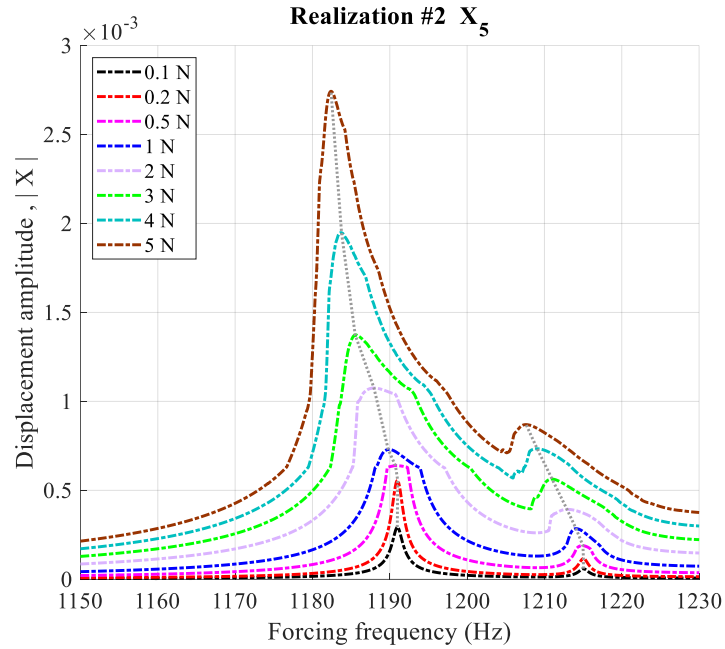
Figure 3-6: Steady-state forced response of the tip of the second blade for a range of external forces between 0.1N and 5N, second mistuning realization
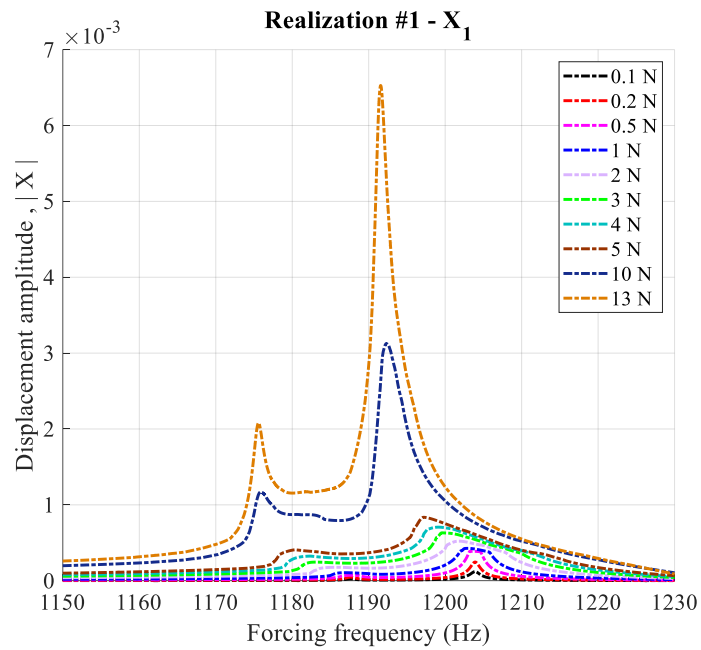
Figure 3-7: Steady-state forced response of the tip of the first blade for a various range of excitation between 0.1N and 13N, first mistuning realization
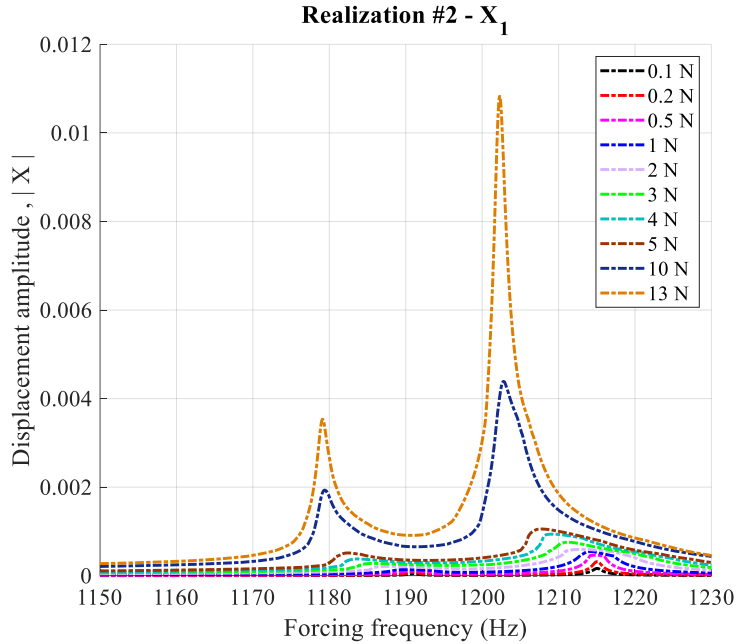
Figure 3-8: Steady-state forced response of the tip of the first blade for a various range of excitation between 0.1N and 13N, second mistuning realization

For two realizations, the backbone curves of the first blade tip are plotted in separate figures, Figure 3-9 and Figure 3-10. These backbone curves are plotted for excitation forces between 0.1 N and 13 N. In Figure 3-9, the right vertical asymptotes at 1187.6 Hz and 1203.9 Hz represent the peak of the response curves for the lower excitation levels. These frequencies are the natural frequencies for the linear model (f_2 and f_3) with bonded assumption presented in Table 3-2. By increasing the excitation level and the activation of the nonlinear force, the backbone curve moves to the lower frequencies (left side of the figure). Due to the softening effect introduced by friction, the backbone curve approaches the natural frequencies of the linear system with the frictionless assumptions, i.e., 1175.6 Hz and 1191.5 Hz, presented in Table 3-2.
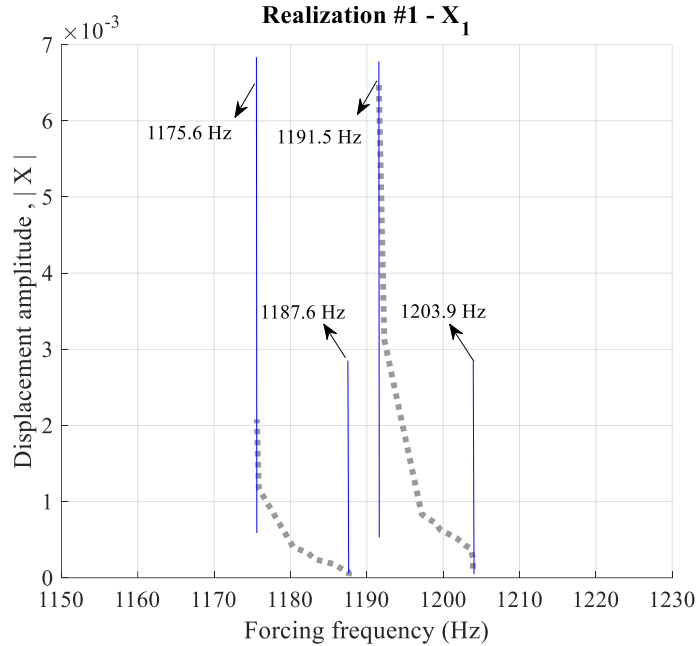
Figure 3-9: Backbone curve based on the forced response of vibration between 0.1-13N, first blade tip, first mistuning realization

The shift in the resonance frequency can be observed for all blades within the same frequency range. Figure 3-10 shows the backbone curve for the first blade tip and the second realization. The backbone curves shift from the bonded frequency to the frictionless frequency presented in Table 3-3. However, due to the change in the stiffness values for the middle and tip springs, frictionless and bonded frequencies vary from the first realization. The figures of backbone curves for other blade tips, including the first and the second mistuning realizations, are demonstrated in Figure A 5 and Figure A 6 of Appendix A, respectively.
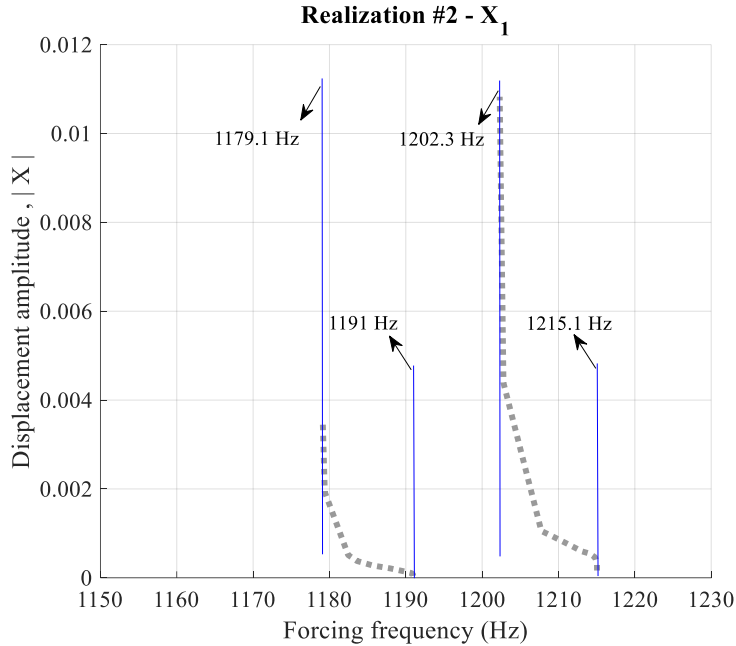
Figure 3-10: Backbone curve based on the forced response of vibration between 0.1-13N, second blade tip, second mistuning realization

In Figure 3-11, it is shown how changing the levels of excitations affects the compliance response of the first blade's tip for the first mistuning realization. Figure 3-12 shows the compliance response of the first blade's tip for the second realization. In both figures, the two peaks of the response are transferred to the lower frequencies after changing the excitation level from 0.1 N to 13 N. Considering the second peak of the compliance for both realizations, the amplitude of compliance decreases when the excitation increases from 0.1 N to 5 N. The reason is the increase of damping, the same for the tuned system, which stops when forces higher than 5 N are applied to the blade tip. By applying forces above 5 N, the second peak of compliance is increased, and the damping is reduced, suggesting that the maximum damping value can be acquired when the excitation level is 5 N.

Considering the first peak of the compliance response for each realization reveals another result. For the first realization, the maximum value of damping can be obtained when the external force is equal to 5 N. However, observing Figure 3-12 for the second realization, the minimum compliance peak is achieved when the external force is 3 N.

The compliance figures for the rest of the blade's tip, including both realizations, are presented in Figure A 7 and Figure A 8 in Appendix A. The results suggest that unlike the tuned system,

where only one excitation level could result in the minimum amplitude of compliance peak (and consequently maximum damping), in the mistuned system, minimizing the peak of compliance can not be achieved by one excitation level. In the mistuned system, the excitation level to minimize the peak of compliance varies based on the targeted peak and the mistuning realization.
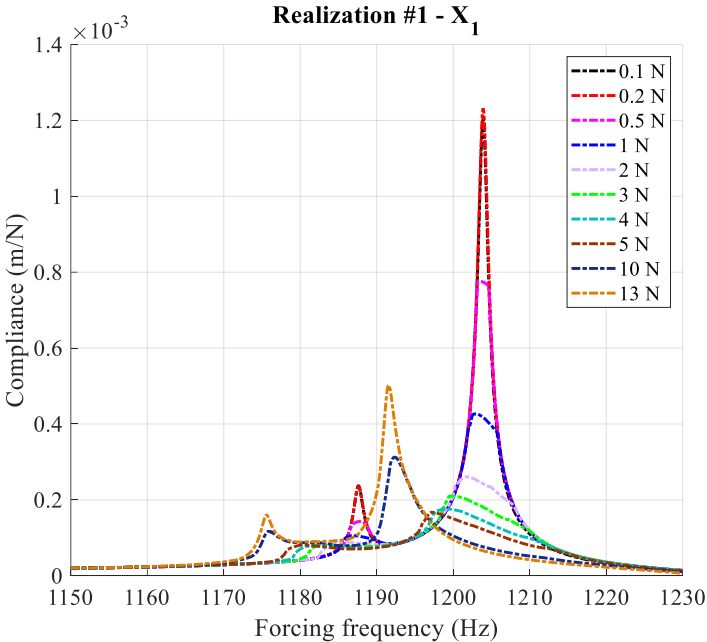
Figure 3-11: Compliance of the first blade tip of the mistuned system for different excitation levels, first mistuning realization
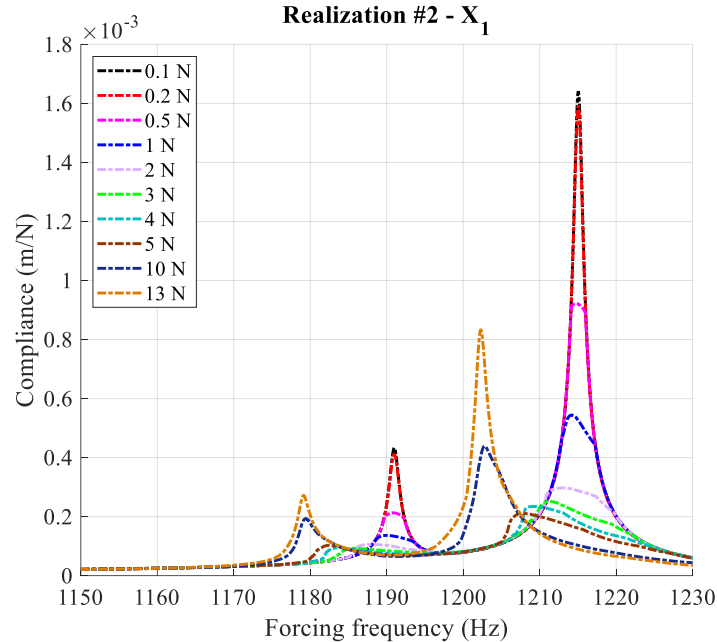
Figure 3-12: Compliance of the first blade tip of the mistuned system for different excitation levels, second mistuning realization

The response of the mistuned system in the time domain shows a combination of traveling and stationary waves. In Figure 3-13, considering the external force equal to 2 N, the time series of the blade tip masses are added to the forced response of the system with the first mistuning realization. These time series show the time response of each blade tip for a period of the response (T) at a specific exciting frequency. Far from the first peak of the response and between two peaks, the time series demonstrate the diagonal pattern that can be expressed as the traveling wave feature. However, close to the resonances (either of the first or second peak of the response curve), the time series patterns are no longer diagonal. Close to the resonances, the traveling wave features in the time series are vanished and are finally replaced with stationary waves when it reaches the peak of the response. This behavior was not observed in the tuned system, resulting from the presence of mistuning in the system. Furthermore, the stationary waves of the time series close the resonances are observed for the second realization, Figure 3-14, and all levels of excitation forces for both realizations.
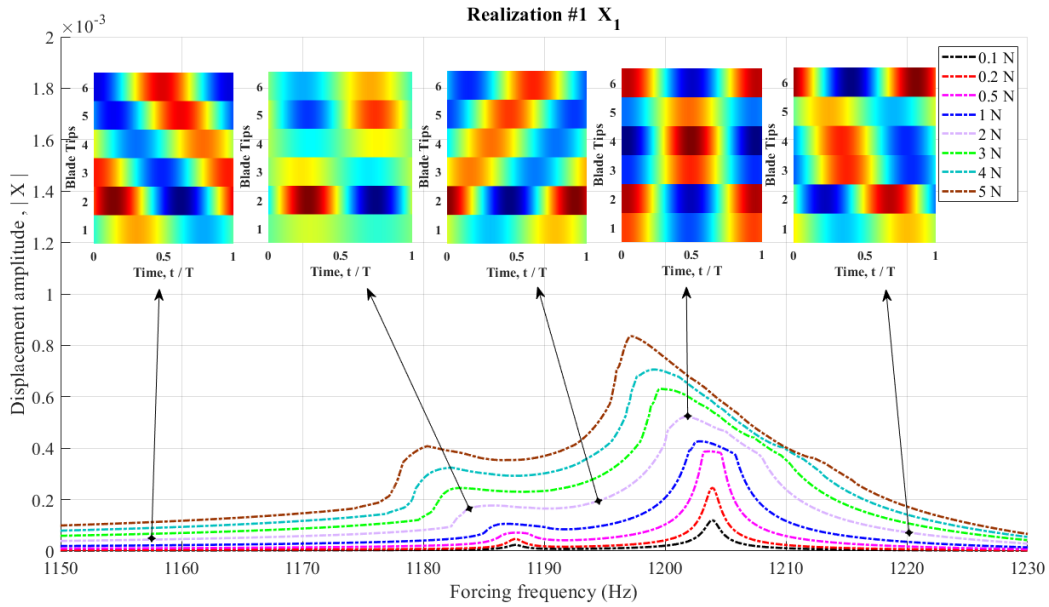
Figure 3-13: Time series of the blade tip of all blades for different exciting frequencies at F= 2 N, first mistuning realization
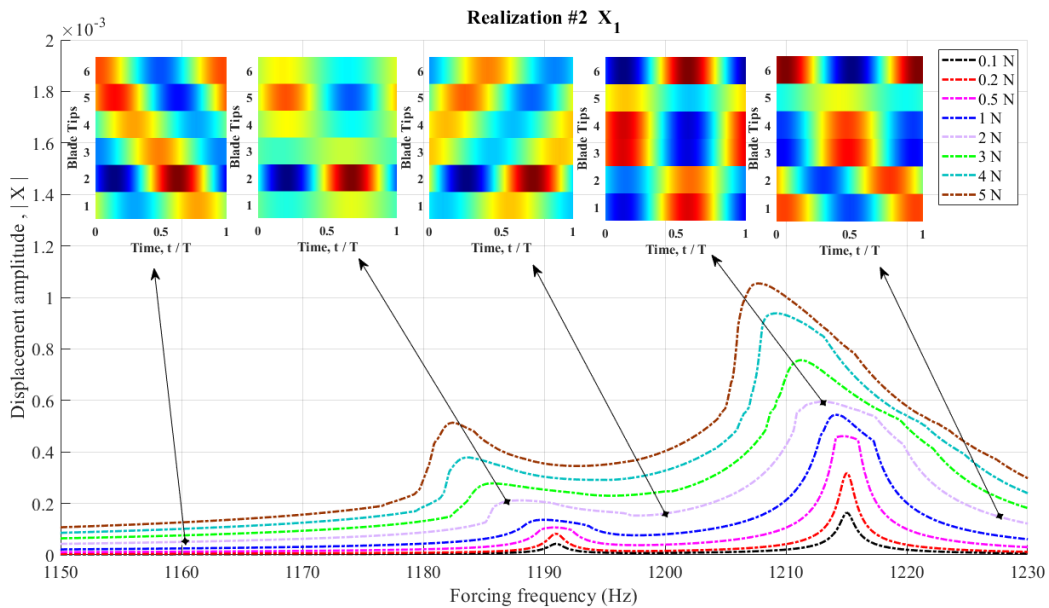
Figure 3-14: Time series of the blade tip of all blades for different exciting frequencies at F= 2 N, second mistuning realization

3.2.2 Effect of Changing the Mistuning Level

The effect of changing the mistuning level, d_m, in Eq. (3-1), on BDA's forced response is studied in this section. For this purpose, the mistuning level is changed between 0 to 160, with a step of 20. The mistuning level of zero represents the tuned system. The excitation level remains

constant through changing the mistuning level, equal to 2 N. Then, for two mistuning realizations, the forced response of the BDA is calculated and discussed. Note that, due to the changing of mistuning level, the tip and middle stiffnesses vary after changing the mistuning level. Thus, it is necessary to check and modify the initial frequency before starting each run.

Considering two different mistuning realizations and various levels of mistuning, the natural frequencies of the linear system with frictionless and bonded boundaries are listed in Table 3-4 and

Table 3-5. In the presence of any level of mistuning, the frequency split phenomenon can be seen, in which the pairs of equal frequencies of the tuned system are split into two different frequencies.

Table 3-4: Natural frequencies of the first linear mistuned system for the first family of bending mode, considering frictionless and bonded assumptions, first mistuning realization

Mistuning level (d_m)	Frequency (Hz)	f_1	f_2	f_3	f_4	f_5	f_6
20	Frictionless	652.63	1186.9	1190.6	1241.2	1246.1	1248.3
	Bonded	653.60	1199.34	1203.15	1253.80	1258.83	1260.91
40	Frictionless	652.61	1184.5	1191.6	1238.5	1247.3	1249.1
	Bonded	653.58	1196.85	1204.18	1251.00	1260.01	1261.85
60	Frictionless	652.6	1181.8	1192.1	1235.7	1247.7	1250.5
	Bonded	653.57	1194.07	1204.65	1248.13	1260.33	1263.27
80	Frictionless	652.57	1178.8	1192.1	1232.8	1247.9	1251.7
	Bonded	653.54	1190.99	1204.56	1245.21	1260.55	1264.36
120	Frictionless	652.52	1172	1190.4	1226.9	1248.4	1252.7
	Bonded	653.49	1183.91	1202.77	1239.20	1261.13	1265.13
140	Frictionless	652.49	1168.1	1188.8	1223.9	1248.6	1252.7
	Bonded	653.46	1179.91	1201.10	1236.12	1261.45	1264.91
160	Frictionless	652.45	1164	1186.8	1220.8	1248.9	1252.4
	Bonded	653.43	1175.60	1198.94	1232.98	1261.61	1264.52

Table 3-5: Natural frequencies of the first linear mistuned system for the first family of bending mode, considering frictionless and bonded assumptions, second mistuning realization

Mistuning level (d_m)	Frequency (Hz)	f_1	f_2	f_3	f_4	f_5	f_6
20	Frictionless	652.68	1188.16	1192.20	1242.61	1247.19	1250.88
	Bonded	653.64	1200.55	1204.74	1255.20	1259.91	1263.56
40	Frictionless	652.71	1186.68	1195.06	1241.09	1249.07	1255.07
	Bonded	653.68	1198.99	1207.68	1253.58	1261.79	1267.91
60	Frictionless	652.74	1184.66	1197.69	1239.43	1250.62	1259.54
	Bonded	653.70	1196.86	1210.37	1251.81	1263.37	1272.50
80	Frictionless	652.76	1182.12	1200.09	1237.65	1252.17	1263.94
	Bonded	653.73	1194.18	1212.83	1249.90	1264.98	1277.02
120	Frictionless	652.80	1175.61	1204.26	1233.67	1255.50	1272.35
	Bonded	653.77	1187.33	1217.07	1245.65	1268.44	1285.58
140	Frictionless	652.82	1171.73	1206.05	1231.42	1257.31	1276.32
	Bonded	653.79	1183.25	1218.88	1243.25	1270.33	1289.62
160	Frictionless	652.84	1167.47	1207.67	1228.94	1259.21	1280.14
	Bonded	653.80	1178.79	1220.51	1240.60	1272.33	1293.49

Figure 3-15 and Figure 3-16 show the effect of changing the mistuning level on the forced response of the first and second blade tips, respectively for the first mistuning realization. For the low mistuning level, such as 20, the response curve shows only one peak, and it is hard to distinguish two different peaks for this level of mistuning. However, after increasing the mistuning level, the frequency split phenomenon happens, and two separate resonance frequencies become clear. Moreover, increasing the mistuning level increases the distance between two peaks in the response curve, and the peaks become more separate compared to the lower mistuning levels.

The effect of changing the mistuning level on the steady-state forced response varies for each blade. Considering each peak in the response curve, the increase in mistuning level results in increasing or decreasing the response's amplitude. In Figure 3-15, considering the first peak, after the occurrence of the frequency split phenomenon, the amplitude of the response is decreased by increasing the mistuning level. The second peak experiences an increase in its amplitude if the mistuning levels are between 0 and 20. However, after $d_m = 20$, the amplitude of the second peak reduces. For the whole range of d_m, while the first peak of the response transfers to the lower frequencies by increasing the mistuning level, the second peak shows a different pattern. For the mistuning levels between 0 and 60, the second peak moves to the higher frequencies, and for the

53

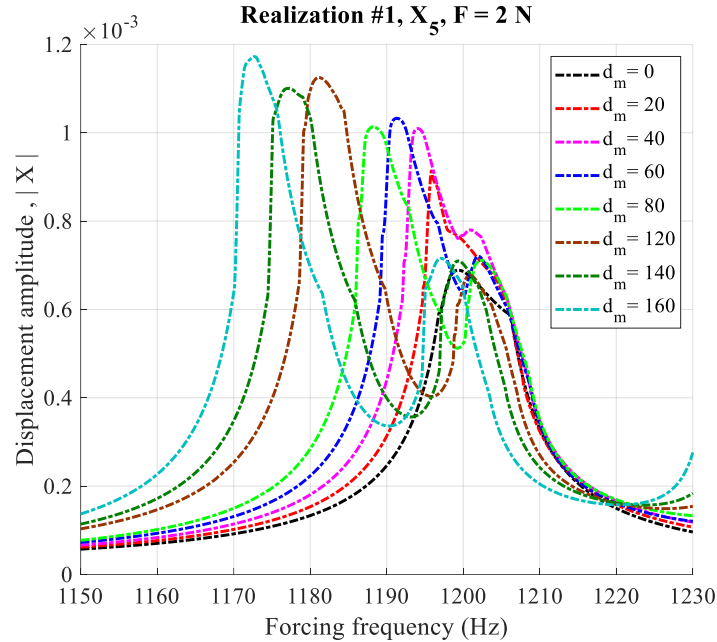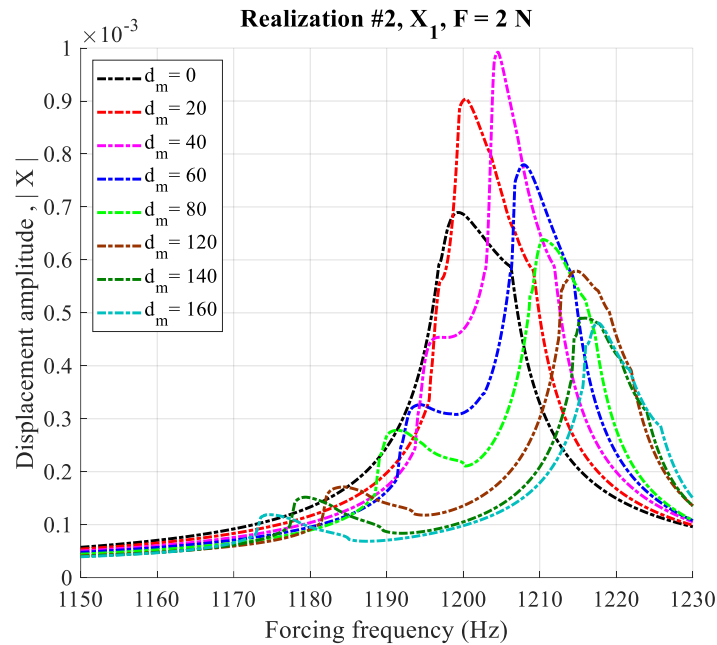mistuning levels between 80 and 160, it moves to lower frequencies, the same behavior as the first peak.
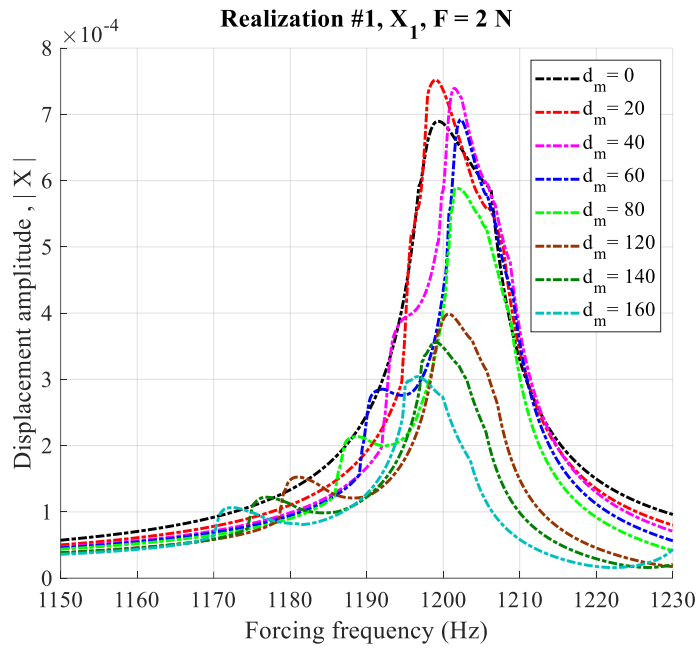
Figure 3-15: Steady-state forced response of the tip of the first blade for a range of mistuning levels between 0 and 160, first mistuning realization

In Figure 3-16, two peaks are not clear, considering mistuning levels of 0 and 20. After increasing the mistuning level, the amplitude of the first peak is higher than the second peak. The amplitude of the first peak fluctuates based on the mistuning level, and it does not increase constantly. For example, a mistuning level of 40 and 60 increases the amplitude, and $d_m = 80$ decreases. Again, the mistuning level of 120 increases the forced response amplitude while $d_m = 140$ decreases. The amplitude of the second peak fluctuates as well. While the mistuning levels of 40, 140, and 160 increase amplitude, the mistuning levels of 60 or 140 decrease the displacement amplitude.

The shifting of the resonance frequencies is another interesting point of Figure 3-16—the first peak transfers to the lower frequencies after increasing the mistuning level. However, the second peaks move to the higher frequencies when $0< d_m <80$, and it moves to lower frequencies when d_m is equal to 120 or 160.
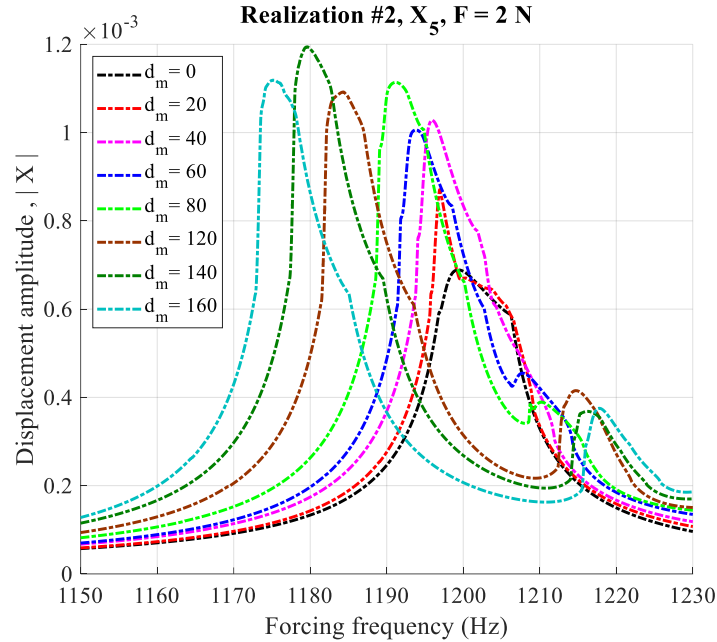
Figure 3-16: Steady-state forced response of the tip of the second blade for a range of mistuning levels between 0 and 160, first mistuning realization

The steady-state forced response for the other blades is presented in Figure A 9 of Appendix A. Considering all the results for the first realization, the first peak of the response curve is lower for most of the blades, except blades #2 and #5, in which the second peak has a lower amplitude than the second peak. Another observed fact is that by increasing the mistuning level, the peak of the response can stay constant. For instance, the first peak of the response curve for the sixth blade, part (d) in Figure A 9, shows a decrease from 20 to 80, while it increases with $d_m = 120$ and remains constant for the rest of the mistuning levels.

Figure 3-17 and Figure 3-18 show the forced response of BDA's blade tips with different mistuning levels for the second mistuning realization. The amplitude of the first resonance peak of the first blade tip, Figure 3-17, shows the same behavior as the first mistuning realization. By increasing the mistuning level, the amplitude first peak decreases. Moreover, the amplitude of the second peak increases for lower mistuning levels, such as 20 and 40. For the rest of the range of mistuning levels, especially for the higher values of mistuning levels, the amplitude of the second resonance peak decreases, and $d_m = 160$ results in a lower amplitude.

As the mistuning level increases, the first resonance peak shifts to a lower frequency, the same behavior for the first mistuning realization and the same blade tip. However, unlike the previous

55

mistuning realization, the second resonance peak shifts constantly to the higher frequencies when d_m increases.

Figure 3-17: Steady-state forced response of the tip of the first blade for a range of mistuning levels between 0 and 160, second mistuning realization

The amplitude of the first peak of the second blade's response curve, Figure 3-18, is the opposite of the one with the first realization. For example, considering the first realization and having a mistuning level of 120 increases the first peak's amplitude, while for the second mistuning realization and the same condition, the amplitude decreases. The second peaks fluctuate by increasing the mistuning level; for instance, $d_m = 60$, 80, 140, and 160 decreases the amplitude of the second peak, and with $d_m = 120$, the amplitude grows.

The shifting of the resonance peak is the same as the first blade, in which the first resonance peak moves to the lower frequencies, and the second peak constantly moves toward higher frequencies when the mistuning level is increased. Furthermore, the forced response of all other blade tips is shown in Figure A 10 of Appendix A. Like the first mistuning realization, the first peak of the response curves of the second and fifth blade tips have higher amplitude than the second peak. For the other blade tips, the second peaks show a higher amplitude than the first.

56

Figure 3-18: Steady-state forced response of the tip of the second blade for a range of mistuning levels between 0 and 160, second mistuning realization

In order to investigate the effect of changing the mistuning level on the forced response of BDA, the amplification factor is defined. Using the amplification factor, comparing the forced response of the mistuned and tuned system is possible. The amplification factor is defined as the ratio of the maximum amplitude of the mistuned system to the maximum amplitude of the tuned system, assuming the desired frequency range [35], [59]. The previous mistuning realizations are used to calculate the variation of the amplification factor based on the change in the mistuning level. The excitation level is constant and equal to 2 N.

Figure 3-19 shows the amplification factor for all the blade tips of the system versus different values of mistuning levels, considering the first mistuning realization. The second and first blades reach the highest and lowest amplification factors, respectively, after increasing the mistuning level. The third and sixth blades show identical behavior; by increasing the mistuning level to 40, the amplification factor reduces and increases for mistuning levels above 40. As opposed to the third and sixth blades, after $d_m = 40$, the amplification factor decreases in the fifth blade. The third blade tip shows the amplification factor under the unit for all the mistuning levels, which means that mistuning leads to the mitigation of the maximum amplitude of the response compared to the tuned system. Another interesting point is that having a mistuning level equal to 160 reduces the maximum amplitude of the response for four blade tips out of six.

57
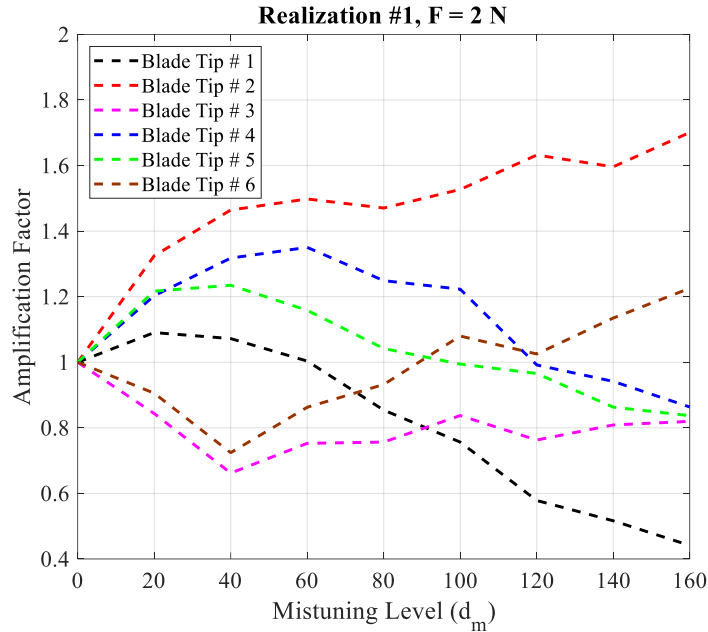
Figure 3-19: Amplification factor for all the blade tips versus different mistuning levels, first mistuning realization

Figure 3-20 demonstrates the amplification factor for all the blade tips, considering the second mistuning realization. The mistuning level of 40 increases the amplification factor for most of the blade tips. The same observation as the previous mistuning realization can be seen for the second realization. The second blade tip and the first one represent the highest and the lowest amplification factor after increasing the mistuning level to 160.

The amplification factor for pairs of the third and sixth blades and the first and the fourth blades has the same trend. In contrast with other blades, having a mistuning level above 80 causes an increase in the amplification factor for the third and the sixth blades. While $d_m = 160$ increases the maximum amplitude of the mistuned system up to 60%, it reduces the maximum amplitude on three blade tips by about 20%. Moreover, comparing the mistuned and tuned results, the third blade shows a lower maximum amplitude when there is any level of mistuning in the system (the amplification factor <1).
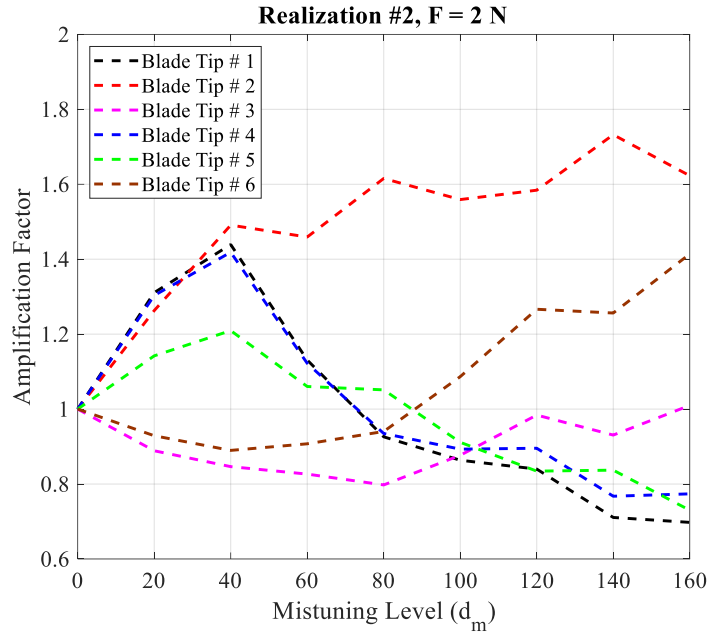
Figure 3-20: Amplification factor for all the blade tips versus different mistuning levels, second mistuning realization

3.3 Conclusion

In this chapter, the effect of mistuning on the BDA model introduced in chapter 2 was studied. Mistuning was introduced as deviations in the values of the stiffness of the middle and tip sections of the blades from the value of the tuned BDA. Two specific realizations of mistuning were used to study the forced response of the blade tips for excitation levels between 0.1 N and 13 N. A splitting effect was observed in the response curves, in which the unique resonance peak in the tuned system was split into two separate frequencies due to mistuning. The transition of the resonance peak and backbone curve from bonded frequency to frictionless frequency was observed, similar to the tuned system.

Unlike the tuned system, the compliance curves showed that one excitation level could not result in a lower compliance peak value. Depending on the first or the second peak of the compliance, and the mistuning realization, different excitation levels could lead to minimizing the compliance and the maximum damping value. For example, considering the first compliance peak and the first realization, the excitation level of about 5 N caused the minimum peak. However, for the second realization and the same blade tip, the first compliance's peak was minimized under the excitation level of 3 N. Unlike the tuned system, in the time series response of the mistuned system, the traveling wave feature was not observed within the whole range of frequencies. The

59

results showed that, far from or between the resonance frequencies of the forced response, the time series had a traveling wave pattern. However, the time series showed the stationary wave feature close to the resonance frequencies.

A range of variable mistuning levels, between 0 to 160, was defined to study the effect of changing the mistuning level under a constant excitation level of 2 N. The changes in the response curves followed a similar pattern for the two realizations. There is no constant trade of increasing or decreasing the amplitude of vibration. The amplitude of the peaks oscillated by increasing the mistuning level.

It was observed that by increasing the mistuning level for two different mistuning realizations, the first peak shifted to the lower frequencies. However, the second peak was shifted to higher frequencies, and in some cases, it moved to the lower frequencies. Increasing the mistuning level in all cases resulted in more separation between two peaks, and the frequency split phenomenon became clear.

The amplification factor was defined to compare the effect of various mistuning levels versus the tuned BDA. The amplification factor for each mistuning realization fluctuated by changing the mistuning level. The results suggested that the amplification factor increased rapidly at low mistuning levels for both mistuning realizations. The increase in the mistuning level could result in an amplification of up to 75% in some blade tips. Furthermore, some blade tips demonstrated amplification factors lower than the unit.

4. Chapter 4: Statistical Effect of Mistuning

The statistical effect of mistuning is studied in this chapter. This is achieved by performing a preliminary statistical analysis of the vibration response of 150 realizations of mistuned BDAs. The effects of changing (a) the amplitude of engine-order excitation and (b) the mistuning level are studied. Various statistical parameters, including the mean of the response amplitude, standard deviation, compliance, coefficient of variation, and amplification factor, are calculated. The results for all blade tips are discussed in the following sections.

4.1 Effect of Changing the Excitation Level

In this section, the effect of changing the excitation level on the forced response for different realizations is investigated. In this study, 150 various realizations are chosen based on the mistuning parameter, ξ, in equation (3-1). The value of ξ is in the range of $[-10^{-3}, 10^{-3}]$, and the value of the mistuning level, d_m, is constant and equal to 100. This corresponds to an average 10% deviation in natural frequencies of the blades across different realizations of the mistuned BDAs.

Statistical analysis is necessary to study the mistuning effect of all mistuning realizations on the forced response of the BDA blade tips. The mean of the amplitude response, the standard deviation, compliance, and the coefficient of variation are calculated for this purpose. The amplitudes of external forces applied on the tips of the blades change between 0.1 N and 10 N to include both linear and nonlinear response regimes. All the results are provided in the same range of frequencies, between 1150 – 1230 Hz.

4.1.1 Mean

The forced response of each realization is calculated to find the mean, μ, of all the realizations, for each external force. Using the "mean" command in MATLAB, the average response of the blade tips displacement amplitude is then calculated considering all 150 realizations. Figure 4-1 and Figure 4-2, respectively, show the mean of the response for the first and second blade tips, X_1 and X_5, for different values of excitation amplitude. The amplitude of the mean of displacement increases with the external force. In the previous chapter, the frequency split phenomenon was observed in the presence of the single mistuned realization. The same phenomenon is observed

61

considering 150 realizations. As a result of the frequency split, two peaks appear in the mean response; one is more evident than the other.
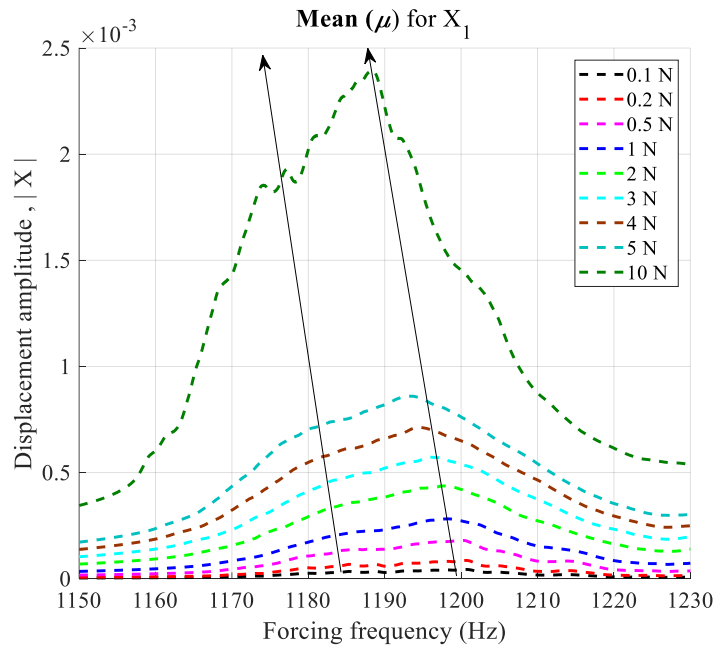
Figure 4-1: Mean of displacement amplitude for the first blade tip, X_1, considering 150 mistuning realizations
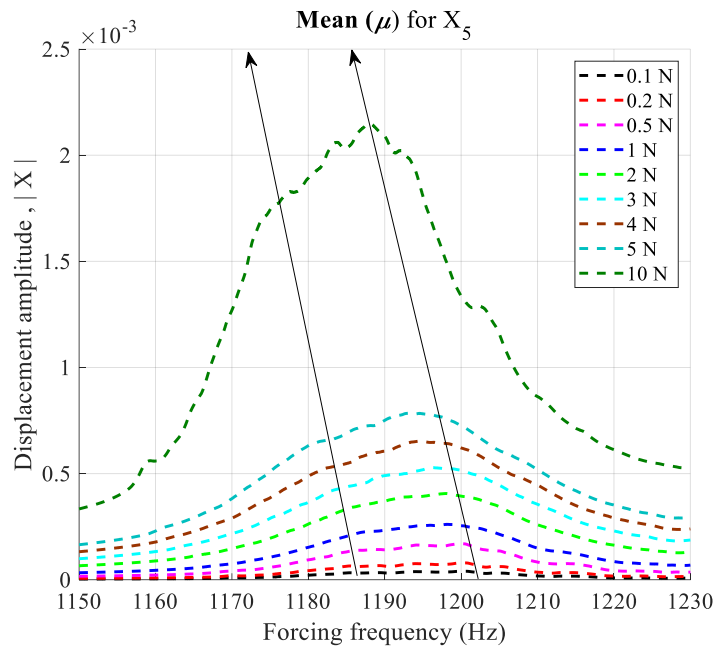
Figure 4-2: Mean of displacement amplitude for the second blade tip, X_5, considering 150 mistuning realizations

Furthermore, the same behavior of shifting resonance frequencies in the single mistuning realization happens when 150 realizations are considered. Looking at Figure 4-1 and Figure 4-2,

the peaks of the response for the lower external forces occur around 1185Hz and 1200 Hz. After increasing the excitation level, and the activation of the nonlinearity due to friction between the blade root and disk, the peaks shift to lower frequencies. This shifting is shown with two black arrows in Figure 4-1 and Figure 4-2. For example, for the excitation level equal to 10 N, the two resonance frequencies are located around 1178 Hz and 1189 Hz. For the sake of brevity, the mean results for other blades are demonstrated in Figure B 1 of Appendix B. All other blade tips show the same behaviors as the tips of the first and second blades. Figure 4-3 shows a detailed view of the mean response of the first blade tip, X_1, in which the external excitation level is low and is equal to 0.1 N or 0.2 N. Comparing Figure 4-3 with Figure 4-1 demonstrates that for lower excitation level, i.e., 0.1 N and 0.2 N, and the highest excitation level, 10 N, the peaks in the mean response are spread across a wide range of frequencies and are not as unique as the peaks in the mean response between 0.5 N-5 N.
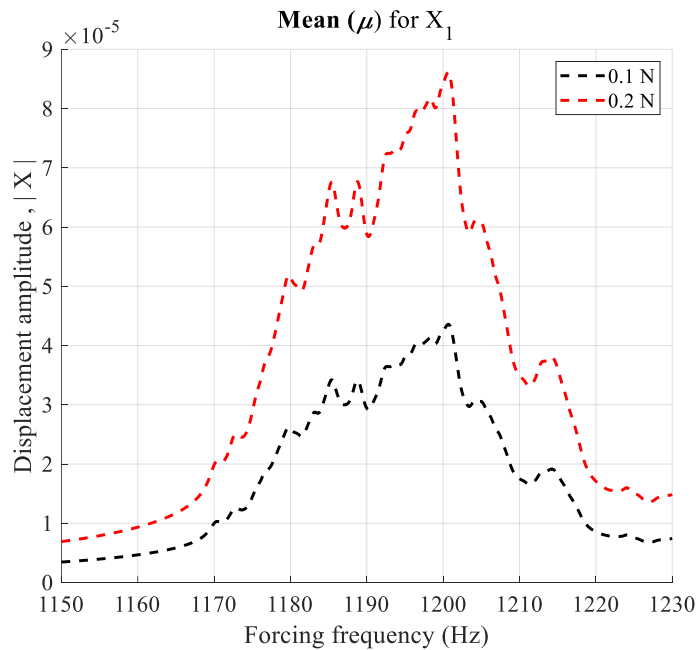
Figure 4-3: Detailed view of the mean displacement response for the first blade, X_1, with an external force equal to 0.1 N and 0.2 N, considering 150 mistuning realizations

4.1.2   Standard Deviation

Standard deviation, σ, is the other statistical term studied in the current work. Standard deviation presents the variation of a set of values. The lower and higher values of standard deviation mean that the values are close to the mean or scattered over a wide range. The value of

the standard deviation for a continuous uniform distribution can be calculated using the following equation:

$$\sigma = (b - a)\frac{1}{\sqrt{12}} \tag{4-1}$$

where a and b are the beginning and the end of the desired interval for the continuous uniform distribution. For a uniform distribution, about 58% of the population lies in the interval $[\mu\text{-}\sigma, \mu+\sigma]$.

To better compare the results, the displacement response within one standard deviation from the mean, $\mu\pm\sigma$, is calculated in this section. Only four excitation levels, i.e., 0.1, 1, 4, and 10 N, are chosen to give a clear vision during the comparison. Figure 4-4 and Figure 4-5 show the space between $\mu\pm\sigma$ as the colored clouds for different excitation levels and the first and second blade tips, respectively. The amplitude covered by the range between $\mu\pm\sigma$ increases when the excitation level increases. For the lower excitation level, such as 0.1 N, there is no intersection between its cloud and the cloud of other excitation levels. After increasing the external force to higher values, some intersections between the range of $\mu\pm\sigma$ of different clouds can be observed.
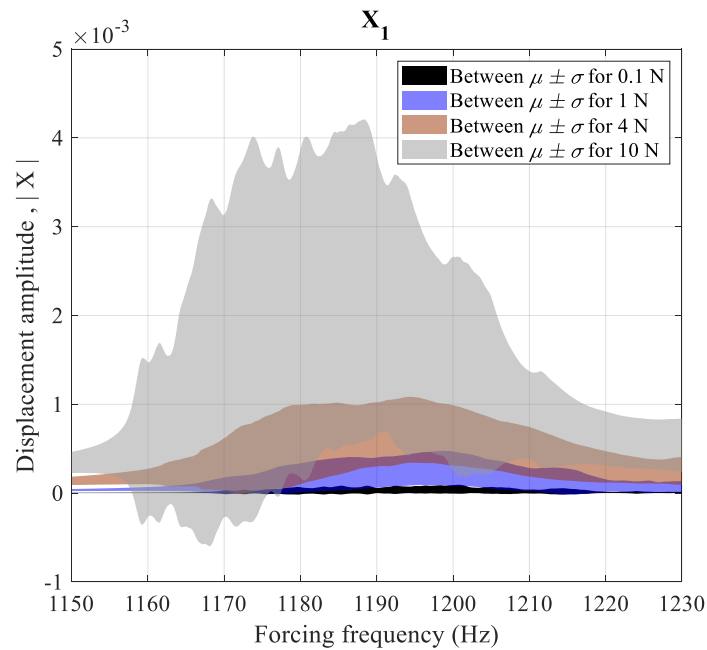
Figure 4-4: Space between $\mu\pm\sigma$ for the first blade tip, X_1, and different excitation levels considering 150 realizations
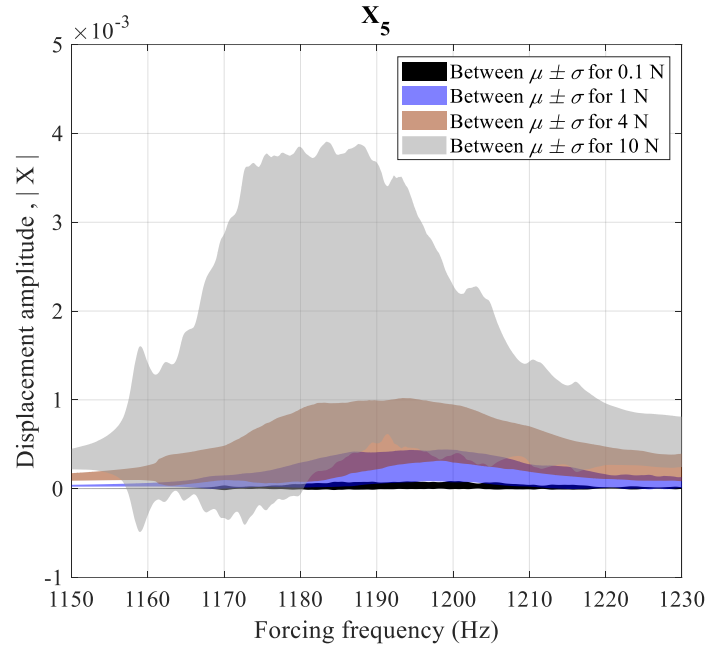
Figure 4-5: Space between *μ±σ* for the second blade tip, *X*₅, and different excitation levels considering 150 realizations

The cloud for the excitation level of 10 N almost covers the cloud of the excitation equal to 4 N in most of the frequency range. Moreover, this coverage can be observed for the other blade tips, presented in Figure B 2 in Appendix B. This coverage can help predict the range of the forced response of the blade tip when BDA is under external excitation within a specific excitation level. For example, the coverage between the clouds of 4 N and 10 N means that for the external forces between 4 N to 10 N, the steady-state forced response of one realization can occur within the range of gray cloud (10 N).

It is hard to recognize a peak for *μ±σ* response, especially when the excitation force is 10 N. However, the frequency shifting phenomenon due to the activation of nonlinearity can be observed with increasing the excitation level.

4.1.3   Compliance

The mean compliance is the third parameter that has been studied in this research considering all 150 mistuning realizations. It can be calculated by dividing each forced response of each mistuning realization by its excitation force or simply by dividing the average forced response of each blade tip by its excitation force, F, as follows:

$$Mean\ Compliance = \frac{\mu}{F} \tag{4-2}$$

Considering 150 mistuning realizations and the excitation level between 0.1 N and 10 N, the mean compliance for the first and second blade tips are presented in Figure 4-6 and Figure 4-7, respectively. Only one peak can be recognized, especially for the excitation level between 1 N and 5 N. The same behavior observed in the previous chapter for only one realization can also be seen for 150 realizations. By increasing the excitation level from 0.1 N to 5 N, the amplitude of the mean compliance decreases, and the peak of the response curves shift to a lower frequency. After increasing the excitation level to 10 N, the amplitude of the mean compliance increases, and the peak of the amplitude continues to shift to the lower frequency, the same as observed in the tuned system and the mistuned system with only one mistuning realization.
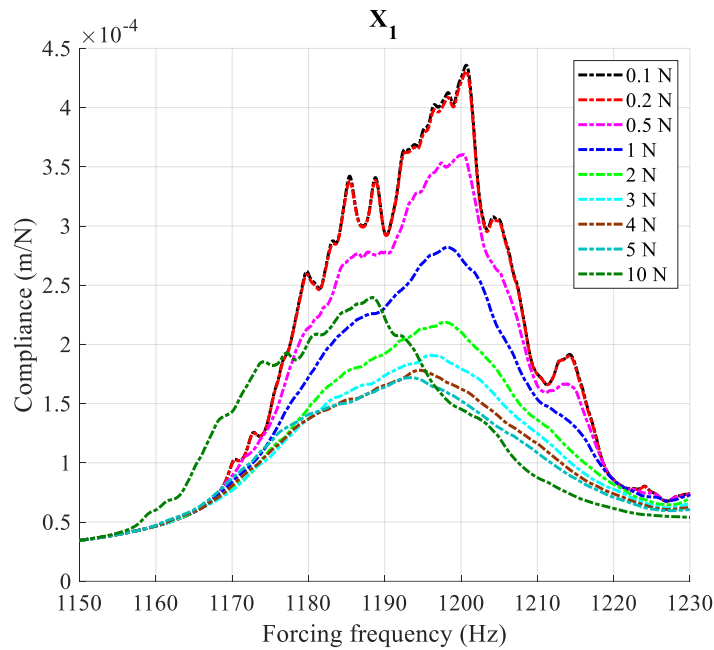
Figure 4-6: Mean compliance of the first blade tip, X_1, for different excitation levels, considering 150 mistuning realizations

Considering the mean compliance for a single excitation level, an external force of 5 N can result in the minimum amplitude. However, the excitation level of 5 N does not cause the minimum amplitude of mean compliance for all ranges of frequencies or all blade tips. For example, in Figure 4-7, at some frequencies, the excitation level of 5 N can result in the minimum amplitude of average compliance, and for some frequencies range, the excitation level of 4 N provides the minimum amplitude. Because the results presented in this chapter combined 150 different

mistuning realizations, there is a possibility that a mistuning realization shows a minimum peak in compliance response with F = 4 N and another mistuning realization shows the minimum peak while F = 5 N. Thus, depending on the mistuning realization, the maximum damping can be acquired by exciting the mistuning system with either 4 N or 5 N of external forces. Because mean compliance shows only one prominent peak for all blade tips, the discussed results can be extended to either the first or second peak of the mistuned compliance response for a single realization. The mean compliance for other blade tips is shown in Figure B 3 of Appendix B.
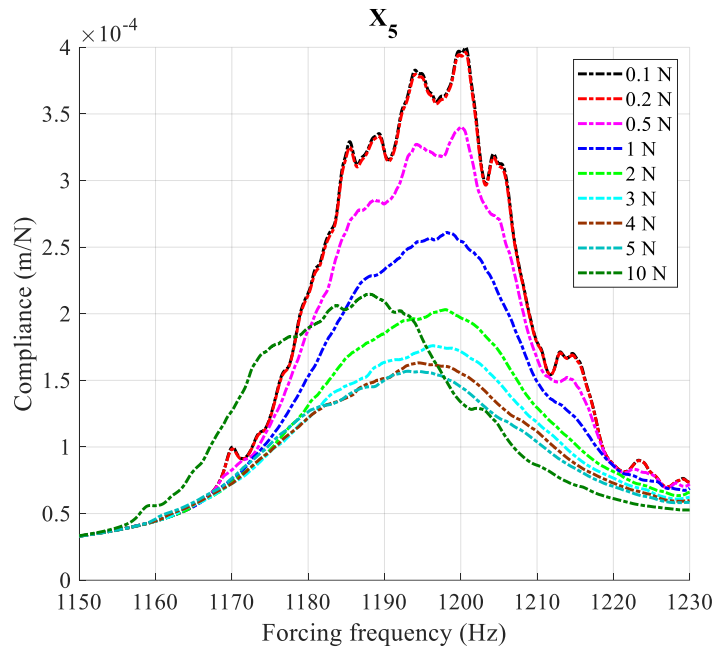
Figure 4-7: Mean compliance of the second blade tip, X_5, for different excitation levels, considering 150 mistuning realizations

4.1.4 Coefficient of Variation

A standardized dimensionless definition that can be used is the coefficient of variation or the relative standard deviation to express the probability distribution of data. The coefficient of variation is defined as follows:

$$CoV = \frac{\sigma}{\mu} \tag{4-3}$$

While the coefficient of variation and standard deviation are different in the definition, both present a measurement of the dispersion of data from the mean. However, because the coefficient of variation is dimensionless, it is useful when different datasets with different units are available

for comparison. For this study, using the coefficient of variation eliminates the increase in standard deviation as a function of the excitation amplitude. Considering 150 realizations, Figure 4-8 and Figure 4-9 show the coefficient of variation for various excitation levels on the first and the second blade tips, respectively. For the excitation levels between 0.1 N and 2 N and all frequency ranges, the coefficient of variation decreases by increasing the excitation level. After changing the excitation level between 3 N to 5 N, the coefficient of variation can be reduced in some frequency ranges while it increases in other frequencies. For example, in Figure 4-8, although around 1210 Hz, the coefficient of variation under 5 N of excitation is lower than the one for the force equal to 2 N, for another frequency, such as 1170 Hz, it is higher for 5 N than 2 N. Thus, increasing of the excitation level does not result in reducing the coefficient of variation in all frequency ranges.

Many oscillations can be observed in the curves for the excitations of 0.1 N, 0.2 N, and 10 N. However, the response curves under the excitations in the range of 0.5 N to 5 N seem more stable within the desired frequency range with fewer oscillations.
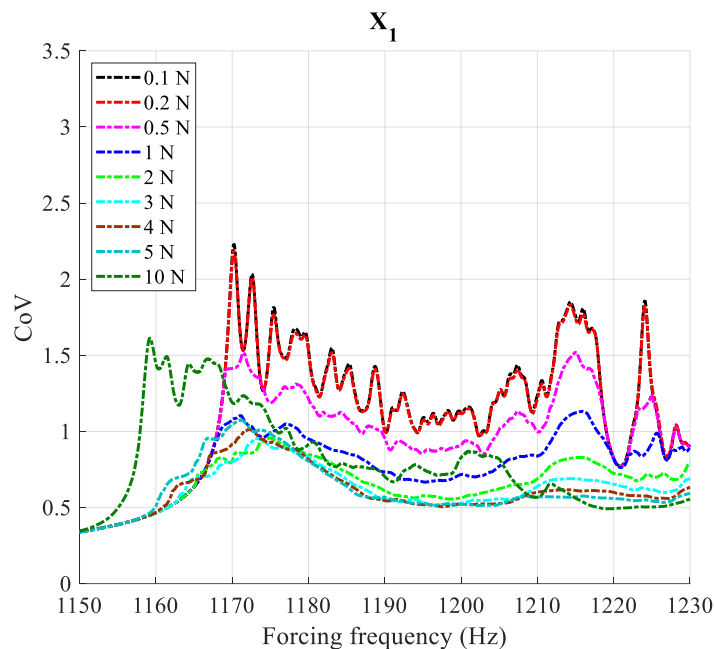
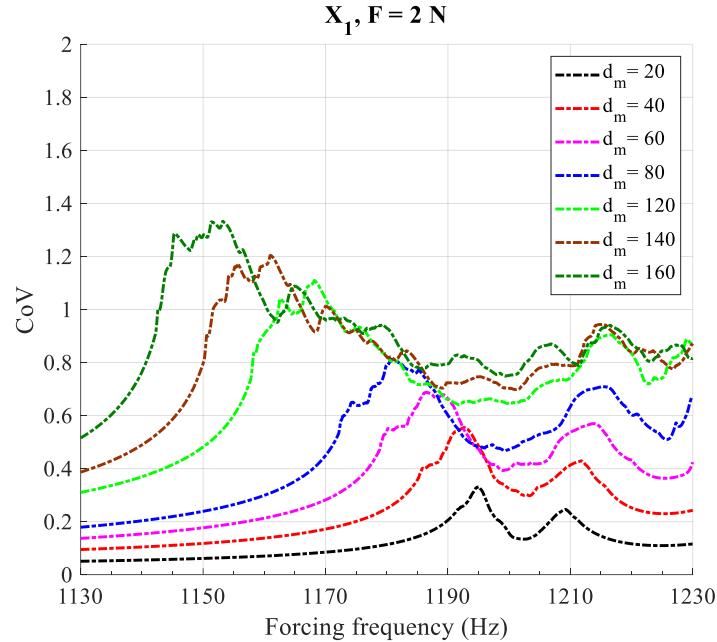Figure 4-8: The coefficient of variation of the first blade tip, X_1, for different excitation levels, considering 150 mistuning realizations

The results for other blade tips, including blade numbers 3, 4, 5, and 6, are presented in Figure B 4 of Appendix B. By comparing the results for all blade tips; generally, the minimum coefficient

of variation happens in the middle range of the demonstrated frequency, i.e., between 1175 Hz and 1210 Hz.

The bigger the coefficient of variation is, the farther dataset is located from the average number. For the curves of 0.1 N and 0.2 N, the coefficient of variation oscillates within the desired frequency range (1150-1230 Hz). This oscillation can be interpreted as the peaks of the displacement response for various mistuning realizations spread on a wide range of frequencies. In Fig 4-9, the peaks in the curves of the coefficient of variation for forces of 0.1, 0.2, and 0.5 N, around 1170 Hz and 1220 Hz explain that the variation in data sets from average values is higher for these frequencies. The high coefficient variation is because outlier data is produced by the peak of the response of some realizations in these frequencies. In contrast, for the excitation levels between 0.5 N and 5 N, the amplitude of the coefficient of variation is low, which means most of the responses from different realizations are close to the average of the response.
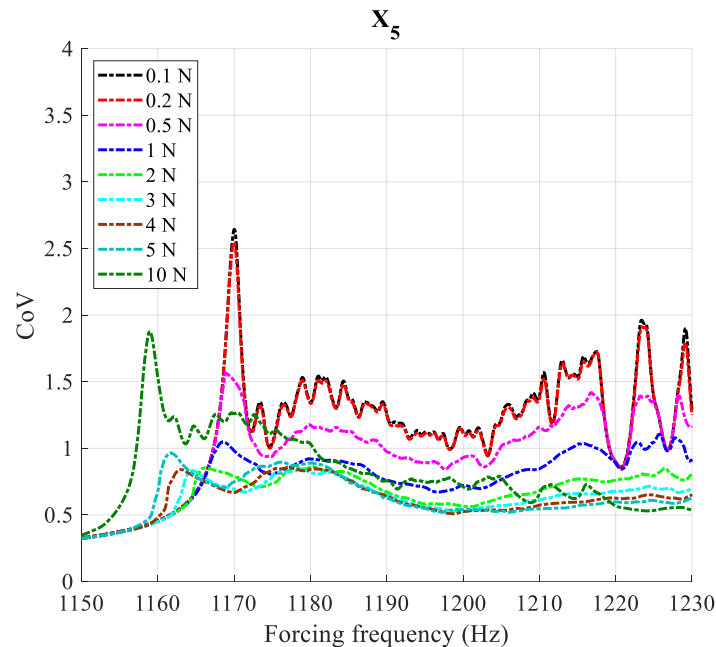
Figure 4-9: The coefficient of variation of the second blade tip, X_5, for different excitation levels, considering 150 mistuning realizations

4.2 Effect of Changing the Mistuning Level

In this section, the effect of changing the mistuning level, d_m, considering 150 mistuning realizations, is investigated. The same investigation, including two mistuning realizations, was

presented in Section 3.2.2. In this part, a constant excitation level equal to 2 N is applied to each blade tip, and a range of mistuning levels, between 0 and 160, are studied. This roughly corresponds to an average variation (with respect to the tuned system) in the natural frequencies of the blades between 0 and 16%. The mistuning level equal to zero represents the tuned system, and $d_m = 100$ is the same mistuning level used in the previous section, Section 4.1. The different statistical results are studied, considering 150 mistuning realizations, including the mean of the steady-state forced response, coefficient of variation, and the amplification factor.

4.2.1 Mean

The mean displacement amplitude for the first and the second blade tips are shown in Figure 4-10 and Figure 4-11. Only one dominant peak can be seen in the mean of the response, considering all 150 mistuning realizations and different mistuning levels. Unlike what was observed in Chapter 3 for two realizations and various mistuning levels, the mean of the response for 150 realizations shows a constant trend in reducing the amplitude and shifting the response peak. For example, after increasing the mistuning level, for one realization, it was observed that the peak amplitude of the response fluctuated or it moved to the higher or lower frequencies based on the blade tip's number and mistuning level. However, including more realizations show a better vision of the general behavior of the system under a random mistuning realization. For instance, in both blade tips in Figure 4-10 and Figure 4-11, the amplitude of the peak of the mean response reduces by increasing the mistuning level.
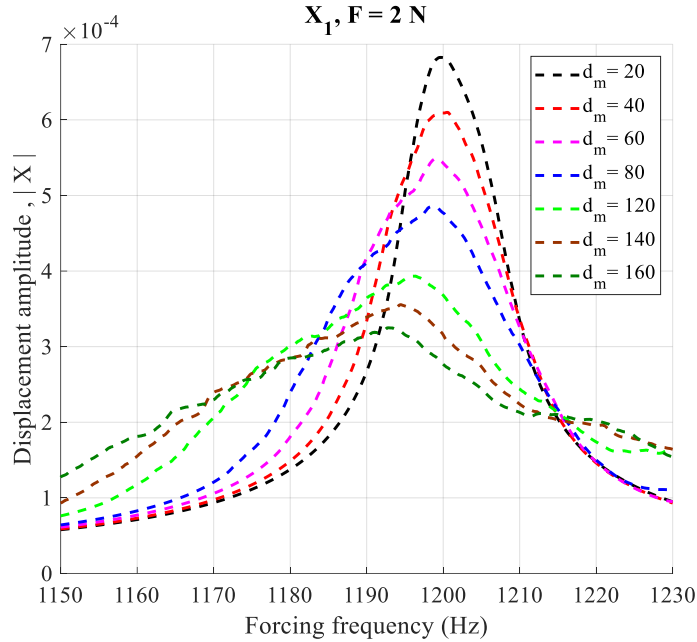
Figure 4-10: Mean of displacement amplitude for the first blade tip, X_1, for a range of mistuning levels, considering 150 mistuning realizations

Moreover, the peak of the mean response shifts to a lower frequency after increasing the mistuning level. However, for single mistuned realization, based on the blade tip number, the number of the response peak, or the mistuning realization, the response peak could move to either lower or higher frequencies.

The mean of the displacement amplitude for the rest of the blade tips, Figure B 5 in Appendix B, shows the same behavior as the first and the second blade tips. Looking at the response of all blade tips, the amplitude of the mean response peak is not equal among the blades. As seen in Section 3.2.2, having lower mistuning levels, such as 20, it was hard to distinguish between the two peaks produced by the frequency split phenomenon. The mean of the response shows a clear peak, considering 150 mistuning realizations, while the result of each mistuning realization in Section 3.2.2 showed either one or two peaks based on the blade number. As the mistuning level increases, the response for each realization produces two peaks. Consequently, the unique peak of the mean response at lower mistuning levels vanishes, and the peak becomes flat for higher mistuning levels.
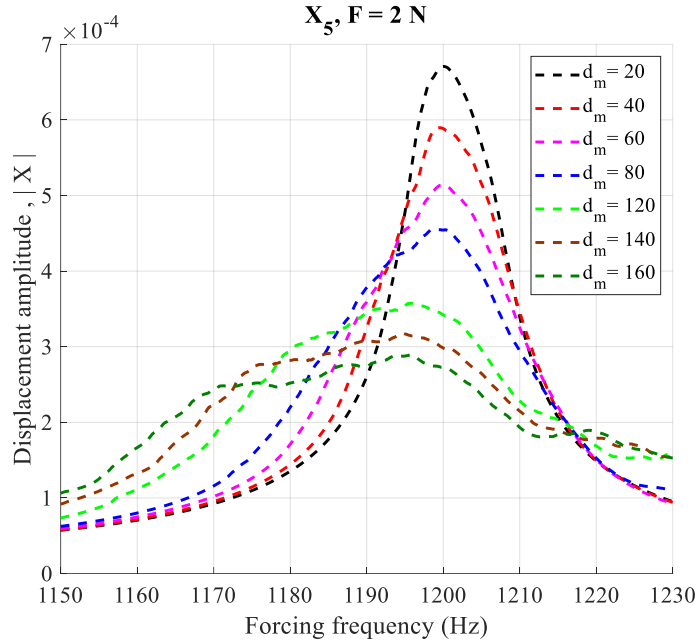
Figure 4-11: Mean of displacement amplitude for the second blade tip, X_5, for a range of mistuning levels, considering 150 mistuning realizations

4.2.2 Coefficient of Variation

The coefficient of variation for blade tips number one and two are presented in Figure 4-12 and Figure 4-13, respectively. Figure B 7 of Appendix B shows the results for other blade tips. Although the amplitude of the coefficient of variation for each blade tip varies, all figures show the same trend in terms of fluctuating within the shown frequency range. The amplitude of the coefficient of variation increases by increasing the mistuning level. The lower values of the mistuning level result in a coefficient of variation close to zero. Also, for lower mistuning levels, the coefficient of variation oscillates less compared with high values of d_m, meaning that data sets for higher values of d_m spread in a wide range of frequencies.

Figure 4-12: Coefficient of variation of the first blade tip, X_1, for a range of mistuning levels, considering 150 mistuning realizations

The higher values for the coefficient of variation appear around lower frequencies. This high value means that there are some outlier data, i.e., the forced response for some realizations spread at lower frequencies and far from the mean of the response. Furthermore, as the mistuning level increases, the peak of the coefficient of variation, or the outlier data, shifts to the lower frequencies. Tracking the peak from lower mistuning levels, it seems that for low mistuning levels, two peaks can be observed. After increasing the mistuning level, one peak transfers to the lower frequencies, while the other moves to the higher frequencies, and finally, it vanishes after reaching $d_m = 120$.

Also, the results show that the best range of frequencies providing a lower coefficient of variations is between 1190 Hz and 1210 Hz, considering all the range of mistuning levels. It points out that within this range of frequencies, the dispersion of data sets from the mean value is lower compared with other frequencies.
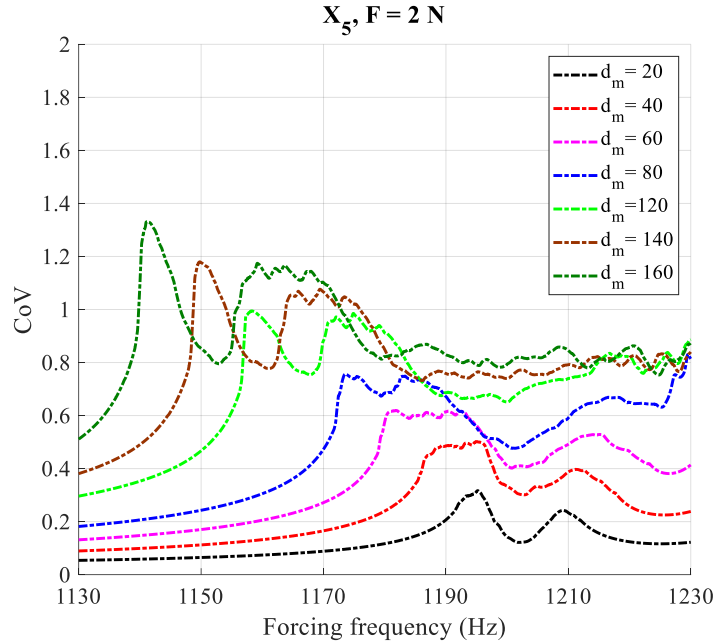
Figure 4-13: Coefficient of variation of the second blade tip, X_5, for a range of mistuning levels, considering 150 mistuning realizations

4.2.3   Amplification Factor

The amplification factor for the first and second blade tips are shown in Figure 4-14 and Figure 4-15. Each point in the figures represents the amplification factor for each mistuned realization based on various mistuning levels, highlighted with different colors. The big red dot in each plot demonstrates the average amplification factor of 150 mistuning realizations for each mistuning level. The black line shows the trend of changing the mean amplification factor on each column of the mistuning level. Figure B 8 of Appendix B presents the results of other blade tips.
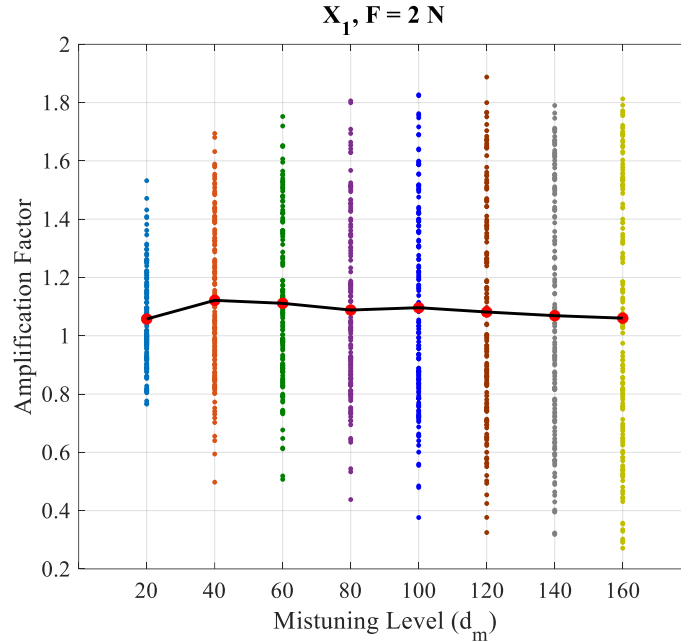
Figure 4-14: Amplification factor of the first blade tip, X_1, for a range of mistuning levels, considering 150 mistuning realizations
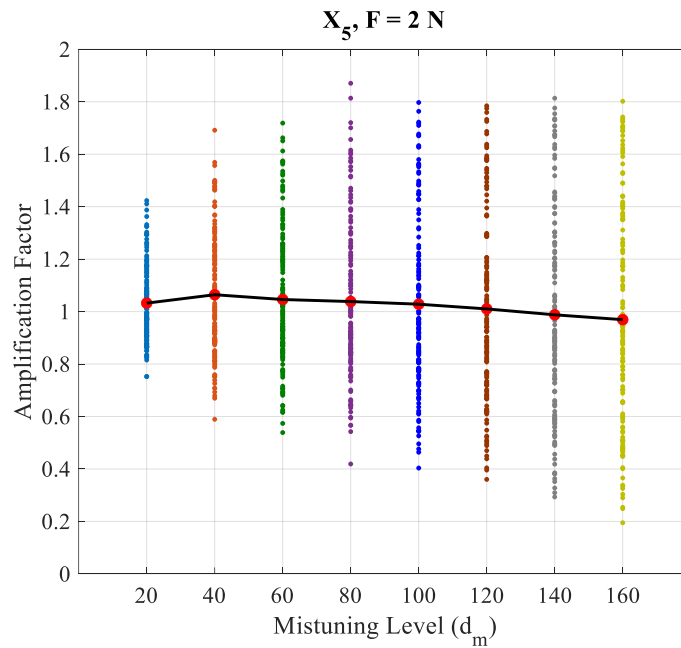
Figure 4-15: Amplification factor of the second blade tip, X_5, for a range of mistuning levels, considering 150 mistuning realizations

Results show that the patterns of the points distributions for each column (mistuning level) become more significant as the mistuning level increases. For example, for the first blade tip, considering $d_m = 20$, the amplification factor spreads between 0.7 and 1.6, while for $d_m = 160$, it spreads between a broader range of 0.2 and 1.8. Also, the mistuning level of 40 leads to the

75

maximum mean amplification factor for all blade tips. While the mistuning level between 20 and 40 increases the amplification factor, it shows a reducing trend for d_m bigger than 40. In some blades, such as the first and fourth ones, the mean amplification factor experiences a minor increase after $d_m = 40$. For instance, the mean amplification factor for the first blade tip is increased by about 0.74% between $d_m = 80$ and $d_m = 100$.

For all blade tips, except the first blade, the lowest value of amplification factor can be reached by adopting $d_m = 160$. For the first blade, $d_m = 20$ provides the lowest amplification factor, 1.057. For the same blade tip, the mistuning level equal to 160 results in an amplification factor of 1.06, representing a slight difference between $d_m = 160$ and 20.

At $d_m = 160$, the amplification factor for the third blade tip, shown in part (a) of Figure B 7 (Appendix B), is slightly above the unit, with a value of 1.0066. However, it is under the unit for the tips of the second, fifth, and sixth blades. The value under the unit means that, for the average response under the mistuning level of 160, the maximum amplitude of the forced response, within the desired frequency range, decreases compared with the maximum response amplitude of the tuned system.

4.3 Conclusion

In this chapter, a statistical analysis was performed on the nonlinear mistuned BDA, over 150 realizations. For this purpose, the random mistuning pattern applied to each blade's tip and middle stiffness coefficients and two different studies with several statistical parameters were investigated. For the first study, under a fixed mistuning level of 100, the effect of changing the excitation level between a range of 0.1 N and 10 N was analyzed. This wide range of excitation brought the effect of nonlinearity into consideration on the forced response of the system. The mean of the response, standard deviation, the mean compliance of the response, and the coefficient of variation were investigated in the first part of the study as the statistical parameters. The results suggested the mean of response increased with the excitation level, and also, the shifting phenomenon due to activation of the nonlinear effect of friction was observed. Moreover, the results of standard deviation showed that the response cloud of 10 N mostly covered the response cloud of 4 N. This coverage showed that the forced response of the tips of the blades, with an excitation between 4 N – 10 N, could fall in the area highlighted with 10 N cloud. The results of

mean compliance demonstrated that only one excitation level could not be suggested to minimize the peak of mean compliance. However, the excitation level that minimized the peak of compliance in most realizations could be limited to two levels of excitation, 4 N and 5 N. The results suggested that the coefficient of variation can be reached to its minimum value within a specific range of frequencies, 1175 Hz and 1210 Hz. It offered that within this range, the majority of forced responses, considering various mistuning realizations, were close to the mean of the response. However, outside this range, the presence of outlier data due to the peaks of response increased the coefficient of variation's amplitude. For the second part of the study, a constant excitation level of 2 N was assumed, and the mistuning level, d_m, was changed between a range of 0 to 160. This assumption provided information about changing the mistuning level from the tuned blade, $d_m = 0$, to the higher levels of mistuning amplitude. The effects of changing the mistuning level on different statistical parameters were studied, such as the mean of forced response, standard deviation, coefficient of variation, and amplification factor. The mean of the response showed that by increasing the mistuning level, the peak amplitude of the mean response decreased and shifted to the lower frequencies. The results were suggestive of an ideal frequency range between 1190 Hz and 1210 Hz, which means that within this frequency range, the variation of data sets is lower than the rest of the frequencies. The patterns of distribution of amplification factor's points offered that the data points distributed on a broader range by increasing the mistuning level. The trend of the amplification factor's variation suggested that $d_m = 40$ caused the highest mean amplification factor compared with the rest of the range. Generally, after $d_m = 40$, the mean amplification factor was decreased. For half of the tips of the blades, $d_m = 160$ provided the mean amplification factor less than the unit, meaning that the maximum amplitude of the forced response of mistuned nonlinear BDA, for most of the mistuning realizations, was less than the maximum response amplitude of the nonlinear tuned system.

5.   Chapter 5: Conclusion

5.1   Main Contributions

The focus of this work was to study the nonlinear vibration characteristics of mistuned bladed disk assemblies (BDAs). Nonlinearity was due to friction forces at the contact interfaces of the blade root and disk. Mistuning was due to deviations in the elasticity of the blades from the tuned blade caused by manufacturing tolerances. Although there are many research studies on the separate effects of mistuning and nonlinearity in BDA, few studies consider the effect of both phenomena on the vibration characteristics of BDA. The main contributions of this study are summarized as follows:

i.   A mathematical model was implemented in MATLAB for a BDA, including the nonlinear friction forces at the blade root and the mistuning of blade elasticity.

ii.   The steady-state vibration response of the BDA subject to engine-order excitation was computed and validated for various configurations.

iii.   A preliminary statistical analysis of the vibration response of the mistuned BDA was performed based on 150 realizations of mistuning. The effects of excitation amplitude and mistuning level were studied.

5.2   Summary of Findings

The main conclusions drawn from this study can be summarized below:

i.   The steady-state forced response curves of the tuned system, under different excitation levels, showed only one resonance peak. The amplitudes of the displacement for different blade tips are equal in response to engine-order excitation, as expected.

ii.   The natural frequencies of the first bending mode family for the tuned linear BDA demonstrated two pairs of equal frequencies corresponding to the double mode and two frequencies associated with the single mode. Mistuning results in splitting the pairs of equal frequencies in the tuned system were split into two separate frequencies.

iii.   The comparison between the natural frequencies of the linear tuned system and the steady-state forced response curves revealed that after increasing the excitation level, the

resonance frequency shifted from the bonded frequencies to the frictionless frequencies. The backbone curves, which trace the locus of maximum displacement amplitude, showed the same behavior in both the tuned and mistuned systems.

iv. The contact nonlinearity in this study has a softening effect, i.e., the resonance frequency shifts gradually to lower frequencies as the amplitude of excitation increases.

v. Analyzing the time-series of the blade tip's response for the tuned system suggested a traveling wave feature before, at, and after resonance frequency. Unlike tuned BDA, the time-series of the mistuned system demonstrated a traveling wave feature far from or between resonance frequencies. Close to the resonance peaks of the mistuned BDA, the time-series of the blades' tips together showed the stationary wave feature.

vi. The compliance curve for the tuned BDA revealed that the maximum damping due to the dry friction occurred under the excitation level of 5N. This was determined by considering the response curve with the smallest peak value. Considering the two individual mistuning realizations of Chapter 3, the compliance curve for the mistuned BDA showed that an individual excitation level cannot ensure the smallest compliance peak for different realizations. Therefore, the maximum damping depends on the mistuning realization and the targeted response peak. This is corroborated by the trends observed for 150 realizations in Chapter 4. However, the excitation level that minimized the peak of compliance in most realizations was limited to two excitation levels, 4 N and 5 N.

vii. The analysis of the amplification factor for the mistuned system with two different mistuning realizations confirmed the expectation that the maximum response amplitude depends on the mistuning level. For the 150 realizations of mistuning considered here, the values of the amplification factor had a larger distribution when the mistuning level increased. Interestingly, the average amplification factor did not change significantly. This suggests that the average value of the amplification factor may not be a suitable design parameter.

viii. The amplification factor for individual blades can sometimes be smaller than 1. This means that in some blade tips a specific range of mistuning levels may decrease the amplitude of steady-state response compared with the tuned BDA. Analyzing the data set provided from 150 mistuning realizations revealed that for half of the blade tips, $d_m = 160$ provided the mean amplification factor less than 1, meaning that the maximum amplitude of the steady-

state response of mistuned BDA, for most of the mistuning realizations, was less than the maximum response amplitude of the nonlinear tuned system.

ix. The results of analyzing the effect of changing the excitation level suggested that the coefficient of variation reached its minimum value in the frequency range of 1175 Hz and 1210 Hz. It offered that within this range, most blade tips' steady-state forced response under each mistuning realization is close to the mean of the response. However, outside this range, outlier data (due to the response's peaks) increased the coefficient of variation's amplitude. The coefficient of variation for the study of changing the mistuning level was suggestive of an ideal frequency range between 1190 Hz and 1210 Hz, which means that within this frequency range, the variation of data sets with respect to the mean value is lower than the rest of the frequencies.

5.3 Suggestions for future work

The current work has provided a study of the effect of nonlinearity and mistuning on the dynamic behavior of BDA. However, there are many aspects that require further development in the future. These are listed below:

i) To better predict the dynamic behavior of BDA under a random mistuning realization, a larger dataset with many samples is required. Thus, more random mistuning realizations are needed to make the population more representative of the typical behavior of BDAs. A larger population makes it possible to calculate the distribution of the response amplitude more accurately. This is important in understanding how uncertainty propagates from blade elasticity to blade displacement amplitude.

ii) In the current study, the effect of the mistuning level was considered only under a constant excitation level of 2 N. The variation of mistuning level may be analyzed under different excitation levels, covering both linear and nonlinear ranges of the steady-state forced response to study any connection between linear and nonlinear amplification factors.

iii) The current study considers only nonlinear forces due to the friction between the blade's root and disk at dovetail joints. The blade-casing contact can play a significant role in the vibration behavior of BDA because of the high linear velocity of the blade tip. The implication of nonlinear forces on the blade tip due to the blade-casing rubbing needs to be

considered. The blade-casing rubbing requires studying different contact models that can be applied to the contact event. Considering both nonlinear forces at the blade-casing interface and blade-disk, along with the statistical analysis of varying mistuning patterns, is another idea that may be worth pursuing.

iv)   Other uncertain parameters should be analyzed considering mistuning and nonlinear forces. For example, in a mistuned system, the pattern in which mistuning is distributed in the system, between different parts of the blades, or the friction coefficient at the contact interface can be studied as other uncertain parameters which affect the behavior of the BDA.

v)   The study of worst-case scenarios based on different target metrics, such as maximum stress at the blade root, root mean square blade displacement, or the maximum blade tip displacement, is another important information for the industry, which we did not explore in this work.

References

[1]   J. Joachim, F. Nyssen, and A. Batailly, "Numerical Investigation of a Mistuned Academic Bladed Disk Dynamics with Blade/Casing Contact," *J. Eng. Gas Turbines Power*, 2020, doi: 10.1115/1.4047780.

[2]   B. Beirow, F. Figaschewsky, A. Kühhorn, and A. Bornhorn, "Modal Analyses of an Axial Turbine Blisk With Intentional Mistuning," *J. Eng. Gas Turbines Power*, vol. 140, no. 1, Jan. 2018, doi: 10.1115/1.4037588.

[3]   M. P. Castanier and C. Pierre, "Modeling and analysis of mistuned bladed disk vibration: Status and emerging directions," *J. Propuls. Power*, vol. 22, no. 2, pp. 384–396, Mar. 2006, doi: 10.2514/1.16345.

[4]   M. Krack, L. Salles, and F. Thouverez, "Vibration Prediction of Bladed Disks Coupled by Friction Joints," *Arch. Comput. Methods Eng.*, vol. 24, no. 3, pp. 589–636, Jul. 2017, doi: 10.1007/s11831-016-9183-2.

[5]   H. Ma, F. Yin, Y. Guo, X. Tai, and B. Wen, "A review on dynamic characteristics of blade–casing rubbing," *Nonlinear Dyn.*, vol. 84, no. 2, pp. 437–472, Apr. 2016, doi: 10.1007/s11071-015-2535-x.

[6]   E. P. Petrov, "Reduction of forced response levels for bladed disks by mistuning: Overview of the phenomenon," *J. Eng. Gas Turbines Power*, vol. 133, no. 7, Jul. 2011, doi: 10.1115/1.4002619.

[7]   D. S. Whitehead, "The maximum factor by which forced vibration of blades can increase due to mistuning," in *ASME 1996 International Gas Turbine and Aeroengine Congress and Exhibition, GT 1996*, Feb. 1996, vol. 5. doi: 10.1115/96-GT-125.

[8]   D. S. Whitehead, "The maximum factor by which forced vibration of blades can increase due to mistuning," *J. Eng. Gas Turbines Power*, vol. 120, no. 1, pp. 115–119, Jan. 1998, doi: 10.1115/1.2818061.

[9]   J. S. Rao, *History of Rotating Machinery Dynamics*, vol. 20. Dordrecht: Springer Netherlands, 2011. doi: 10.1007/978-94-007-1165-5_16.

[10] G. Jacquet-Richardet *et al.*, "Rotor to stator contacts in turbomachines. Review and application," *Mech. Syst. Signal Process.*, vol. 40, no. 2, pp. 401–420, Nov. 2013, doi: 10.1016/j.ymssp.2013.05.010.

[11] T. M. Bartsch, "High Cycle Fatigue (HCF) Science and Technology Program 2002 Annual Report," Aug. 2003. Accessed: May 20, 2021. [Online]. Available: https://apps.dtic.mil/sti/citations/ADA423347

[12] D. S. Whitehead, "Effect of Mistuning on the Vibration of Turbo-Machine Blades Induced by Wakes," *J. Mech. Eng. Sci.*, vol. 8, no. 1, pp. 15–21, Mar. 1966, doi: 10.1243/jmes_jour_1966_008_004_02.

[13] C. Martel and R. Corral, "Asymptotic description of maximum mistuning amplification of bladed disk forced response," *J. Eng. Gas Turbines Power*, vol. 131, no. 2, Mar. 2009, doi: 10.1115/1.2968868.

[14] P. W. Anderson, "Absence of diffusion in certain random lattices," *Phys. Rev.*, vol. 109, no. 5, pp. 1492–1505, Mar. 1958, doi: 10.1103/PhysRev.109.1492.

[15] H. Yiu and D. J. Ewins, "Dependence on blade arrangements of mistuned bladed disc of the optimal and critical resonant responses," in *Rotating Machinery, Proceedings of the 6th International Symposium on Transport Phenomena and Dynamics of Rotating Machinery*, 1986, vol. 1, pp. 237–251.

[16] E. P. Petrov and D. J. Ewins, "Search for the best blade arrangement in a mistuned bladed disc assembly," 2002.

[17] T. Butlin and A. Batailly, "Anti-optimisation applied to the analysis of rotor/stator interaction," in *Proceedings of the ASME Turbo Expo*, Nov. 2013, vol. 7 A. doi: 10.1115/GT2013-94633.

[18] T. Butlin, "Anti-optimisation for modelling the vibration of locally nonlinear structures: An exploratory study," *J. Sound Vib.*, vol. 332, no. 26, pp. 7099–7122, Dec. 2013, doi: 10.1016/j.jsv.2013.06.028.

[19] E. F. Crawley and K. C. Hall, "Optimization and mechanisms of mistuning in cascades," *J.*

Eng. Gas Turbines Power, vol. 107, no. 2, pp. 418–426, Apr. 1985, doi: 10.1115/1.3239742.

[20]   S. Quaegebeur, B. Chouvion, F. Thouverez, S. Quaegebeur, B. Chouvion, and F. Thouverez, "Nonlinear cyclic reduction for the analysis of mistuned cyclic systems To cite this version : HAL Id : hal-03020831," Nov. 2020, Accessed: Dec. 07, 2020. [Online]. Available: https://hal.archives-ouvertes.fr/hal-03020831

[21]   C. Joannin, F. Thouverez, and B. Chouvion, "Reduced-order modelling using nonlinear modes and triple nonlinear modal synthesis," *Comput. Struct.*, vol. 203, pp. 18–33, Jul. 2018, doi: 10.1016/j.compstruc.2018.05.005.

[22]   L. Ouyang, H. Shang, H. Chen, Q. Bi, and L.-M. Zhu, "The Mechanism on Prediction of Transient Maximum Amplitude for Tuned and Mistuned Blisks," *J. Eng. Gas Turbines Power*, vol. 142, no. 5, May 2020, doi: 10.1115/1.4046761.

[23]   T. Butlin, J. Woodhouse, and A. R. Champneys, "The landscape of nonlinear structural dynamics: An introduction," *Philosophical Transactions of the Royal Society A: Mathematical, Physical and Engineering Sciences*, vol. 373, no. 2051. Royal Society of London, p. 20140400, Sep. 28, 2015. doi: 10.1098/rsta.2014.0400.

[24]   E. Piollet, F. Nyssen, and A. Batailly, "Blade/casing rubbing interactions in aircraft engines: Numerical benchmark and design guidelines based on NASA rotor 37," *J. Sound Vib.*, vol. 460, p. 114878, Nov. 2019, doi: 10.1016/j.jsv.2019.114878.

[25]   A. Batailly, M. Meingast, and M. Legrand, "Unilateral contact induced blade/casing vibratory interactions in impellers: Analysis for rigid casings," *J. Sound Vib.*, vol. 337, pp. 244–262, Feb. 2015, doi: 10.1016/j.jsv.2014.10.010.

[26]   A. Batailly, M. B. Meingast, M. Legrand, and J.-P. Ousty, "Rotor-Stator Interaction Scenarios for the Centrifugal Compressor of a Helicopter Engine." Aug. 04, 2013. doi: 10.1115/DETC2013-12211.

[27]   C. Padova, M. G. Dunn, J. Barton, K. Turner, A. Turner, and D. DiTommaso, "Casing treatment and blade-tip configuration effects on controlled gas turbine blade tip/shroud rubs at engine conditions," *J. Turbomach.*, vol. 133, no. 1, Jan. 2011, doi: 10.1115/1.4000539.

[28] E. P. Petrov and D. J. Ewins, "Analytical formulation of friction interface elements for analysis of nonlinear multi-harmonic vibrations of bladed disks," *J. Turbomach.*, vol. 125, no. 2, pp. 364–371, Apr. 2003, doi: 10.1115/1.1539868.

[29] C. Joannin, B. Chouvion, F. Thouverez, J. P. Ousty, and M. Mbaye, "A nonlinear component mode synthesis method for the computation of steady-state vibrations in non-conservative systems," *Mech. Syst. Signal Process.*, vol. 83, pp. 75–92, Jan. 2017, doi: 10.1016/j.ymssp.2016.05.044.

[30] M. Krack and J. Gross, *Harmonic Balance for Nonlinear Vibration Problems*. Springer, 2019. doi: 10.1007/978-3-030-14023-6.

[31] R. Murthy and M. P. Mignolet, "On the benefits of intentional mistuning of friction dampers to reduce the response of tuned and mistuned bladed disks," in *Proceedings of the ASME Turbo Expo*, Nov. 2013, vol. 7 A. doi: 10.1115/GT2013-95792.

[32] Y. Han, R. Murthy, M. P. Mignolet, and J. Lentz, "Optimization of intentional mistuning patterns for the mitigation of the effectsof random mistuning," *J. Eng. Gas Turbines Power*, vol. 136, no. 6, Jun. 2014, doi: 10.1115/1.4026141.

[33] A. Tacher, F. Thouverez, and J. Armand, "Interaction Between Coriolis Forces and Mistuning on a Cyclic Symmetric Structure with Geometrical Nonlinearity," *J. Eng. Gas Turbines Power*, Oct. 2020, doi: 10.1115/1.4048844.

[34] W. Zhao, D. Zhang, L. Sun, and Y. Xie, "Nonlinear dynamics analysis of mistuned turbine bladed disks with damped shrouds," in *American Society of Mechanical Engineers, Power Division (Publication) POWER*, Sep. 2017, vol. 2. doi: 10.1115/POWER-ICOPE2017-3433.

[35] C. Joannin, B. Chouvion, F. Thouverez, M. Mbaye, and J.-P. Ousty, "Nonlinear Modal Analysis of Mistuned Periodic Structures Subjected to Dry Friction," *J. Eng. Gas Turbines Power*, vol. 138, no. 7, Dec. 2015, doi: 10.1115/1.4031886.

[36] T. Liu, Y. Xie, and D. Zhang, "Investigation of vibration characteristics for bladed-disks with dry friction nonlinearity," in *MATEC Web of Conferences*, Sep. 2018, vol. 207, p. 04009. doi: 10.1051/matecconf/201820704009.

[37]   H. She, C. Li, Q. Tang, H. Ma, and B. Wen, "Computation and investigation of mode characteristics in nonlinear system with tuned/mistuned contact interface," *Front. Mech. Eng.*, vol. 15, no. 1, pp. 133–150, Mar. 2020, doi: 10.1007/s11465-019-0557-7.

[38]   S. Quaegebeur, B. Chouvion, F. Thouverez, and L. Berthe, "Energy transfer between nodal diameters of cyclic symmetric structures exhibiting polynomial nonlinearities: Cyclic condition and analysis," *Mech. Syst. Signal Process.*, vol. 139, p. 106604, May 2020, doi: 10.1016/j.ymssp.2019.106604.

[39]   S. Quaegebeur, B. Chouvion, F. Thouverez, and L. Berthe, "On a New Nonlinear Reduced-Order Model for Capturing Internal Resonances in Intentionally Mistuned Cyclic Structures," *J. Eng. Gas Turbines Power*, vol. 143, no. 2, Feb. 2021, doi: 10.1115/1.4049138/1091628.

[40]   R. M. Rosenberg, "The normal modes of nonlinear n-degree-of-freedom systems," *J. Appl. Mech. Trans. ASME*, vol. 29, no. 1, pp. 7–14, Mar. 1962, doi: 10.1115/1.3636501.

[41]   M. Krack, L. Panning-Von Scheidt, and J. Wallaschek, "A method for nonlinear modal analysis and synthesis: Application to harmonically forced and self-excited mechanical systems," *J. Sound Vib.*, vol. 332, no. 25, pp. 6798–6814, Dec. 2013, doi: 10.1016/j.jsv.2013.08.009.

[42]   M. Mitra and B. I. Epureanu, "Dynamic Modeling and Projection-Based Reduction Methods for Bladed Disks with Nonlinear Frictional and Intermittent Contact Interfaces," *Appl. Mech. Rev.*, vol. 71, no. 5, Sep. 2019, doi: 10.1115/1.4043083.

[43]   T. Butlin, "Response bounds for complex systems with a localised and uncertain nonlinearity," *J. Sound Vib.*, vol. 384, pp. 227–252, 2016, doi: https://doi.org/10.1016/j.jsv.2016.08.015.

[44]   T. Butlin, P. Ghaderi, G. Spelman, W. J. B. Midgley, and R. Umehara, "A novel method for predicting the response variability of friction-damped gas turbine blades," *J. Sound Vib.*, vol. 440, pp. 372–398, Feb. 2019, doi: 10.1016/j.jsv.2018.10.013.

[45]   T. Butlin, G. Spelman, P. Ghaderi, W. J. B. Midgley, and R. Umehara, "Predicting response bounds for friction-damped gas turbine blades with uncertain friction coupling," *J. Sound*

Vib., vol. 440, pp. 399–411, 2019, doi: https://doi.org/10.1016/j.jsv.2018.08.037.

[46]   H. Liao, W. Wu, and D. Fang, "The reduced space Sequential Quadratic Programming (SQP) method for calculating the worst resonance response of nonlinear systems," *J. Sound Vib.*, vol. 425, pp. 301–323, Jul. 2018, doi: 10.1016/j.jsv.2017.12.020.

[47]   A. Mahmoodi and H. Ahmadian, "Forced Response Vibration Analysis of the Turbine Blade with Coupling between the Normal and Tangential Direction," *Shock Vib.*, vol. 2022, 2022, doi: 10.1155/2022/2413022.

[48]   E. Pennestrì, V. Rossi, P. Salvini, and P. P. Valentini, "Review and comparison of dry friction force models," *Nonlinear Dynamics*, vol. 83, no. 4. Springer Netherlands, pp. 1785–1801, Mar. 01, 2016. doi: 10.1007/s11071-015-2485-3.

[49]   "MATLAB Documentation," *MathWorks*, 2022. https://www.mathworks.com/help/matlab/ref/ode45.html

[50]   R. L. Burden, J. D. Faires, and A. M. Burden, *Numerical analysis*, 10th ed. Cengage Learning, 2015. doi: 10.1201/9781315274980.

[51]   S. Chapra and R. Canale, *Numerical Methods for Engineers*, 6th ed. McGraw-Hill Science/Engineering/Math, 2009.

[52]   T. C. Yuan, J. Yang, and L. Q. Chen, "A harmonic balance approach with alternating frequency/time domain progress for piezoelectric mechanical systems," *Mech. Syst. Signal Process.*, vol. 120, pp. 274–289, Apr. 2019, doi: 10.1016/j.ymssp.2018.10.022.

[53]   J. J. Thomsen, *Vibrations and Stability*, Third. Springer International Publishing, 2021. doi: 10.1007/978-3-030-68045-9.

[54]   E. Sarrouy and J.-J. Sinou, "Non-Linear Periodic and Quasi-Periodic Vibrations in Mechanical Systems - On the use of the Harmonic Balance Methods," in *Advances in Vibration Analysis Research*, F. Ebrahimi, Ed. InTech, 2011.

[55]   W. Govaerts *et al.*, "MATCONT: Continuation toolbox for ODEs in Matlab," *Univ. Gent, Belgium Utr. Univ.*, p. 124, 2019.

[56]   D. Laxalde, F. Thouverez, J. J. Sinou, and J. P. Lombard, "Qualitative analysis of forced

response of blisks with friction ring dampers," *Eur. J. Mech. A/Solids*, vol. 26, no. 4, pp. 676–687, Jul. 2007, doi: 10.1016/j.euromechsol.2006.10.002.

[57] D. Laxalde and F. Thouverez, "Complex non-linear modal analysis for mechanical systems: Application to turbomachinery bladings with friction interfaces," *J. Sound Vib.*, vol. 322, no. 4–5, pp. 1009–1025, May 2009, doi: 10.1016/j.jsv.2008.11.044.

[58] H. She, C. Li, G. Zhang, and Q. Tang, "Investigation on the parameter sensitivity of bladed assemblies undergoing mistuning features," *Appl. Acoust.*, vol. 178, p. 107998, Jul. 2021, doi: 10.1016/j.apacoust.2021.107998.

[59] M. Mitra, "Modeling and Analysis of Nonlinear Damping and Mistuning Mechanisms in Rotating Systems," University of Michigan, 2018. Accessed: Sep. 22, 2020. [Online]. Available: http://deepblue.lib.umich.edu/handle/2027.42/144064

Appendix A
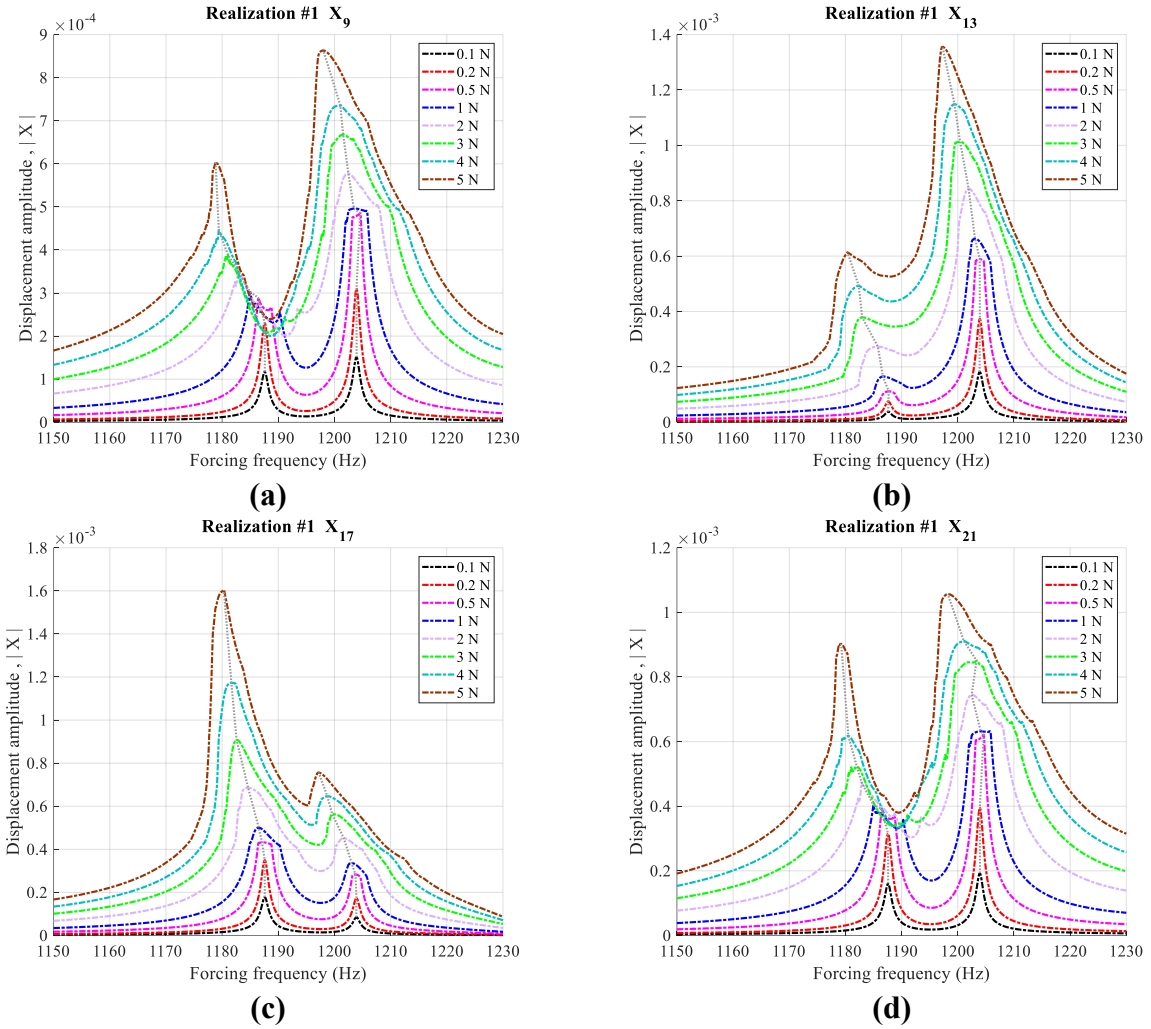
Figure A 1: Steady-state forced response of the tip of (a) third, (b) fourth, (c) fifth, and (d) sixth blades for a range of external forces between 0.1N and 5N, first mistuning realization
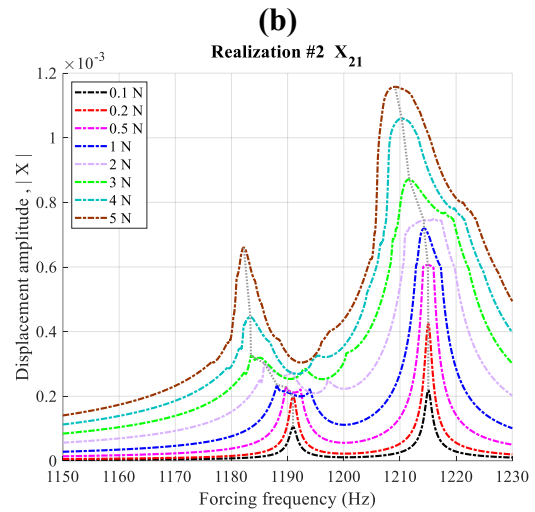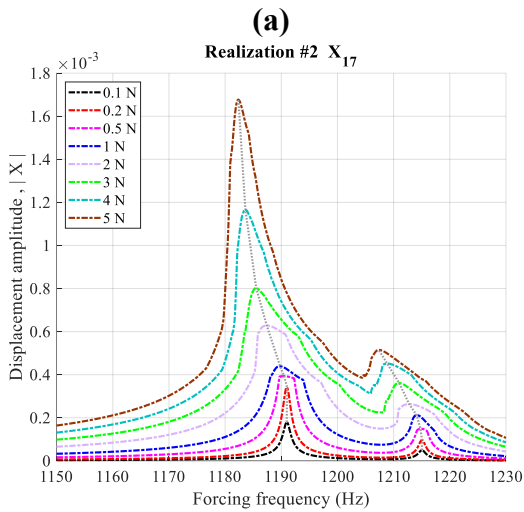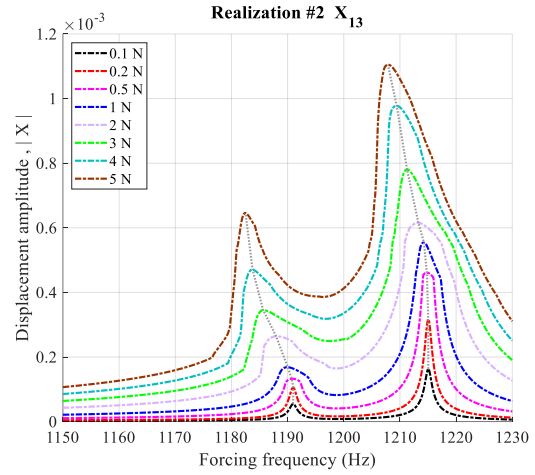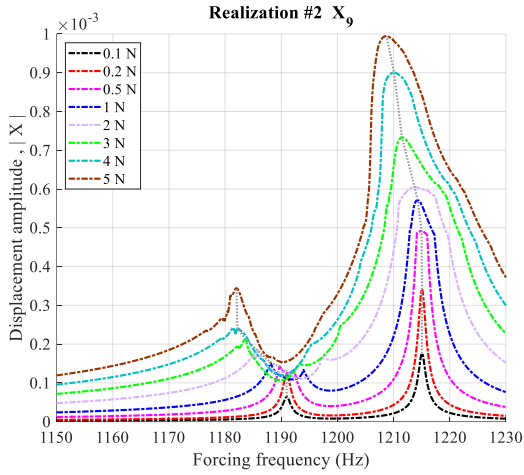
Figure A 2: Steady-state forced response for the blades #3, #4, #5, and #6, for a range of external forces between 0.1 N and 5 N, second mistuning realization
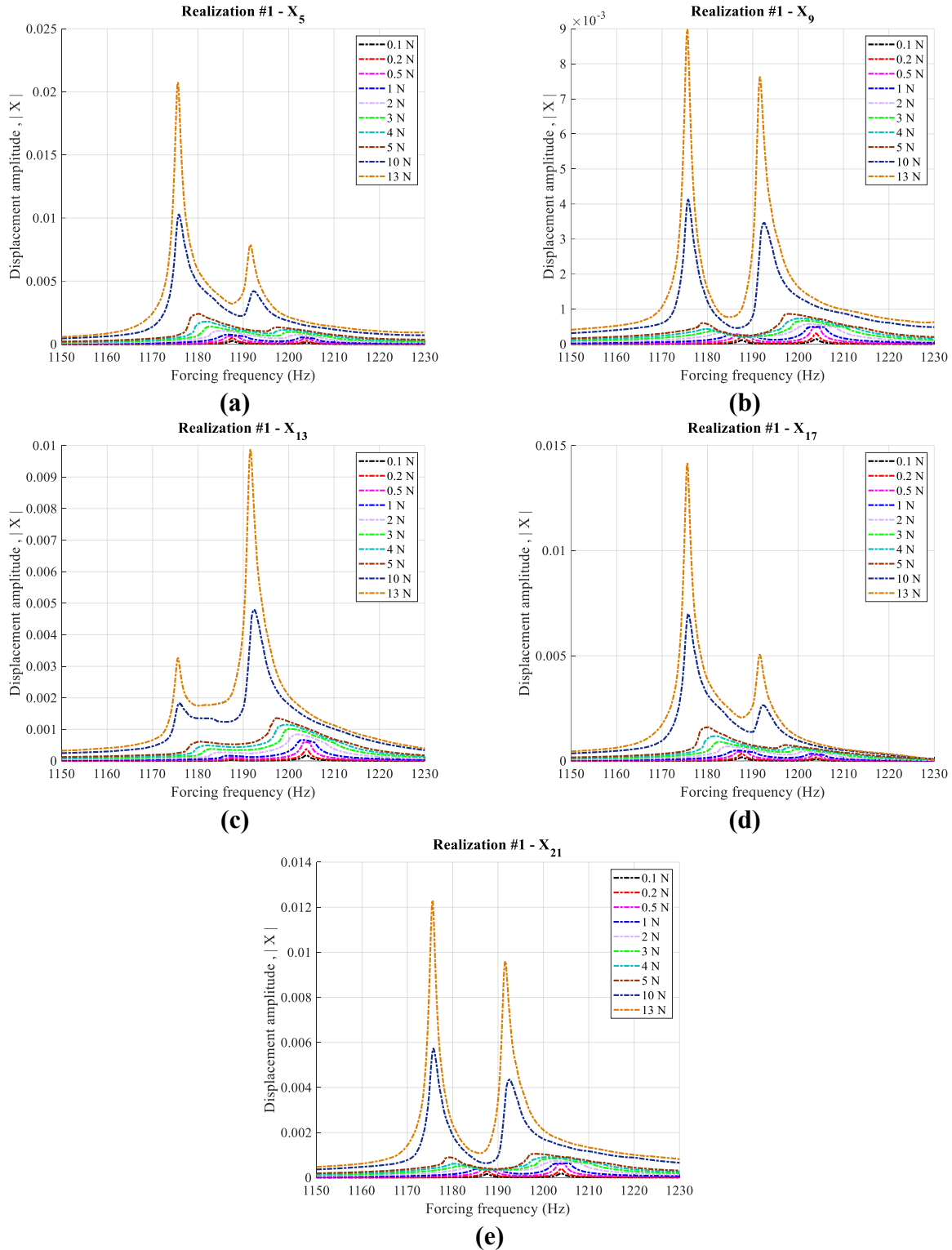
Figure A 3: Steady-state forced response for the blades #2, #3, #4, #5, and #6, for a range of external forces between 0.1 N and 13 N, first mistuning realization

(a)

(b)

(c)

(d)

(e)
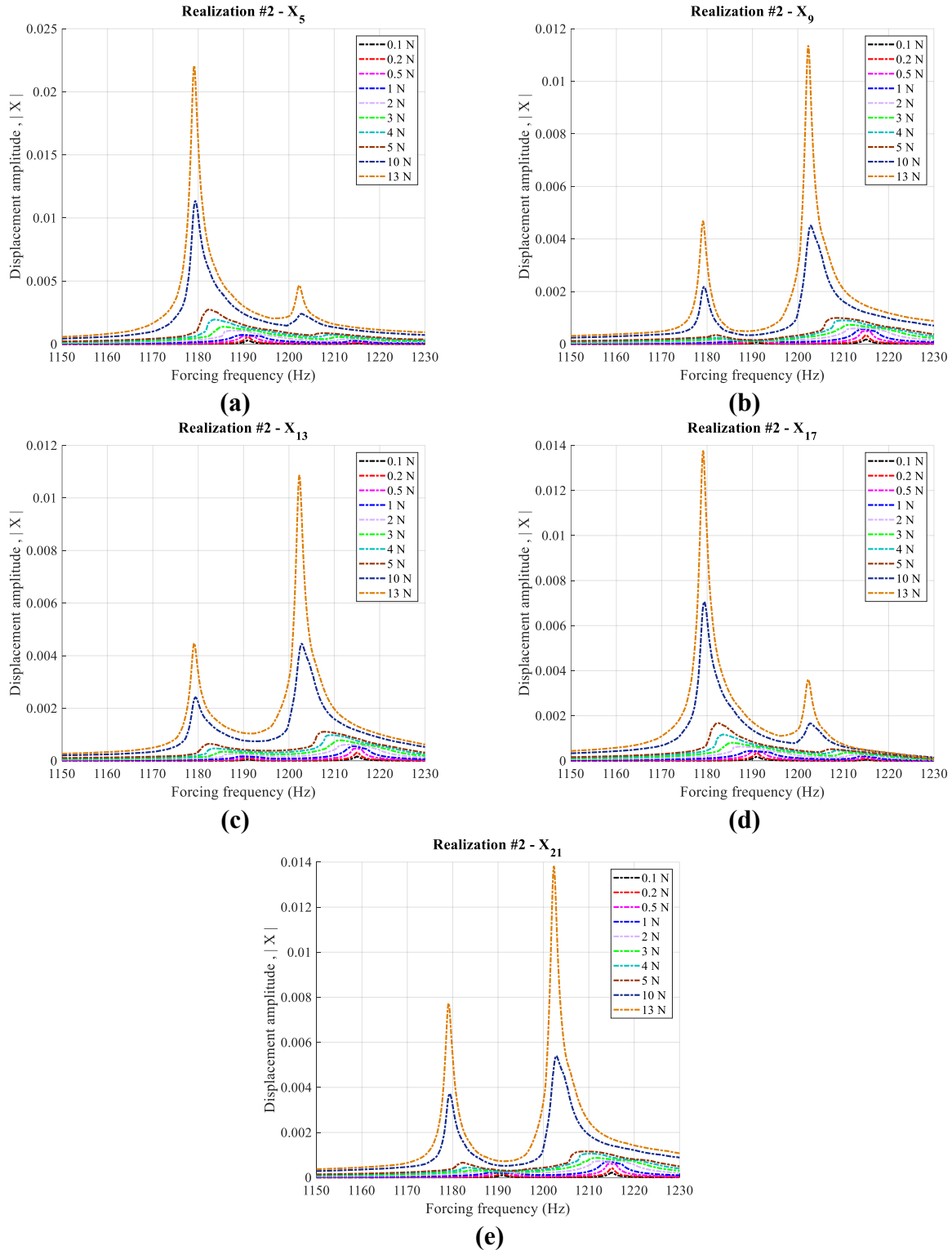
Figure A 4: Steady-state forced response for the blades #2, #3, #4, #5, and #6, for a range of external forces between 0.1 N and 13 N, second mistuning realization
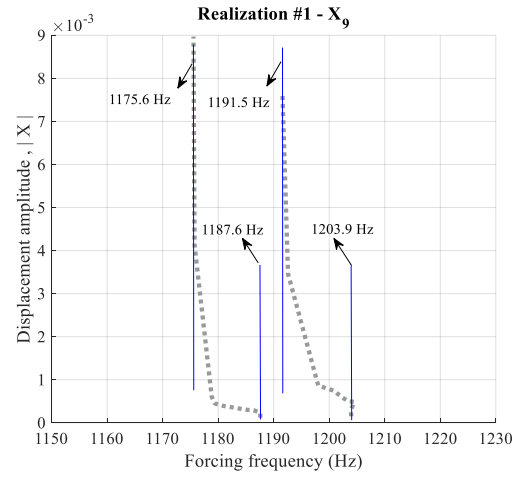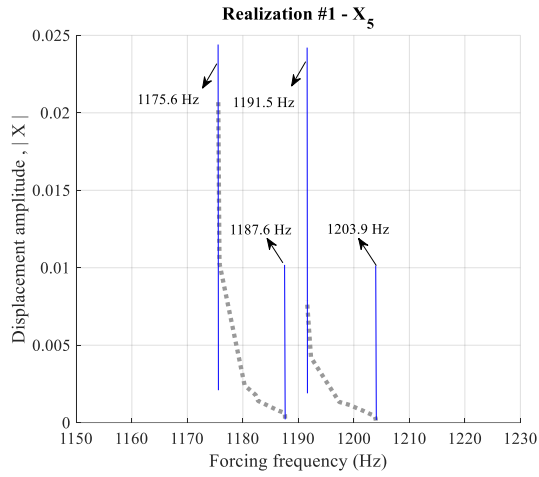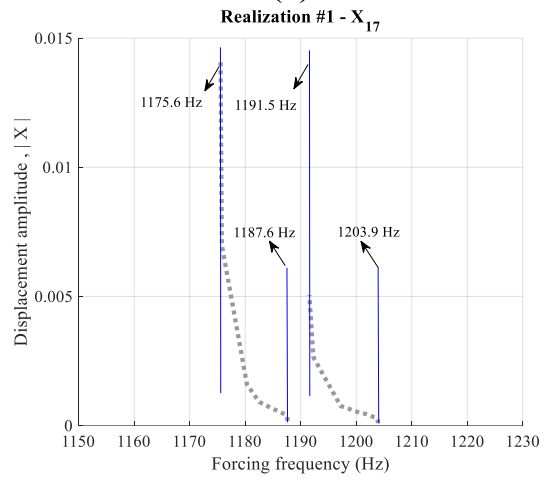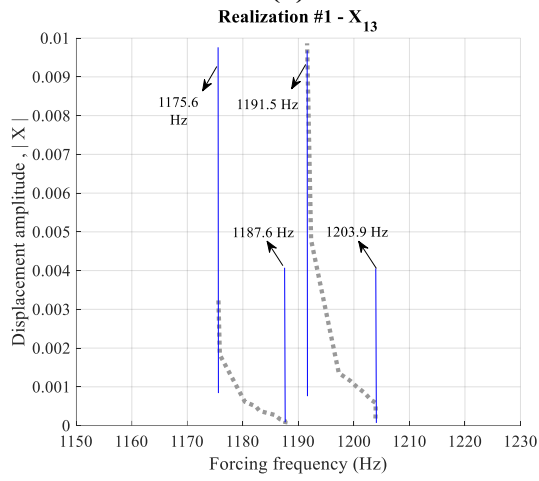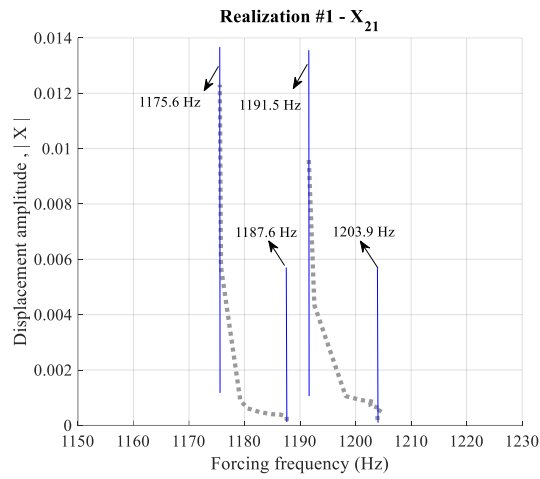
Figure A 5: Backbone curve based on the forced response of vibration between 0.1-13N, blade tips #2, #3, #4, #5, and #6, first mistuning realization
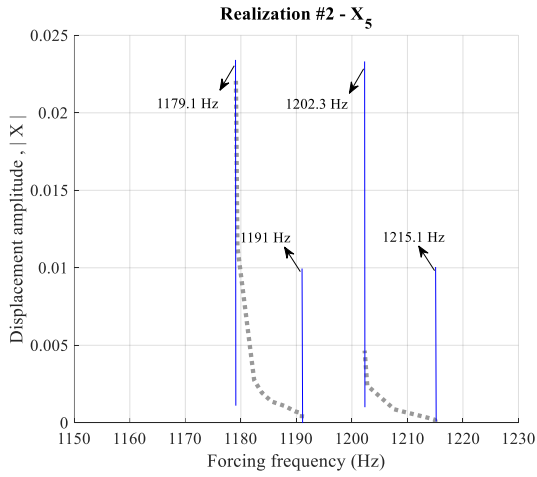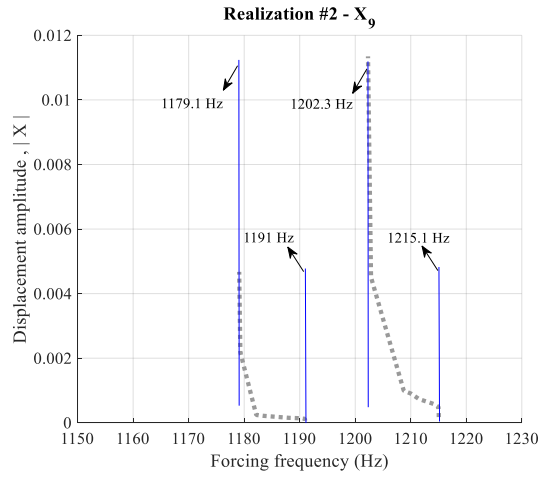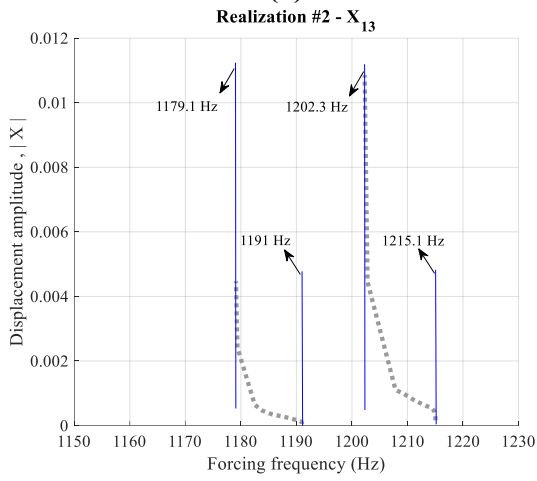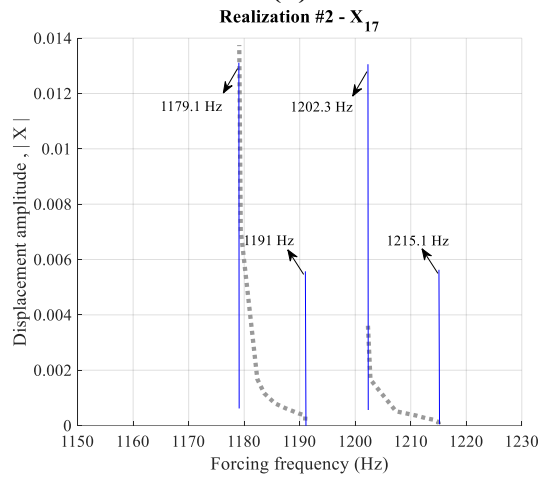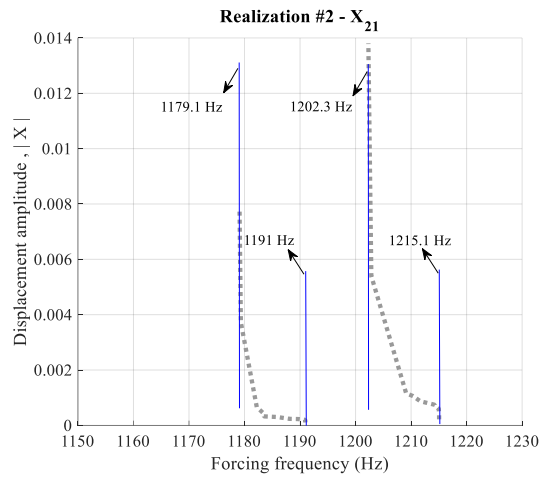
Figure A 6: Backbone curve based on the forced response of vibration between 0.1-13N, blade tips #2, #3, #4, #5, and #6, second mistuning realization
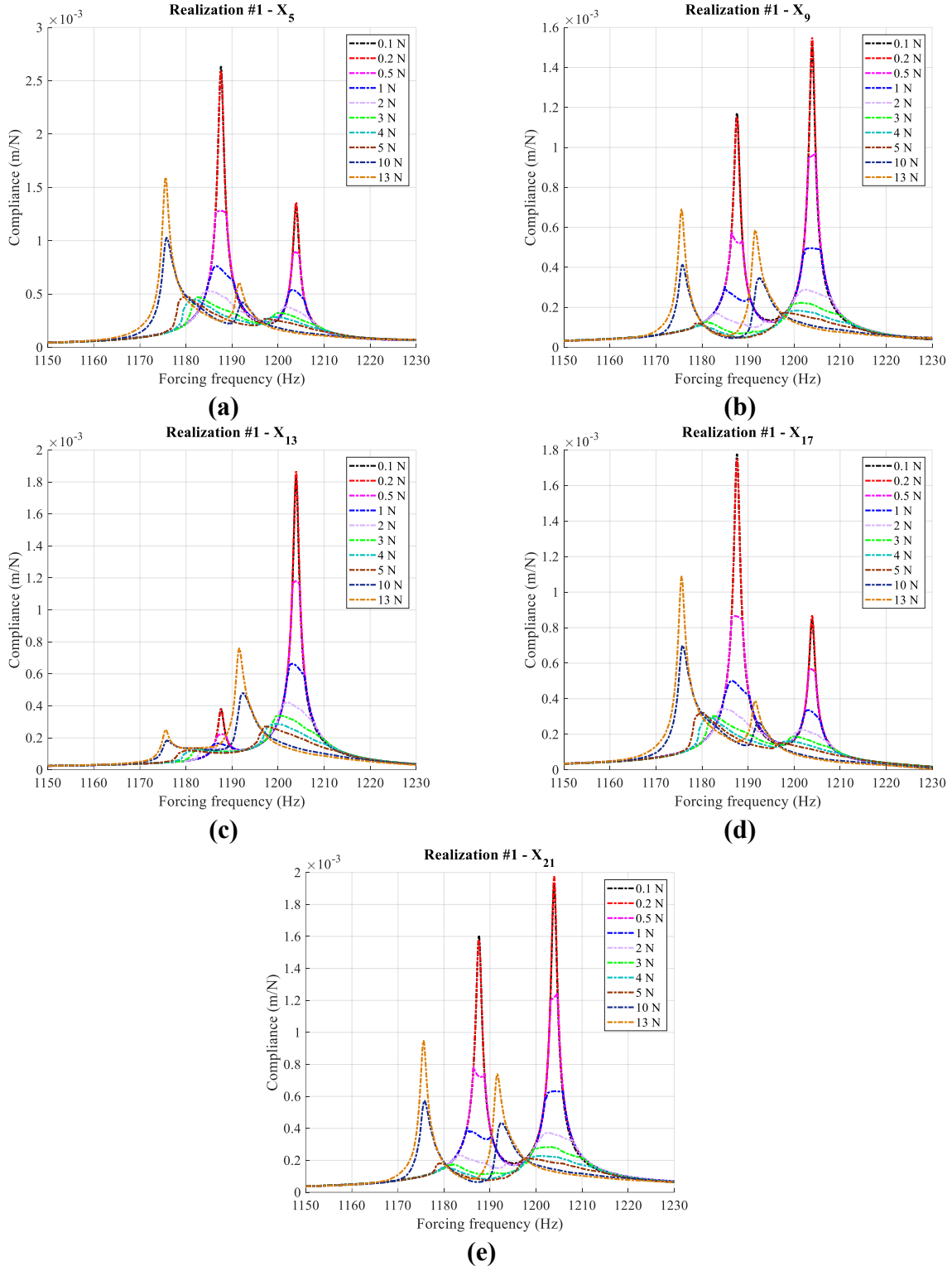
Figure A 7: Compliance of the blade tips #2, #3, #4, #5, and #6 for different excitation level, first mistuning realization
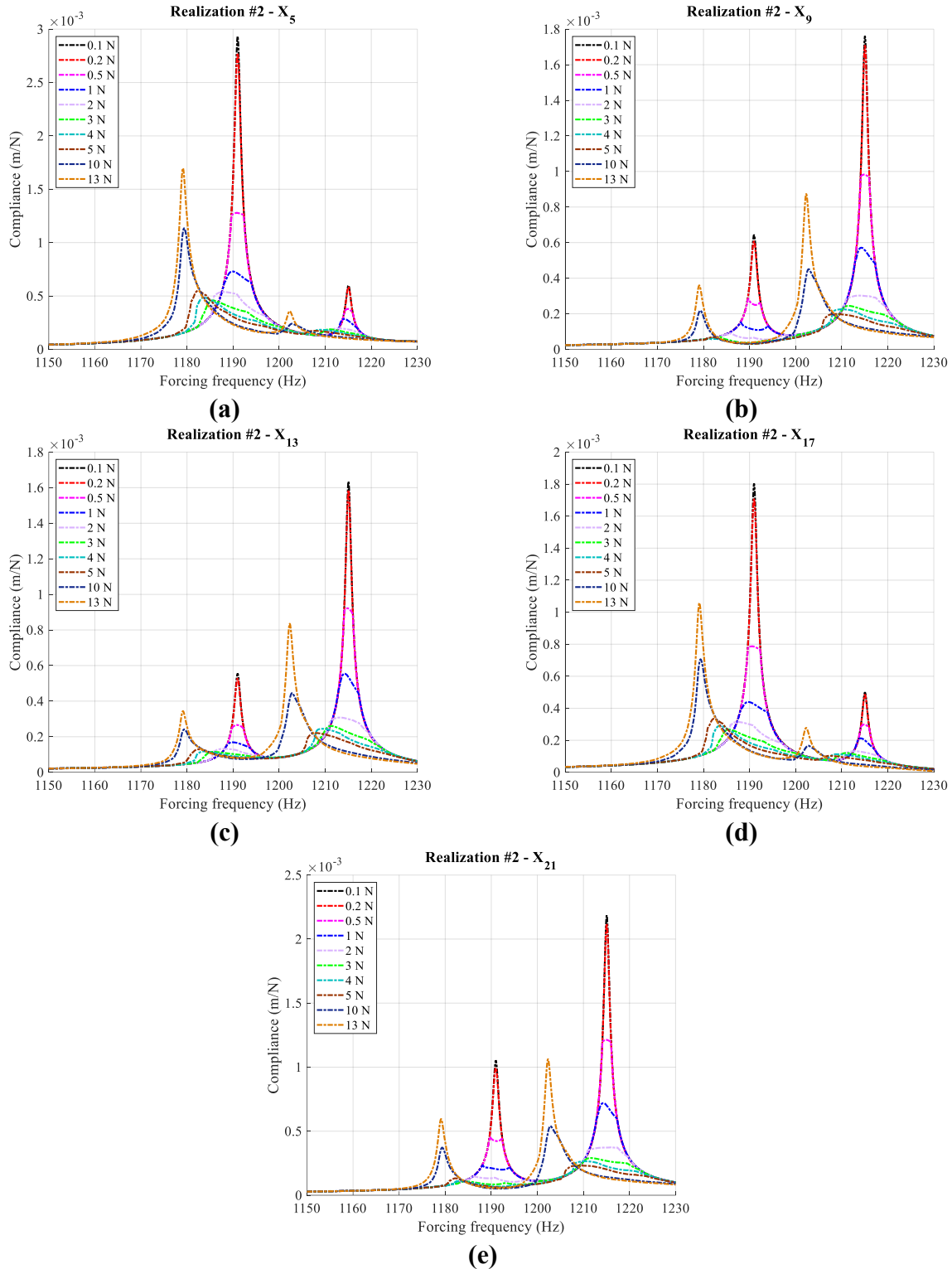
Figure A 8: Compliance of the blade tips #2, #3, #4, #5, and #6 for different excitation level, second mistuning realization
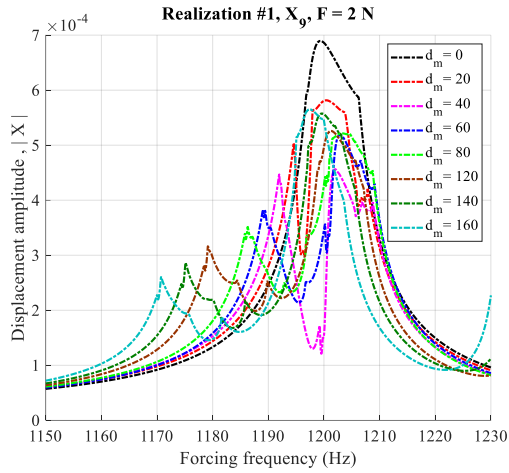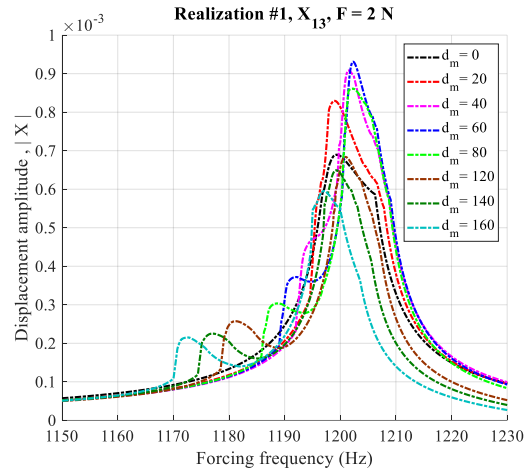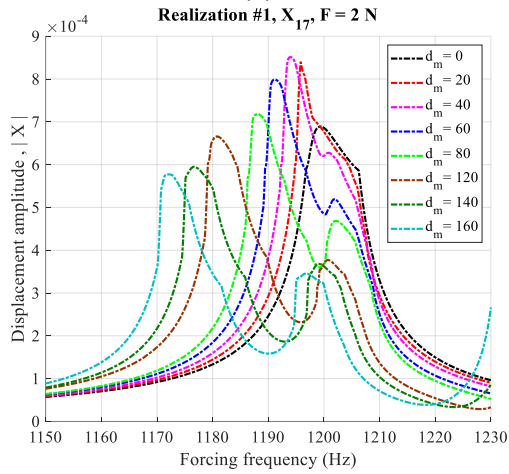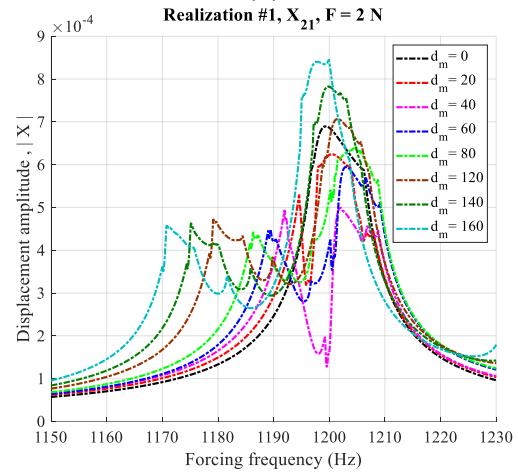
Figure A 9: Steady-state forced response of the tips of blades #3, #4, #5, and #6 for a range of mistuning levels between 0 and 160, first mistuning realization
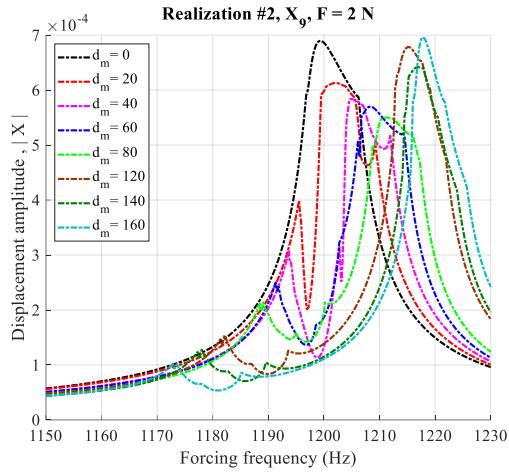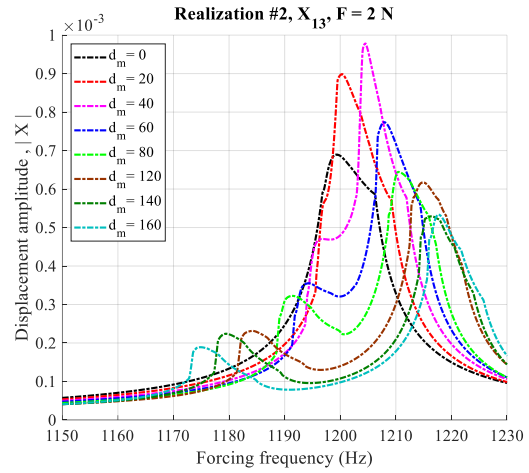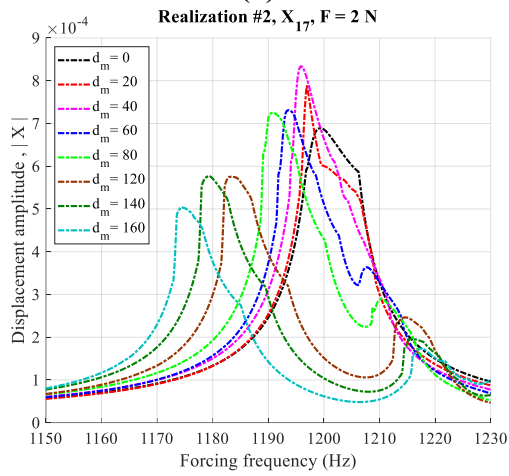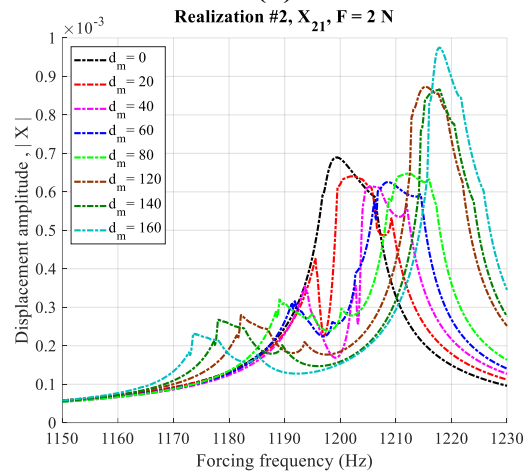
Figure A 10: Steady-state forced response of the tips of blades #3, #4, #5, and #6 for a range of mistuning levels between 0 and 160, second mistuning realization

Appendix B
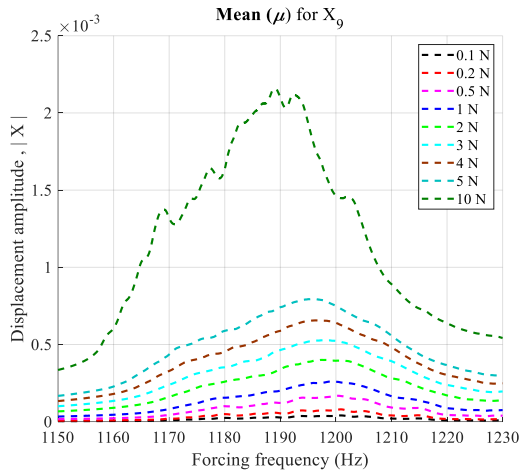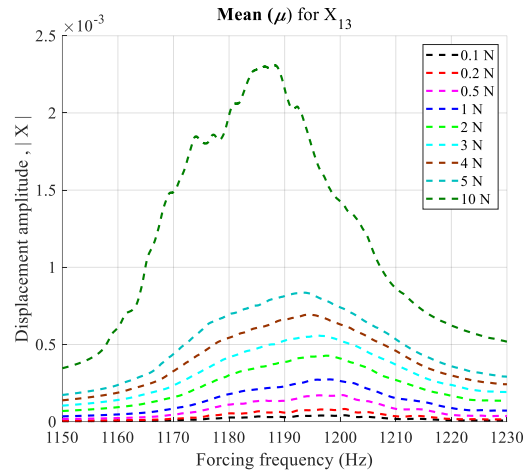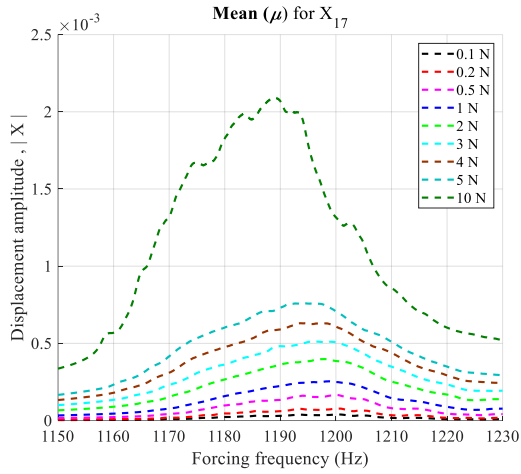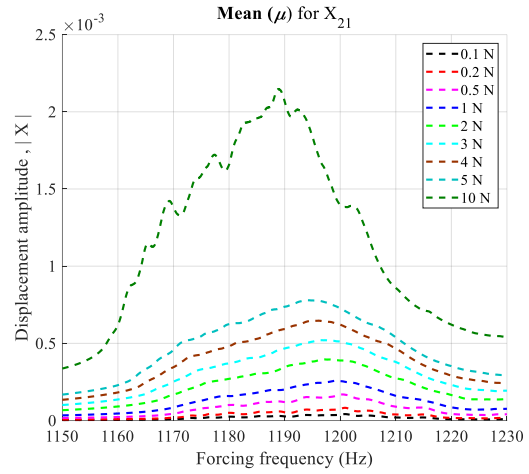
Figure B 1: Mean of displacement amplitude for the blade tips #3 to #6, considering the 150 mistuning realizations
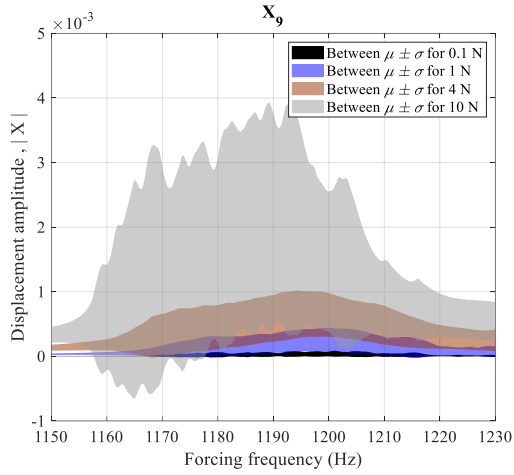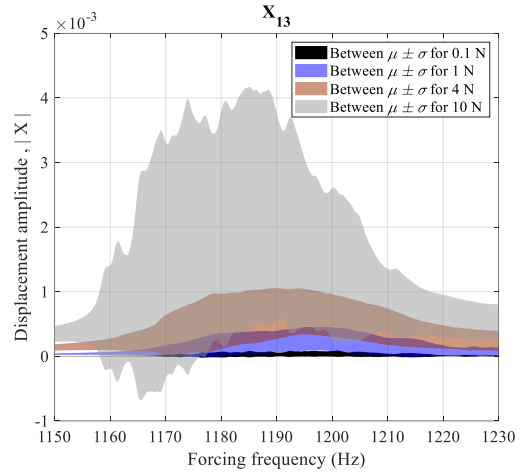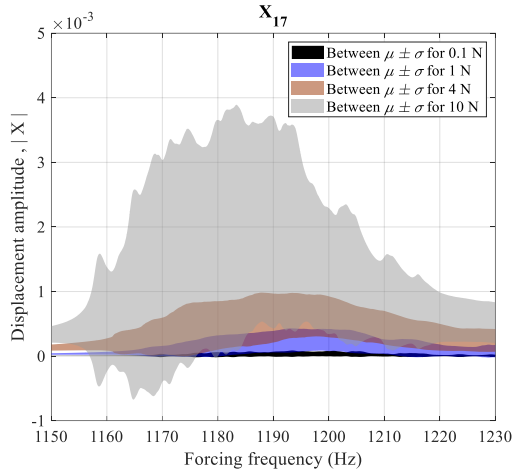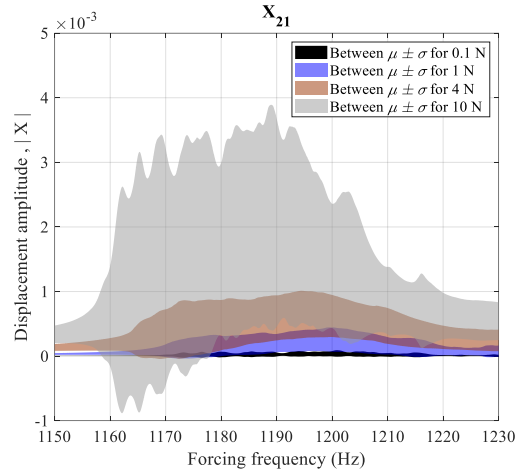
Figure B 2: Space between $\mu \pm \sigma$ for blade tips #3, #4, #5, and #6, and different excitation levels, considering 150 realizations
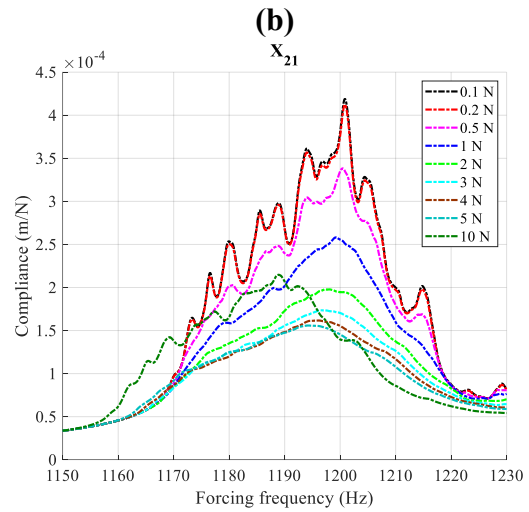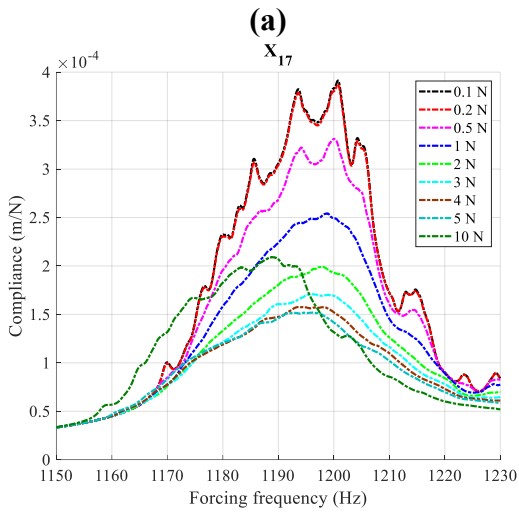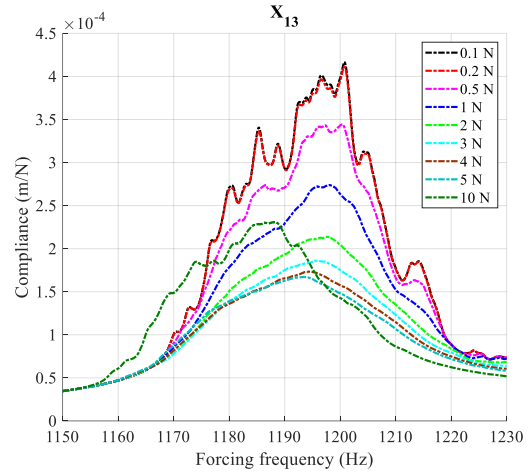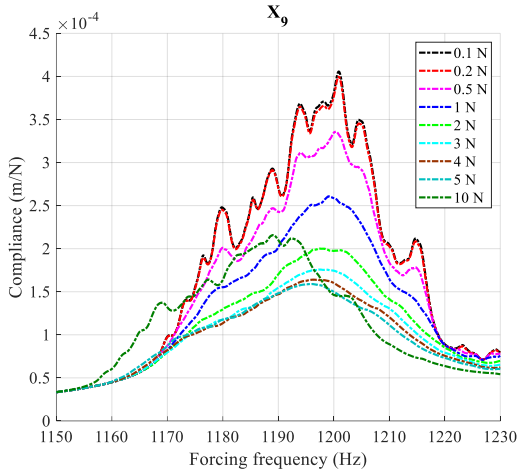
Figure B 3: Mean compliance of the blade tips #3, #4, #5, and #6 for different excitation levels, considering 150 mistuning realizations
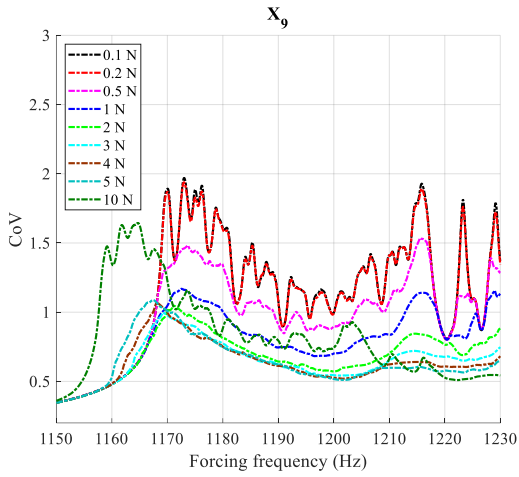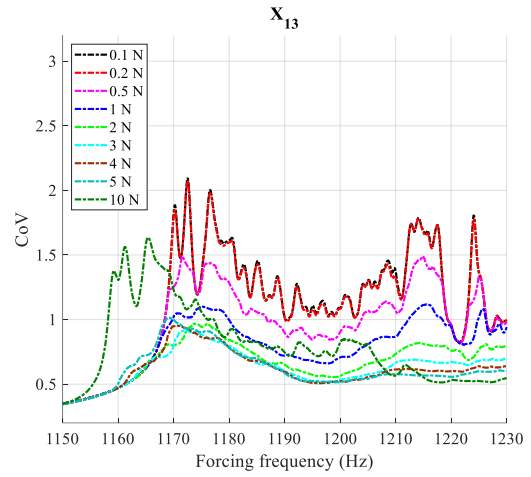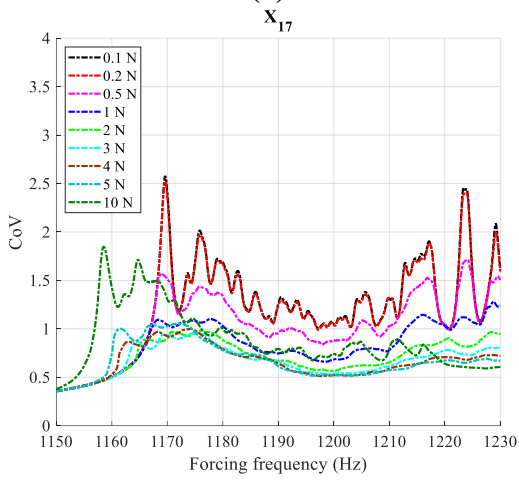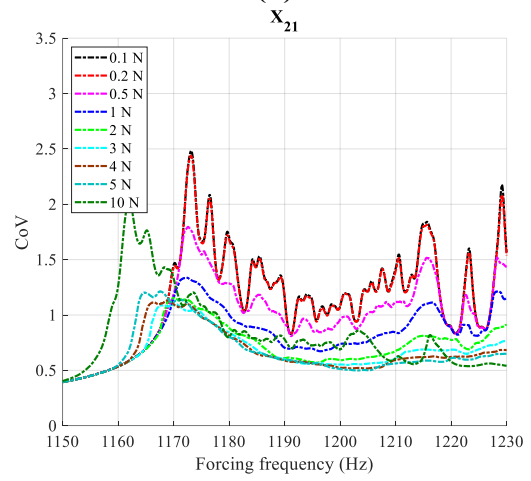
Figure B 4: Coefficient of variation of blade tips #3, #4, #5, and #6, for different excitation levels, considering 150 mistuning realizations
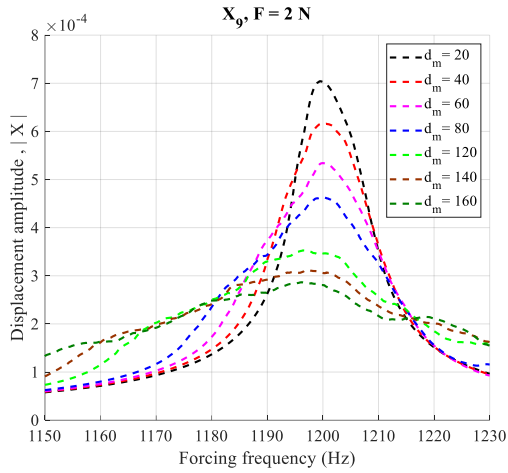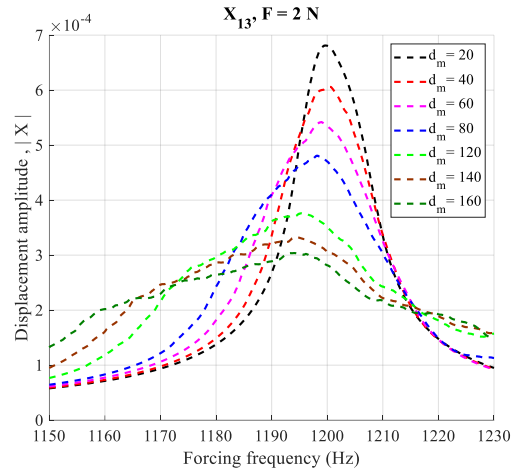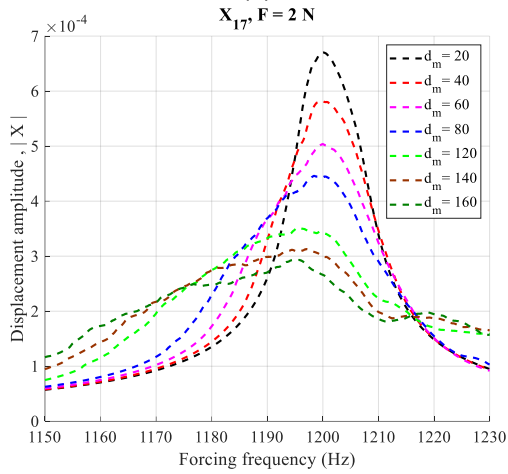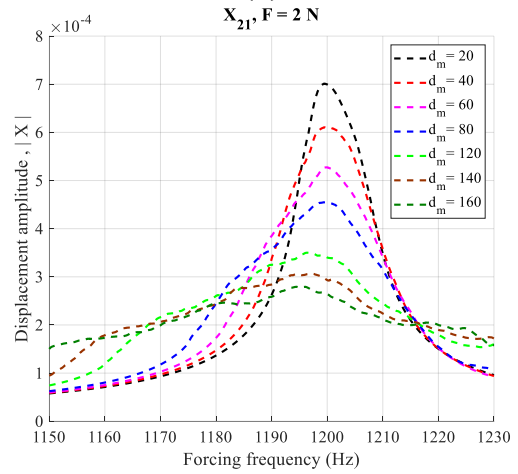
Figure B 5: Mean of displacement amplitude for the blade tips #3, #4, #5, and #6, for a range of mistuning levels, considering 150 mistuning realizations
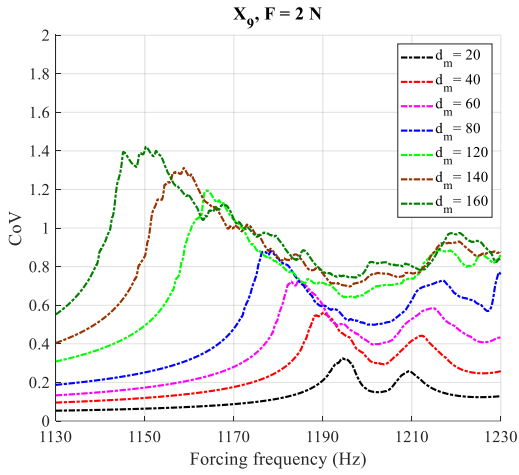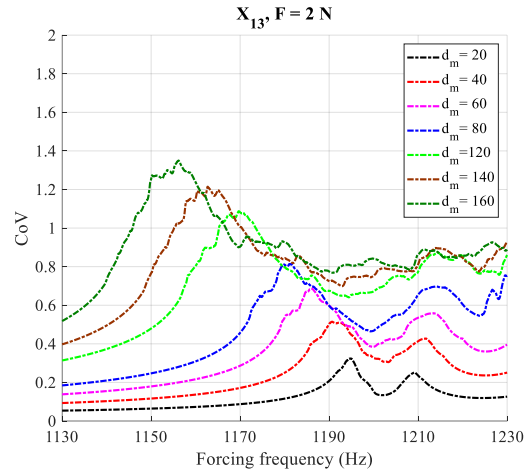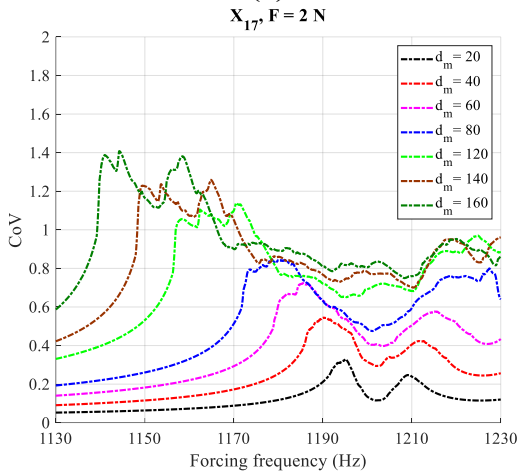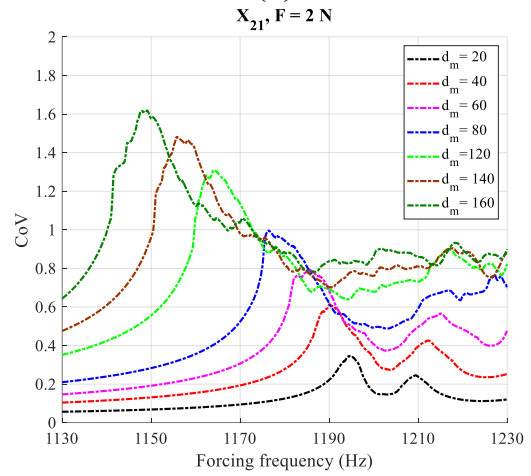
Figure B 6: Coefficient of variation of the blade tips #3, #4, #5, and #6, for a range of mistuning levels, considering 150 mistuning realizations
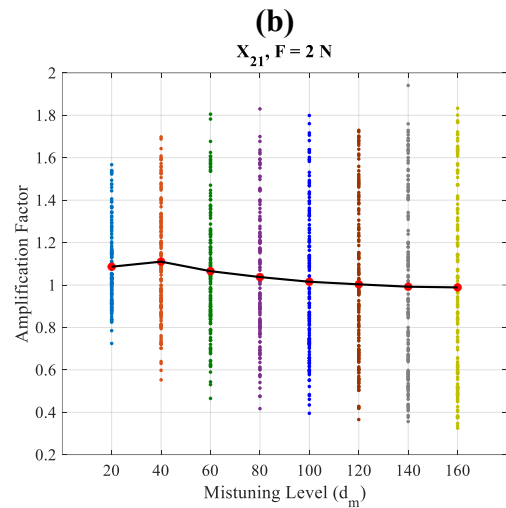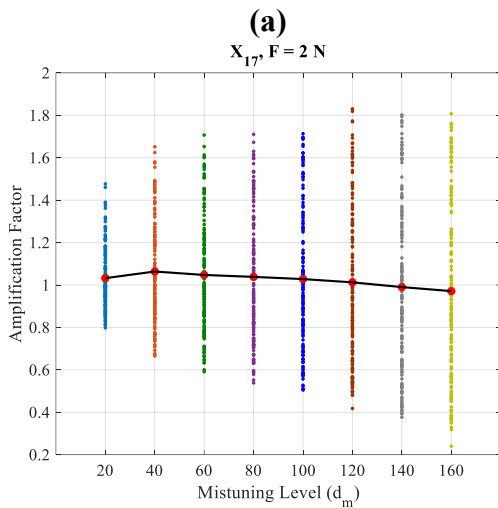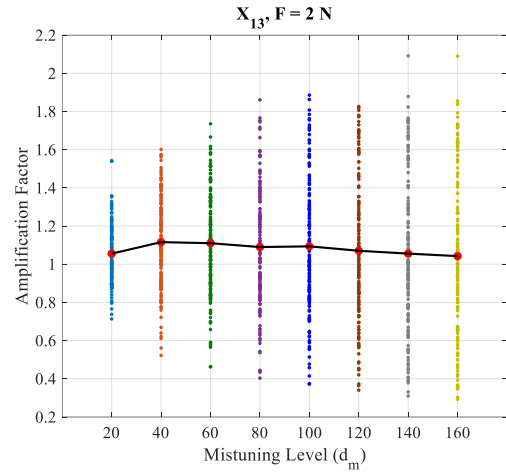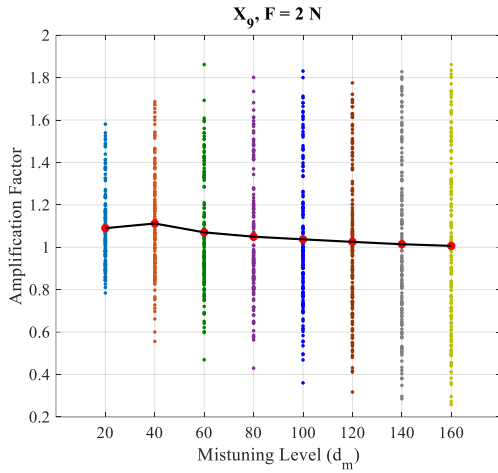
Figure B 7: Amplification factor of blade tips #3, #4, #5, and #6, for a range of mistuning levels, considering 150 mistuning realizations